UC Davis

Title

Advancing the understanding and measurement of phagocyte vomocytosis of Cryptococcus neoformans

Permalink

Author

Pacifici, Noah

Publication Date

2022

Advancing the understanding and measurement of phagocyte vomocytosis of
Cryptococcus neoformans

By

NOAH PACIFICI
DISSERTATION

Submitted in partial satisfaction of the requirements for the degree of

DOCTOR OF PHILOSOPHY

in

Biomedical Engineering

in the

OFFICE OF GRADUATE STUDIES

of the

UNIVERSITY OF CALIFORNIA

DAVIS

Approved:

_____
Jamal Lewis, Chair

_____
Angela Gelli

_____
Alyssa Panitch

_____
Sharon Aviran

Committee in Charge

2022

i

ABSTRACT

Following digestion by phagocytes, the fungal pathogen Cryptococcus neoformans (CN) has been observed to survive within the normally fatal phagosome and trigger nonlytic expulsion through a process called "vomocytosis". This phenomenon is believed to play a key role in dissemination of the fungal pathogen, allowing CN to use immune cells as shuttles to travel throughout the body and to even cross the blood brain barrier through a "Trojan Horse" method. Very little is known about the underlying mechanisms of vomocytosis; however, prior studies have correlated its rate of occurrence with a small number of physicochemical, protein, and immunological cues. Understanding vomocytosis could open the doors for development of new therapies against Cryptococcal infection, as well as new drug delivery biomaterial vehicles that can escape phagosome-mediated degradation. The primary goal of this dissertation is to uncover further understanding of vomocytosis. The work includes characterization of this phenomenon in a new cell type, development of a new fluorescent tool to measure expulsions, and transcriptomic analysis of CN-infected phagocytes.

Vomocytosis has primarily been studied in macrophages (MΦs), the primary phagocyte that interacts with CN. However, recently neutrophils were also observed to perform vomocytosis, indicating that this phenomenon may be conserved among other phagocyte cell types. To further investigate, we characterized the first documented occurrence of vomocytosis in dendritic cells (DCs), a phagocyte and key immune cell player bridging the innate and adaptive immune system. The unique lymph node trafficking and antigen presentation properties of this cell type made DCs of high interest for studying this phenomenon. This work characterized the vomocytosis rates, timing, and

CN per phagosome of DCs under different ratios of infection, immune phenotypes, and drug-treated conditions.

In studying vomocytosis, it was clear that the methods by which to measure the occurrence of expulsion via manual counting of time lapse microscopy videos were extremely difficult and inefficient. Therefore, we devised a new reporter system staining scheme as a novel tool to measure vomocytosis events via flow cytometry with simple, high throughout, and accurate means. This new method, consisting of fluorescent streptavidin and antibody staining during infection, allowed for measurement of vomocytosis rates of both MΦs and DCs, and could measure differences in rates under drug treated conditions that affect phagosome properties and actin polymerization. Furthermore, through single cell Raman scattering analysis, vomocytosed CN were observed to have unique compositional phenotypes that likely affect their biological functions. Finally, the reporter system was translated to inert poly(lactic-co-glycolic acid) (PLGA) microparticles (MPs). This modified staining scheme was shown to successfully function to measure induced expulsion events for proof of concept of reporter-mediated particle vomocytosis measurements.

Lastly, an RNA sequencing study was conducted on CN-infected MΦs and DCs to further understand the internal gene expression changes that occur in phagocytes during vomocytosis occurrence. Like most biological processes, vomocytosis is tied to protein expression and internal signaling pathways. As a precursor to proteins that is easily measured through sequencing, RNA acts as a valuable detection method for potential protein changes and pathway modulations within cells. The RNA expression of MΦs and DCs were measured over the course of 10 hours of CN infection to generate lists of

differentially expressed genes. These gene sets were filtered and analyzed to identify three key signaling pathways that may be involved in vomocytosis— PI3K/Akt, p53, and FoxO. Additionally, the 4 highest modulated genes in each pathway were identified as candidate target genes that might affect vomocytosis.

Together, this work furthers the research of vomocytosis on multiple fronts. We have documented the discovery of vomocytosis occurrence in DCs, developed a superior fluorescence-based method to quantify expulsion occurrence, and screened for potential signaling pathways linked to this process using RNA sequencing.

ACKNOWLEDGEMENTS

TABLE OF CONTENTS

CHAPTER 1: INTRODUCTION AND BACKGROUND

1.1 Abstract

Macrophages are well known for their phagocytic activity and their role in innate immune responses. Macrophages eat non-self particles, via a variety of mechanisms, and typically breakdown internalized cargo into small macromolecules. However, some pathogenic agents have the ability to evade this endosomal degradation through a non-lytic exocytosis process termed vomocytosis. This phenomenon has been most often studied in *Cryptococcus neoformans*, a yeast that causes roughly 180,000 deaths per year, primarily in immunocompromised (e.g. human immunodeficiency virus [HIV]) patients. Existing dogma purports that vomocytosis involves distinctive cellular pathways and intracellular physico-chemical cues in the host cell during phagosomal maturation. Moreover, it has been observed that the immunological state of the individual and macrophage phenotype affects vomocytosis outcomes. Herein, we compile the current knowledge on the factors (with respect to the phagocytic cell) that promote vomocytosis of *C. neoformans* from macrophages.

1.2 Introduction: What goes in, must come out?

Phagocytosis by innate immune cells is important for cell-to-cell communication, metabolism, homeostasis, and organism survival[1–4]. Macrophages are critical players in the innate immune host defense system that recognize, internalize and neutralize foreign bodies[5]. These specialized cells use a variety of mechanisms, which are often concurrent and intertwined, to internalize particulate matter. Some of the most characterized uptake pathways in macrophages include: (1) clathrin-mediated endocytosis, (2) caveolae/raft-

1

dependent endocytosis, (3) macropinocytosis, (4) micropinocytosis and (5) phagocytosis (**Figure 1.1A**). The specific entry process depends on both the physico-chemical and biological properties of the particulate[6–9]. Accordingly, the intracellular fate of internalized cargo is influenced by the type of internalization executed and nature of the internalized particulate[6,8–10].

In the case of a fungal infection, macrophages are among the early immune cell responders that typically internalize and clear fungal cells. This clearance involves the accumulation of these phagocytes at the site of infection, recognition of cell-surface, fungal-specific characteristics, internalization and degradation in an acerbic vacuole, called the phagolysosome[6,11]. However, some fungi, such as *Cryptococcus neoformans*, are capable of not only skirting innate immune actions, but escaping from the grasp of these phagocytic cells after capture.

C. neoformans is a globally distributed and free-living basidiomycetous, mostly found residing within the decaying wood within tree trunk hollows and avian excreta[12]. Therefore, this species' survival does not depend on infection of animal hosts. However, the ease of exposure to *C. neoformans*, presumably by inhalation of infectious particles, resulted in an estimated 220,000 *cryptococcal meningitis* cases in people living with HIV/AIDS in 2017[13]. This organism has developed phagocyte escape capabilities that contribute to its virulence within immunocompromised hosts. Some theorize *C. neoformans* may have developed these defenses against phagocytes in response to pressure from environmental amoeba[14]. However, the amoeba *Dictyostelium discoideum* was shown to expel phagocytosed *C. neoformans* primarily via Wiskott-Aldrich syndrome protein and Scar homolog (WASH)-mediated constitutive exocytosis—an 80-minute-long

process involving actin restructuring and membrane recycling pathways, which is distinct from vomocytosis[15]. When WASH-mediated exocytosis is blocked, a secondary, vomocytosis-like route of escape appears, characterized as a stochastic, non-lytic exocytosis process that takes place over several hours. *C. neoformans* can evade amoeba using constitutive exocytosis alone, therefore the existence of vomocytosis as a secondary exit process seems evolutionarily redundant; the true evolutionary driver for this phenomenon has yet to be discovered. Vomocytosis (often referred to as non-lytic exocytosis) has also been observed in *C. neoformans*-infected macrophages. After expulsion from innate immune cells, *C. neoformans* is carried in the bloodstream and disseminated to the brain[16].
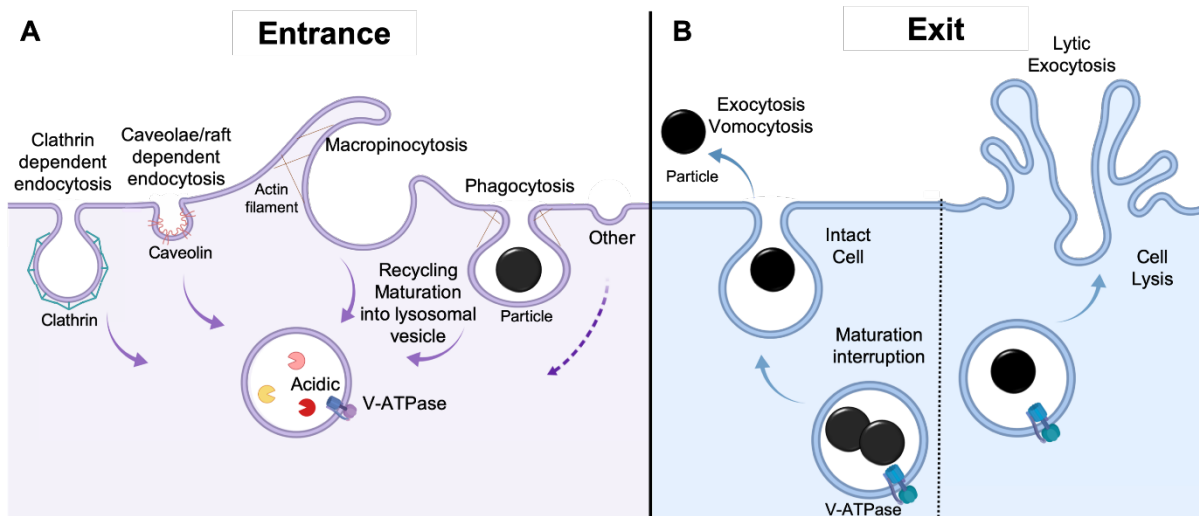
Figure 1.1. Foreign particulate entry and exit pathways into macrophages. Internalized cargo is typically directed to its degradation in a harsh, degradative environment driven by acidity and lysosomal enzyme activity. *C. neoformans*, however, has the ability to manipulate the progression of this process by exiting the cell via the non-lytic exocytosis mechanism, vomocytosis, which leaves the host cell intact or by lytic

exocytosis, which results in the lysis of host cell. This figure depicts the types of internalization mechanism that have been observed in macrophages. Their relative frequency of occurrence is not represented in this figure nor discussed in this article. Figure created with BioRender.

In this review, we highlight the biological, chemical and physical changes within the phagocytic cell that are connected to vomocytosis. As a postscript, we discuss the potential contributions of engineering to the study of this incredible behavior and the prospective exploitation of this phenomenon for advances in biotechnology and medicine.

1.3 Escape from Alcatraz: Breakout from Macrophages

Most mammalian cells are not only capable of internalizing materials, but also have built-in mechanisms to deliver intracellular contents externally. Vacuolar contents can exit the cell via exocytosis, a mechanism in which a vacuole fusses with the cell membrane releasing its contents outside the cell[17]. Exocytosis is particularly relevant in macrophages for a variety of intrinsic functions such as phagocytosis, inflammation and also play a role in diseased state[18–21]. For instance, exocytosis of intracellular compartments is required for phagosome formation in order to compensate for the membrane utilized in phagocytosis, a dynamin-dependent process called focal exocytosis[22]. The secretion of the cytokine tumor necrosis factor (TNF) via secretory carrier membrane protein 5 (SCAMP5) is another example of exocytosis[23]. Moreover, lysosomal enzymes delivered via exocytosis are also reported in the initial degradation of dying or dead adipocytes in obesity and in tumorigenic cells clearance, processes called exophagy and

heterocytolysis, respectively[19,20]. Some internalized pathogens such as *C. neoformans*, *Candida albicans, C. gatti*, among others, have developed a mechanism to fuse their containment vacuoles with the cell membrane, evading lysosomal degradation[24–26].

C. neoformans has developed unique lytic and non-lytic exocytosis mechanisms to escape from phagolysosome degradation (**Figure 1.1B**). Several studies have identified virulence factors that promote escape such as capsule shedding, laccase and phospholipase B1[27–31]. Noting that they mediate escape from the phagosome suggests that they may contribute in modifying host signaling events. Early studies on phagosomal escape demonstrated that *C. neoformans* and the phagosome can be co-localized with phagosomal maturation indicators such as major histocompatibility complex II (MHC II), CD63[32,33], and LAMP-1[26,33], suggesting that the phagosome is at least partially matured. However, more recent studies have identified phagosome maturation disruption at the protein and physicochemical level[34–36]. Another mechanism of escape for *C. neoformans* is cell-to-cell transfer or dragocytosis. Altogether, these exit mechanisms, which are further discussed below, aid in *C. neoformans* survival and dissemination in human hosts.

Lytic Exocytosis

The lysis of host cells is an important route of escape from the intracellular environment for many pathogens[12,37]. However, pore-forming proteins, which are commonly used by other pathogens to lyse host cells, have not been identified in *C. neoformans*. Studies suggest *C. neoformans* mechanically disrupt host cells through proliferation within the phagosome and possibly via production of large amounts of polysaccharide capsule[38,39]. Macrophages can undergo apoptosis in response to

intracellular cryptococcal signaling via the alternative NF-kB pathway[40]. Further, macrophage lysis in response to intracellular *C. neoformans* has recently been linked to phagosome membrane permeabilization and apoptosis[36].

Vomocytosis

Among the different exit mechanisms, vomocytosis (or non-lytic exocytosis) by *C. neoformans* has been the most studied. In vomocytosis, a live fungal cell is expelled from the phagosome whilst keeping the host cell intact[26,41]. Similar phagocytic escape has been described for *Candida albicans*[25], *Chlamydia* spp.[42], *Orientia tsutsugamushi*[43], and *Cryptococcus gatti*[44,45]. However, each of these species have distinguishing features to their vomocytic mechanisms. In vomocytosis, the phagosome fuses with the plasma membrane releasing the cryptococcal cell[46]. In recent years, studies have demonstrated that this mechanism is highly regulated and driven by *C. neoformans* since the heat-killed pathogen is unable to promote vomocytosis[26,47].

Dragotcytosis / Cell-to-cell transfer

Vomocytosis followed by phagocytosis by a nearby cell has been characterized as a new *C. neoformans* phagosomal escape process called dragotcytosis[48]. The distinct feature of this mechanism is that there is interaction between the donor and acceptor macrophage prior to and shortly after the pathogen transfer event. Further molecular studies are needed to elucidate the crosstalk between macrophages and the internalized *C. neoformans* during dragotcytosis.

Noteworthy, the escape of *C. neoformans* from phagocytic cells via the two latter described processes, vomocytosis and dragotcytosis, potentially explain how *C. neoformans* may exploit phagocytes to penetrate the blood brain barrier (BBB) in a Trojan horse manner[49,50]. In previous studies, *C. neoformans* was detected inside phagocytes on the outer side of a meningeal capillary, which suggests that *C. neoformans* may have been transported within circulating phagocytes[51,52]. Moreover, Santiago-Tirado and co-workers demonstrated the occurrence of this mechanism *in vitro*[16]. However, due to the difficulty of studying this mechanism *in vivo*, the extent at which *C. neoformans* may use the Trojan-horse dissemination model to traverse into the brain remains unknown.

Transcytosis

Transcytosis, possibly an indirect innate immune system evasion, is the most employed blood brain barrier (BBB) cells penetration mechanism by *C. neoformans,* which takes advantage of cellular endocytosis[53,54]. Transcytosis of the BBB has been widely reported *in vitro* by showing the ability of *C. neoformans* to adhere to one or more receptors on the endothelial cell barrier[55,56]. The process causes marked morphological changes in the host cell including membrane ruffling, irregular nuclear morphology and swelling of the mitochondria and the ER[57]. Studies suggest that transcytosis involves the migration of *C. neoformans* across the BBB in a glycoprotein cluster of differentiation (CD44)-dependent manner. *C. neoformans* activates EphrinA2 (EphA2) pathway via CD44, creating a permeable barrier that promotes the migration of *C. neoformans* across the BBB[58]. More molecular events detailing the mechanisms underlying *C. neoformans* transcytosis remain to be fully resolved.

Collectively, these mechanisms of escape aid in the survival and dissemination of *C. neoformans* in the human body. However, the relationships between these processes is currently unknown. Converse to phagocytosis, many questions remain over vomocytosis, which was only identified in 2006[26]. Below, we discuss the characterized features of macrophages that have been linked to vomocytosis of *C. neoformans*.

1.4 Vomocytosis involves cytoskeletal remodeling

The cytoskeleton has a prominent role in phagocytosis and therefore, its relevance in *C. neoformans* expulsion should not be surprising. Reports have shown in detail how changes in the cytoskeleton promote pathogen survival and innate immune evasion[26,46,59]. For instance, Johnston et al. found via three dimensional confocal time lapse imaging *in vitro*[46] that there is a dynamic and repeated actin coat assembly around *C. neoformans* containing phagosomes. They also observed that vomocytosis occurred via the fusion of phagosomal compartments and plasma membrane in J774 cells (a macrophage-like cell line). This event was preceded by phagosomal permeabilization and followed by actin coat assembly. When modulating actin polymerization they found that "flash" (actin polymerization cycle) events are inversely related to non-lytic exocytosis, suggesting its role in temporarily inhibiting vomocytosis.

1.5 Protein Networks involved in Vomocytosis

RabGTPases protein family

The Rab GTPase protein family are integral players in phagosomal maturation[60,61]. Rab 5 is an early phagosome marker that recruits for the progression of phagosomal

maturation. Another early phagosome marker is Rab 11, which is relevant for phagosome fusion and fission with other intracellular compartments by contributing to the dynein-dependent transport of recycling endosomes. Whereas, Rab 9 and Rab 7 are proteins associated with late phagosomal stage. The former is a marker of endoplasmic reticulum-derived membrane and the latter plays an essential role in the fusion of the late phagosome with a lysosome to form the phagolysosome[61]. Smith et al. demonstrated that live *C. neoformans* promote the rapid removal of the early phagosome markers Rab5 and Rab11 in J774 cells (**Figure 1.2**)[34]. This removal did not occur when infecting macrophages with heat-killed pathogen or inert beads. Additionally, Rab9 levels were significantly higher on phagosomes containing live *C. neoformans* two hours after phagocytosis compared to phagosomes containing heat-killed pathogen and latex beads. This report demonstrated how *C. neoformans* affects phagosomal maturation at the protein level.
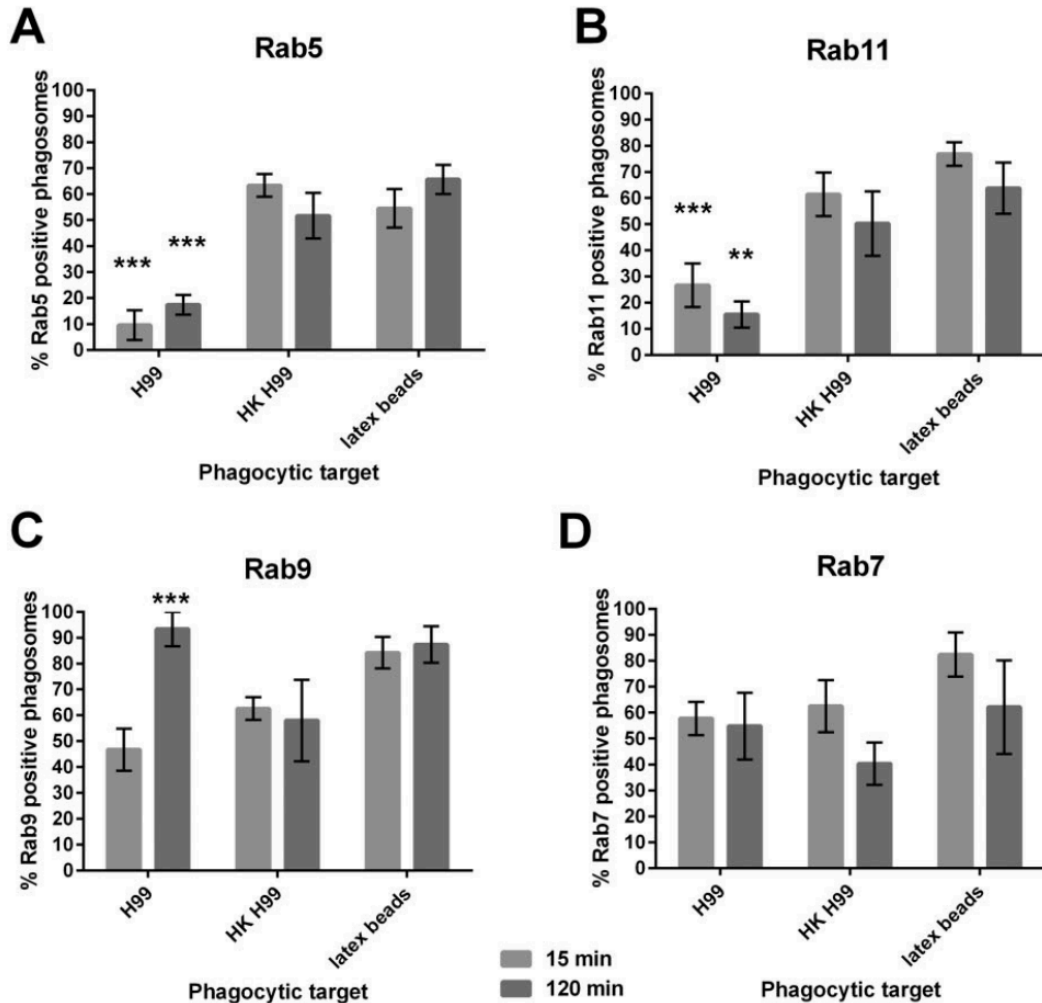
Figure 1.2. Recruitment of Rab GTPases onto the Cryptococcus-containing phagosome. Immunofluorescence analysis at 15 min and 2 h to detect Rab5 (A), Rab11 (B), Rab9 (C) and Rab7 (D) recruitment to phagosomes containing live *C. neoformans* on J774 cells. Figure adapted and data described previously[34].

ERK5 signaling modulation

Another host protein that has been identified to play a role in vomocytosis, as well as in phagocytosis is extracellular-signal-regulated kinase 5 (ERK5). At the cellular level, ERK5 pathway is required for colony-stimulating factor-1 (CSF-1)-induced proliferation

and is linked to cell metabolism in macrophages[62–65]. Gilbert et al. demonstrated its critical role at suppressing the frequency of vomocytic events[64]. Pharmacological inhibition and genetic manipulation of ERK5 activity both significantly raise vomocytosis rates in human macrophages, whereas stimulation of the ERK5 signaling pathway inhibits vomocytosis. Using a zebrafish model of cryptococcal disease, this study showed that reducing ERK5 activity *in vivo* stimulates vomocytosis and results in reduced dissemination of infection, likely due to expulsion before macrophage migration (limiting the chance for Trojan horse transport). Interestingly, modulation of ERK5 signaling pathway did not induce expulsion of heat-killed *C. neoformans* or inert beads, suggesting the active role of the pathogen and a more complex molecular mechanism. Notably, ERK5 inhibition suppressed M2 macrophage polarization in J774 and human-monocyte derived macrophages (HMDM) cells[64], suggesting an interesting dynamic between macrophage polarization and vomocytosis.

Cathepsin Activity

Cathepsins are hydrolytic enzymes that have optimal activity at acidic conditions. They are important players in phagosomal maturation and are also implicated in inflammasome activation. The NLRP3 inflammasome is a multimeric protein complex important for infection eradication via the activation of IL-1β and IL-18, which has a central role in host defense[66]. In a study by Lei et al., *C. neoformans* biofilm was found to stimulate NLRP3 inflammasome activation in human monocytic THP-1 cells. Moreover, an increased rate of death was observed in *C. neoformans* biofilm-infected mice if there was no activation of this protein complex[67]. Further, this group demonstrated that

11

inhibition of Cathepsin B resulted in IL-1β activation interruption in a dose-dependent manner on cells and subsequent host protection. While this report showed the importance of Cathepsin B in the activation of host protection against *C. neoformans in vivo*, Smith et al. showed that macrophage infection with *C. neoformans* results in lack of Cathepsin L activation, which is a phagosome maturation late-stage marker. In this latter study, heat-killed *C. neoformans* had significant activation of Cathepsin L[34]. There is no clear link between vomocytosis and cathepsins. However, these studies demonstrate that this class of proteins may play a role in this special event as cathepsin activity is affected by *C. neoformans* infection. Moreover, these studies implicate the role of phagosomal pH and other physicochemical factors, which influence cathepsin activation, in vomocytosis.

Annexin A2 Expression

Annexin A2 is a membrane-bound protein involved in many processes including phagocytosis, endocytosis, and exocytosis. Gene expression for this protein is upregulated in brain endothelial cells during transmigration of *C. neoformans*[55]. As such, Stukes et al. investigated the role of annexin A2 in the interaction between macrophages and *C. neoformans*[68]. Murine bone marrow-derived cells (BMDMs) were harvested and grown from wild type mice and annexin A2 knockout mice. They found that, compared to wild-type macrophages, annexin A2-deficient macrophages exhibited lower rates of phagocytosis, reduced frequency of vomocytosis, and higher occurrences of lytic exocytosis. Other notable observations of infected annexin A2-deficient macrophages included an increase in *C. neoformans* capsule size, lower production of reactive oxygen species, and decreased levels of LC3 in phagosomes. These results align with previous

findings that free radicals can damage and reduce the *C. neoformans* capsule[69]. Stukes

and co-workers also tested the significance of annexin A2 during infection, by infecting

wild-type and annexin A2 knockout mice with *C. neoformans*. The A2 knockout mice had

lower rates of survival, suggesting that this protein is important in controlling fungal

infections, with vomocytosis potentially protecting macrophages from eventual lysis.

These findings highlighted the role of annexin A2 in phagocytosis, anti-fungal defense

mechanisms, and vomocytosis. While the exact underlying mechanisms of this protein's

involvement are unclear, the authors theorized that during vomocytosis annexin A2

complexes with its known binding partner, fusogenic protein SNAP-23, promote fusion

between the phagosome and plasma membrane[70]. Furthermore, the Ca^{2+} dependence of

annexin A2 could be linked to the intracellular calcium changes observed during

vomocytosis.

1.6 Physicochemical Characteristics of Vomocytosis

Phagosomal pH

An important characteristic of phagosomal maturation is its acidification. Several

studies have demonstrated the ability of *C. neoformans* to affect the pH of phagosomes

as an indication of phagosomal maturation inhibition. The pH in the phagosomal

environment is highly regulated and controlled by vacuolar membrane ATPase activity.

This protein is responsible for the acidification of the phagosomal compartment to a pH

as low as 4.5. This H^+ release is balanced by Cl^- anions[71,72]. Smith and co-workers

demonstrated that significant acidification of the phagosome, which is distinctive of

phagolysosomal stage, only occurred on phagosomes containing heat-killed and UV-

killed *C. neoformans*[34], while acidification was hindered by the presence of live *C. neoformans* in phagosomes of J774 and HMDM cells. Moreover, inhibition of the microbiocidal environment resulted in intraphagosomal cryptococcal budding and vomocytic activity of the internalized *C. neoformans*. These observations validated an earlier study by Moraes-Nicola et al. that noted a relationship between the increased in phagosomal pH and the enhancement of vomocytosis events[73]. Succinctly, they reported an increase in non-lytic exocytosis events when supplementing *C. neoformans*-containing macrophages with the weak bases chloroquine and ammonium chloride.

Later, Fu et al. showed that production of urease was connected with increased phagolysosomal pH[74]. Urease is a major virulence factor of *C. neoformans* upon interaction with macrophages. This enzyme breaks down urea into ammonia, which in turn increases the phagosomal pH in infected macrophages[75,76]. In the study by Fu and coworkers, the alkalinization of phagosomes containing *C. neoformans* was clearly demonstrated and this increase in pH resulted in: (1) reduced proliferation of urease-positive *C. neoformans* compared to urease-negative strain, (2) a decrease in phagolysosomal damage, and (3) an increase in vomocytic events. An interesting finding of this study was that even co-incubating J774 cells with heat-killed *C. neoformans* resulted in an increase in phagosomal pH, in comparison to latex beads containing phagosomes (**Figure 1.3**). The discrepancy between the latter report and what was observed in Smith et al. study could be due to the use of different techniques to measure pH. Fu et al. attributed the alkalinization of phagosomes containing heat-killed *C. neoformans* to heterogenicity in maturation of evaluated phagosomes and secretion of molecules that could affect the concentration of hydronium ions by heat-killed pathogen.

14

Noteworthy, they also observed that the addition of urea promoted an increase in non-lytic exocytosis events in macrophages infected with *C. neoformans*. Interestingly, urea also promoted non-lytic exocytosis events in urease-negative *C. neoformans*-infected macrophages. Taken together, these observations emphasize that increased phagosomal pH facilitates but does not cause vomocytosis. Moreover, vomocytosis is affected by the presence of urea and urease. Additionally, this report noted an increase in intracellular replication of *C. neoformans* in acidic vesicles, corroborating previous findings of *C. neoformans* growth in acidic conditions[77]. In an *in vivo* infection model, urease-deficient *C. neoformans* were less virulent than wild type *C. neoformans*, which reiterates the importance of vomocytosis to *C. neoformans* dissemination and infection.

More recently, De León and co-workers studied the role of the *C. neoformans* capsule in the pH microenvironment of the phagosome[35]. They hypothesized that glucuronic acid residues in the capsular polysaccharide had buffering capacity in the phagosome. They infected BMDM with non-encapsulated *C. neoformans* that were previously coated with different amounts of encapsulated *C. neoformans* conditioned media, which resulted in the attachment of soluble polysaccharide to their surface. More coating on non-encapsulated cells promoted an increase in phagosomal pH, compared to phagosomes infected with encapsulated *C. neoformans*. With these findings they suggested that the presence of glucuronic acid residues in the capsule of *C. neoformans* makes the polysaccharide a weak acid capable of modulating pH in the phagosome. The capsule's acid-base properties promote fungal cell survival in the phagosome by the buffering capacity during microbicidal conditions. While interesting, the characterization

of encapsulated *C. neoformans* conditioned media is necessary to elucidate if there are other factors that would be capable of affecting phagosomal pH.
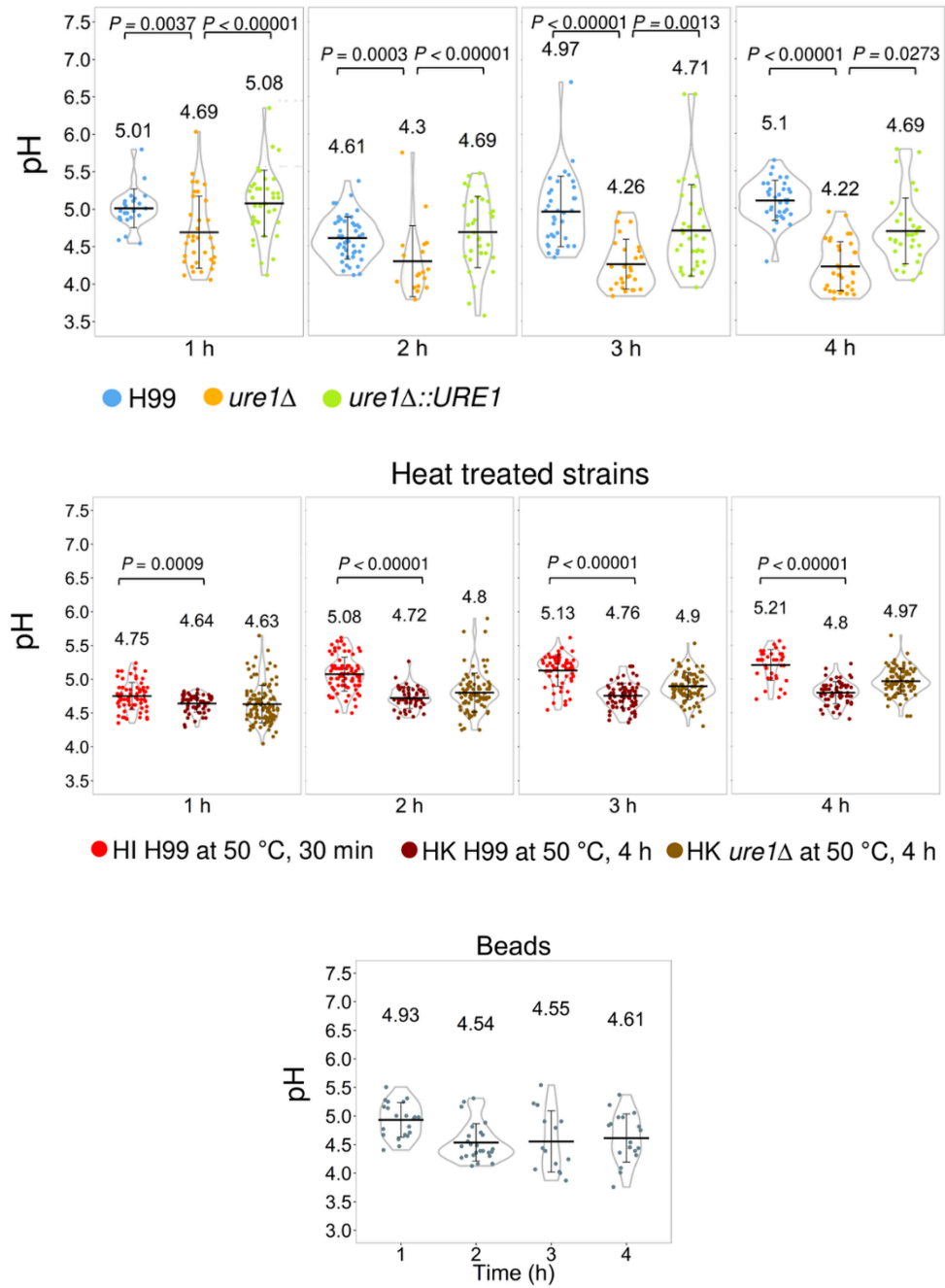
Figure 1.3. The presence of urease increases the phagolysosomal pH. (A–C)

BMDMs were infected with Oregon green labelled (Top) H99, ure1Δ or ure1Δ::URE1, (Middle) heat-inactivated (HI) H99 (heat inactivated at 50 ˚C for 30 min), heat-killed (HK) H99 or ure1Δ (heat killed at 50 ˚C for 4 h), and (Bottom) IgG-coated polystyrene beads, and phagolysosomal pH was measured by using dual-excitation ratio fluorescence imaging at the indicated time points. Each dot represents pH of individual phagolysosomes. Violin plot displays the probability density of dataset with means (middle bar) and standard deviation. Figure adapted and described previously[74].

Phagosome Permeabilization

Phagosome permeabilization has been observed in several studies with *C. neoformans*-infected macrophages[36,51,78,79]. Davis and coworkers studied lysosomal permeabilization in bone marrow derived macrophages infected by *C. neoformans* via flow cytometry[51]. They detected significant phagosome permeabilization up to 72 hours post *C. neoformans* infection. Conversely, no significant permeabilization was observed in macrophages infected with heat-killed *C. neoformans*. Since the majority of *C. neoformans* exocytosis occurs between 5-14 hours after macrophage uptake[26,41], they proposed that if permeabilization is needed for *C. neoformans* to escape from lysosomal degradation, *C. neoformans* exocytosis and *C. neoformans*-mediated lysosomal damage are chronologically independent mechanisms[51].

Three years later, a study by De León-Rodríguez et al. sought to further unravel the relationship between phagosomal pH, phagosomal membrane permeabilization (PMP), lytic exocytosis and vomocytosis[36]. They found that most *C. neoformans*-infected J774.16 cells experiencing PMP were positive for apoptotic markers, demonstrating a

17

relationship between PMP and apoptosis. However, they still observed populations of live cells experiencing PMP on BMDM. Nevertheless, their observations demonstrated that macrophages undergoing apoptosis did not maintain an acidic phagolysosomal pH. They investigated the role of phospholipase B1, a virulence factor for both *C. neoformans* and *C. gattii*, in the *C. neoformans* induction of PMP. Macrophages infected with a *C. neoformans* Δplb1 mutant had a decrease in PMP compared to those infected with wildtype and phospholipase B1–complemented strains, suggesting a mechanism of action for this virulence factor. However, when evaluating if phospholipase B1 deficiency affected phagosomal pH, their data suggested pH was unchanged. Induction of PMP with ciprofloxacin, a membrane permeabilizing agent, enhanced macrophages to trigger lytic exocytosis in apoptotic BMDMs. On the other hand, vomocytic events were common in cell populations without PMP[36]. Vomocytosis occurs with a frequency of 10–30% in macrophages and can be modulated by increase in phagosomal pH with ammonium chloride and chloroquine[73]. Interestingly, these two compounds not only raise the phagolysosomal pH, but also build osmotic pressure across the phagolysosomal membrane through the proton sponge effect, thereby affecting its permeability[80,81]. De León and coworkers showed that chemical induction of PMP in *C. neoformans*–infected macrophages leads to a decrease of vomocytic events to mainly lytic exocytosis, signifying that vomocytosis occurs when there is no PMP. The basis of this inference is that the frequency of non-lytic exocytosis peaks before 4 h, when most macrophages still have intact phagolysosomal membranes. However, they fail to account for dragotcytosis[82].

Calcium transport

Calcium ions (Ca^{2+}) are critical second messengers that regulate key signaling pathways in eukaryotic cells. In the context of phagocytosis, Ca^{2+} elevations are necessary for efficient ingestion of foreign particles by some phagocytic receptors and subsequent phagosomal maturation. Ca^{2+} is required for the solubilization of the actin meshwork that surrounds nascent phagosomes, for the fusion of phagosomes with granules containing lytic enzymes, for the assembly and activation of the superoxide-generating NADPH oxidase complex, and for exocytosis[83–89]. Given the role of Ca^{2+} ions in these related phenomena, some studies have delved into its role in vomocytosis. For instance, Smith et al. investigated the effect of *C. neoformans* on phagosomal and cytosolic calcium levels after infection[34]. They observed reduced levels of Ca^{2+} in phagosomes containing *C. neoformans* compared to cytosolic levels up to 120 minutes after infection (**Figure 1.4**). Interestingly, they found that phagosomes that contained heat-killed *C. neoformans* had greater calcium concentrations when compared to cytosolic Ca^{2+} levels after infection[34]. Although they did not study the relationship between phagosomal Ca^{2+} levels and vomocytic events, this is a good indication of the relevance calcium may have in this process.
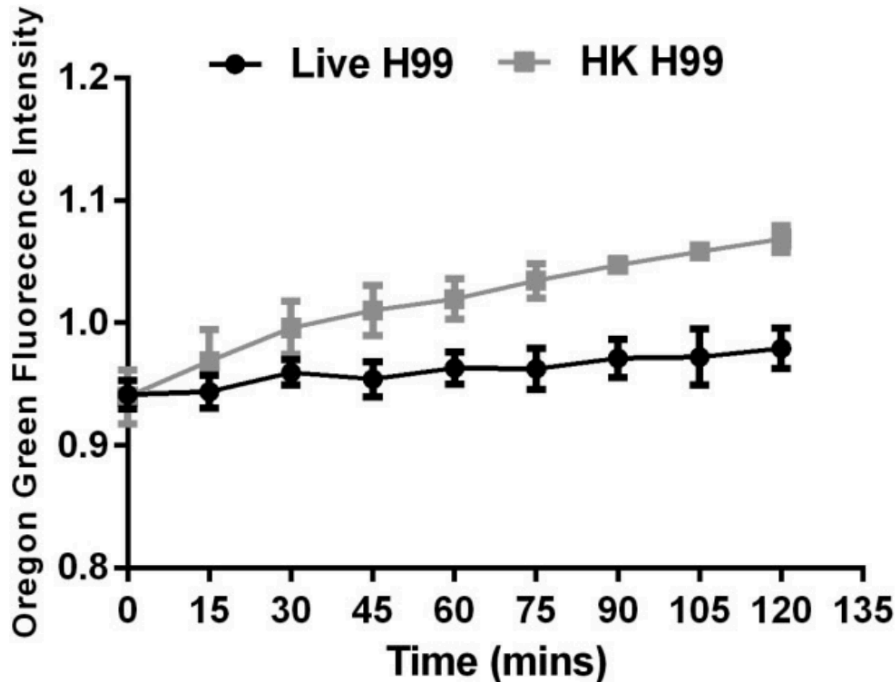
Figure 1.4. Phagosomes containing live *C. neoformans* do not accumulate calcium compared to phagosomes containing heat-killed *C. neoformans*. Fluorescent intensity data from each cryptococcal-containing phagosome (live *C. neoformans* H99 or heat-killed H99 [HK H99]) were normalized to a randomly selected region of cytoplasm within the same cell pre-loaded with Oregon Green BAPTA-1 1 hour before infection. Data displayed are fluorescent intensity relative to cytoplasm, sampled every 15 min over the course of a time lapse experiment, mean ± SEM (n < 35 phagosomes) across three biological repeats. Data as described previously[34].

In a later report, Samantaray et al. investigated the relationship between phagosomal calcium levels and *C. neoformans* survival and proliferation via the use of the L-type calcium channel blocker, fendiline hydrochloride[90]. This drug is thought to trigger endoplasmic reticulum calcium stores release, thus, elevating cytosolic Ca^{2+} and its signaling pathways[91,92]. They found that *C. neoformans*-containing phagosomes

acidify when macrophages were exposed to the drug. This acidification promoted *C. neoformans* death and decreased their proliferation rate. Thus, enhancement of calcium intracellular signaling pathways promoted phagosomal maturation. They did not specifically determine phagosomal pH of experimental groups, which makes it difficult to relate these results with previous discussed studies that demonstrate increase in *C. neoformans* proliferation in acidic phagosomal conditions. Nevertheless, Samantaray et al. and Smith et al. studies make evident that Ca^{2+} influx-dependent signaling is affected by *C. neoformans* and the pathogen's virulence potential can be modulated by manipulating Ca^{2+} concentrations.

1.7 Effect of Immune State on Vomocytosis

Viral Infection and Type-I Interferon

 Cryptococcus neoformans primarily infects immunocompromised hosts such as HIV patients. Seoane et al. investigated the effect of viral infection on vomocytosis[93]. They found that infection with HIV or measles viruses significantly boosts the frequency of vomocytosis in *C. neoformans*-containing human monocyte-derived macrophages, while leaving phagocytic uptake and intracellular fungal proliferation rates unaffected. Polyinosinic-polycytidilic acid (polyIC), a potent TLR3 agonist that induces antiviral responses in macrophages, alone was also shown to increase vomocytosis rates. These findings suggest that the macrophage response to viral infection, rather than active viral pathogenicity, is the factor that is modulating vomocytosis. Furthermore, since viral infections are known for inducing expression of type-I interferons (such as IFN-α and IFN-β), these researchers tested how stimulation with IFN-α affects vomocytosis rates.

Addition of IFN-α to non-virally infected macrophages was shown to produce a comparable enhancement of vomocytosis frequency to that of the virally-infected group. Moreover, pharmacological inhibition of type-I interferon receptors blocked the increase of vomocytosis during viral infections, confirming the role of type-I interferon signaling in modulating this process. This study shows that vomocytosis likely occurs at a high rate in HIV patients and is likely linked to pathways involving type-I interferon receptors.

Cytokines

Many cytokines have been investigated for their effect on the interaction between macrophages and *C. neoformans*. Various studies on Th1 cytokines, IFN-γ[94], IL-12[95], and TNF-α[96], demonstrated significantly increased fungal control in mouse models of *C. neoformans* infection. Additionally, Th17 cytokines IL-17[97] and IL-23[98] are linked to fungal protection in *C. neoformans*-infected mice. Conversely, Th2 cytokines IL-4[99] and IL-13[100] promote fungal disease progression in mice. However, none of these studies linked their observations to vomocytosis.

Therefore, Voelz et al. tested the different T helper cell cytokines for their effect on infected murine J774 cells and primary monocyte-derived human macrophages[49]. Macrophages were stimulated to Th1 (IFN-γ and TNF-α), Th2 (IL-4 and IL-13), or Th17 (IL-17) states. Interestingly, Th2 cytokines caused higher rates of intracellular *C. neoformans* proliferation and lower expulsion rates. Th1 and Th17 cytokines, on the other hand, reduced intracellular proliferation and caused comparably higher expulsion rates. Voelz et al. theorize that these distinct T helper cytokines modify the phagosome to result in different *C. neoformans* fates—intracellular proliferation (Th2) or expulsion (Th1 &

22

Th17). The Th2 cytokines IL-4 and IL-13 have been linked to increased iron availability in macrophages[101]; these metal ions could play a role in affecting the characteristics of *C. neoformans* in the phagosome.

The latter observation of vomocytosis rate in macrophages treated with Th2 cytokines for M2 polarization is in agreement with the aforementioned study by Gilbert et al., where higher vomocytosis rates were observed in ERK5-inhibited macrophages, along with reduction of their M2 polarization markers. ERK5 inhibition in macrophages lead to a modified inflammatory profile that prevented anti-inflammatory polarization without modifying their response to inflammatory stimuli. They also observed a decrease in the presence of actin filament ruffles on macrophages treated with ERK5 inhibitor. Concisely, Gilbert et al. suggested that vomocytosis enhancement by ERK5 inhibition was a result of reduced M2 macrophage polarization and decline in actin filament ruffle formation.
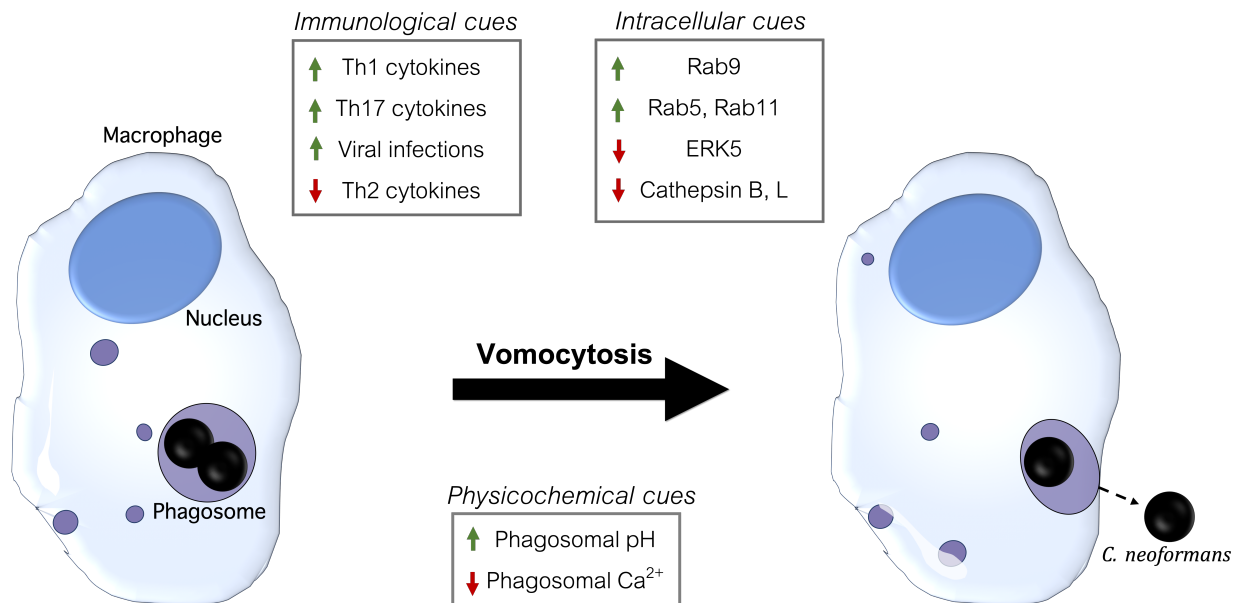
Figure 1.5. Vomocytosis occurrence is characterized by distinct intramolecular, physicochemical and extracellular factors. Rab GTPases recruitment to phagosomes, which affects phagosomal maturation and cathepsin activity is relevant for the occurrence of vomocytosis. Moreover, the manipulation of ERK5 signaling pathway, Annexin A2, phagosomal pH, and Ca^{2+} fluxes are capable of promoting vomocytosis occurrence. Finally, the immunological state of the individual and macrophage phenotype can affect vomocytosis. The arrows point out if the presence of each factor promotes or inhibits vomocytic events.

1.8 Conclusions and Future Perspectives

Vomocytosis is a fascinating mechanism that allows select pathogens to escape from phagocyte degradation while keeping the host cell alive. Specifically, the fungal pathogen *C. neoformans* has developed this mechanism that boosts its survival in the human body. As of today, researchers have identified distinct biological, immunological and physicochemical factors involved in this phagolysosomal escape event.

In terms of biological factors, the protein composition of the phagosome is highly altered prior to and during the expulsion of *C. neoformans* (**Figure 1.5**). Early phagosomes containing live *C. neoformans* show lack of Rab5 and Rab11 endosomal markers and significantly more Rab9 marker at late phagosomal stages than their counterparts containing heat-killed cells or latex beads. Also lack of cathepsins activity is observed in *C. neoformans* containing-phagosomes. These findings implicate the strong inhibition of phagosome maturation in macrophages that are actively vomocytosing cells. Other host proteins involved in vomocytosis include the MAP kinase ERK5 and the

membrane phospholipid binding protein annexin A2, but their exact role in this process is unknown. Outside of biological factors within the cells, the immune state of this host has shown a strong effect on vomocytosis. This is unsurprising since vomocytosis has been observed in macrophages and the phagosome is a crucial component of the innate immune system. Specifically, viral infections, Th1/2/17 cytokine exposure, and macrophage M1/M2 polarization all affect vomocytic rates. Lastly, vomocytosis has been linked to alterations in the physicochemical factors in the phagosome. For instance, Ca^{2+} levels in *C. neoformans*-containing phagosomes decline, relative to the cytosol, during vomocytosis. Also, the pH in the phagosome (due to urease activity and capsule acid-base properties) or in the external media influences the frequency of vomocytosis. These physicochemical factors may also contribute to rates of PMP which are linked to decreased vomocytosis rates and increased probability for lytic exocytosis.

While we have advanced our understanding of this phenomenon, revisiting its science using fresh technologies and an interdisciplinary approach could prove knowledge rich. For instance, the relationship between macrophage polarization and vomocytosis was explored 10 years ago[49]. However, current technological advances could allow us to understand, in more depth, the complexity of macrophage phenotypes and their role in disease prevention and progression. Newer, next generation sequencing technologies could provide new insights on the transcriptional and epigenetic profile of the infected host and fungal cells at different times after infection. This information could facilitate the identification of key signaling pathways in infection and vomocytosis (as well as lytic exocytosis). Moreover, the gene expression profile of pathogens during this phenomenon could inspire novel strategies to manipulate phagosomal escape for a

variety of purposes, including the design of drugs to combat the infection or mimic vomocytosis[102]. Some physico-chemical changes that occur during vomocytosis (intracellular Ca^{2+} concentration, direct phagosomal pH modulation, and PMP) have been characterized. However, there are still challenges in understanding their relationships to vomocytosis. Moreover, there are other key phagosomal physicochemical features that have yet to be investigated with respect to vomocytosis (e.g. Oxygen ions). New technology to accurately record and report this event could also be instrumental for new findings on vomocytosis. Most studies on vomocytosis use time-lapse microscopy as a quantitative and monitoring tool, which is quite labor intensive and inaccurate. Engineering new reporter systems to study vomocytosis will help to elucidate the interplay between biological, physical and chemical factors that influence this behavior. Similarly, accurate measurement of vomocytosis-influencing factors can draw links to the intracellular fate of phagocytosed *C. neoformans* in macrophages. This knowledge will potentially help in designing treatments that target this fungal pathogen. Excitingly, a comprehensive view of vomocytosis can also lead to the development of biomimetic drugs that evade the innate immune system for improved therapeutic outcomes in a plethora of diseases.

1.9 Acknowledgments

1.10 References

(1)   Iwasaki, A.; Medzhitov, R. Control of Adaptive Immunity by the Innate Immune System. *Nat Immunol* **2015**, *16* (4), 343–353. https://doi.org/10.1038/ni.3123.

(2)   Maderna, P.; Godson, C. Phagocytosis of Apoptotic Cells and the Resolution of Inflammation. *Biochim Biophys Acta* **2003**, *1639* (3), 141–151. https://doi.org/10.1016/j.bbadis.2003.09.004.

(3)   Gordon, S. Phagocytosis: An Immunobiologic Process. *Immunity* **2016**, *44* (3), 463–475. https://doi.org/10.1016/j.immuni.2016.02.026.

(4)   Henson, P. M. Cell Removal: Efferocytosis. *Annual Review of Cell and Developmental Biology* **2017**, *33* (1), 127–144. https://doi.org/10.1146/annurev-cellbio-111315-125315.

(5)   Mosser, D. M.; Edwards, J. P. Exploring the Full Spectrum of Macrophage Activation. *Nat Rev Immunol* **2008**, *8* (12), 958–969. https://doi.org/10.1038/nri2448.

(6)   Erwig, L. P.; Gow, N. A. R. Interactions of Fungal Pathogens with Phagocytes. *Nat Rev Microbiol* **2016**, *14* (3), 163–176. https://doi.org/10.1038/nrmicro.2015.21.

(7)   Doshi, N.; Mitragotri, S. Macrophages Recognize Size and Shape of Their Targets. *PLoS One* **2010**, *5* (4), e10051. https://doi.org/10.1371/journal.pone.0010051.

(8)   Walkey, C. D.; Olsen, J. B.; Guo, H.; Emili, A.; Chan, W. C. W. Nanoparticle Size and Surface Chemistry Determine Serum Protein Adsorption and Macrophage

Uptake. *J. Am. Chem. Soc.* **2012**, *134* (4), 2139–2147.
https://doi.org/10.1021/ja2084338.

(9)   Nel, A. E.; Mädler, L.; Velegol, D.; Xia, T.; Hoek, E. M. V.; Somasundaran, P.;
Klaessig, F.; Castranova, V.; Thompson, M. Understanding Biophysicochemical
Interactions at the Nano–Bio Interface. *Nature Mater* **2009**, *8* (7), 543–557.
https://doi.org/10.1038/nmat2442.

(10)   Gustafson, H. H.; Holt-Casper, D.; Grainger, D. W.; Ghandehari, H. Nanoparticle
Uptake: The Phagocyte Problem. *Nano Today* **2015**, *10* (4), 487–510.
https://doi.org/10.1016/j.nantod.2015.06.006.

(11)   Lim, J. J.; Grinstein, S.; Roth, Z. Diversity and Versatility of Phagocytosis: Roles
in Innate Immunity, Tissue Remodeling, and Homeostasis. *Frontiers in Cellular
and Infection Microbiology* **2017**, *7*.

(12)   May, R. C.; Stone, N. R. H.; Wiesner, D. L.; Bicanic, T.; Nielsen, K.
Cryptococcus: From Environmental Saprophyte to Global Pathogen. *Nat Rev
Microbiol* **2016**, *14* (2), 106–117. https://doi.org/10.1038/nrmicro.2015.6.

(13)   Rajasingham, R.; Smith, R. M.; Park, B. J.; Jarvis, J. N.; Govender, N. P.; Chiller,
T. M.; Denning, D. W.; Loyse, A.; Boulware, D. R. Global Burden of Disease of
HIV-Associated Cryptococcal Meningitis: An Updated Analysis. *The Lancet
Infectious Diseases* **2017**, *17* (8), 873–881. https://doi.org/10.1016/S1473-
3099(17)30243-8.

(14)   Levitz, S. M. Does Amoeboid Reasoning Explain the Evolution and Maintenance
of Virulence Factors in Cryptococcus Neoformans? *Proceedings of the National*

Academy of Sciences **2001**, *98* (26), 14760–14762.
https://doi.org/10.1073/pnas.261612398.

(15)   Watkins, R. A.; Andrews, A.; Wynn, C.; Barisch, C.; King, J. S.; Johnston, S. A.
Cryptococcus Neoformans Escape From Dictyostelium Amoeba by Both WASH-
Mediated Constitutive Exocytosis and Vomocytosis. *Front Cell Infect Microbiol*
2018, *8*, 108. https://doi.org/10.3389/fcimb.2018.00108.

(16)   Santiago-Tirado, F. H.; Onken, M. D.; Cooper, J. A.; Klein, R. S.; Doering, T. L.
Trojan Horse Transit Contributes to Blood-Brain Barrier Crossing of a Eukaryotic
Pathogen. *mBio* **2017**. https://doi.org/10.1128/mBio.02183-16.

(17)   Casem, M. L. *Case Studies in Cell Biology*; Academic Press, 2016.

(18)   Murray, R. Z.; Stow, J. L. Cytokine Secretion in Macrophages: SNAREs, Rabs,
and Membrane Trafficking. *Frontiers in Immunology* **2014**, *5*.

(19)   Haka, A. S.; Barbosa-Lorenzi, V. C.; Lee, H. J.; Falcone, D. J.; Hudis, C. A.;
Dannenberg, A. J.; Maxfield, F. R. Exocytosis of Macrophage Lysosomes Leads
to Digestion of Apoptotic Adipocytes and Foam Cell Formation [S]. *Journal of
Lipid Research* **2016**, *57* (6), 980–992. https://doi.org/10.1194/jlr.M064089.

(20)   Hibbs, J. B. Heterocytolysis by Macrophages Activated by Bacillus Calmette-
Gurin: Lysosome Exocytosis into Tumor Cells. *Science* **1974**, *184* (4135), 468–
471. https://doi.org/10.1126/science.184.4135.468.

(21)   Singh, R. K.; Barbosa-Lorenzi, V. C.; Lund, F. W.; Grosheva, I.; Maxfield, F. R.;
Haka, A. S. Degradation of Aggregated LDL Occurs in Complex Extracellular
Sub-Compartments of the Lysosomal Synapse. *Journal of Cell Science* **2016**,
129 (5), 1072–1082. https://doi.org/10.1242/jcs.181743.

(22) Di, A.; Nelson, D. J.; Bindokas, V.; Brown, M. E.; Libunao, F.; Palfrey, H. C. Dynamin Regulates Focal Exocytosis in Phagocytosing Macrophages. *MBoC* **2003**, *14* (5), 2016–2028. https://doi.org/10.1091/mbc.e02-09-0626.

(23) Han, C.; Chen, T.; Yang, M.; Li, N.; Liu, H.; Cao, X. Human SCAMP5, a Novel Secretory Carrier Membrane Protein, Facilitates Calcium-Triggered Cytokine Secretion by Interaction with SNARE Machinery. *The Journal of Immunology* **2009**, *182* (5), 2986–2996. https://doi.org/10.4049/jimmunol.0802002.

(24) Bielska, E.; May, R. C. What Makes Cryptococcus Gattii a Pathogen? *FEMS Yeast Research* **2016**, *16* (1), fov106. https://doi.org/10.1093/femsyr/fov106.

(25) Bain, J. M.; Lewis, L. E.; Okai, B.; Quinn, J.; Gow, N. A. R.; Erwig, L.-P. Non-Lytic Expulsion/Exocytosis of Candida Albicans from Macrophages. *Fungal Genetics and Biology* **2012**, *49* (9), 677–678. https://doi.org/10.1016/j.fgb.2012.01.008.

(26) Alvarez, M.; Casadevall, A. Phagosome Extrusion and Host-Cell Survival after Cryptococcus Neoformans Phagocytosis by Macrophages. *Current Biology* **2006**, *16* (21), 2161–2165. https://doi.org/10.1016/j.cub.2006.09.061.

(27) Evans, R. J.; Li, Z.; Hughes, W. S.; Djordjevic, J. T.; Nielsen, K.; May, R. C. Cryptococcal Phospholipase B1 Is Required for Intracellular Proliferation and Control of Titan Cell Morphology during Macrophage Infection. *Infection and Immunity* **2015**, *83* (4), 1296–1304. https://doi.org/10.1128/IAI.03104-14.

(28) Erb-Downward, J. R.; Noggle, R. M.; Williamson, P. R.; Huffnagle, G. B. The Role of Laccase in Prostaglandin Production by Cryptococcus Neoformans.

Molecular Microbiology **2008**, *68* (6), 1428–1437. https://doi.org/10.1111/j.1365-2958.2008.06245.x.

(29)   Qiu, Y.; Davis, M. J.; Dayrit, J. K.; Hadd, Z.; Meister, D. L.; Osterholzer, J. J.; Williamson, P. R.; Olszewski, M. A. Immune Modulation Mediated by Cryptococcal Laccase Promotes Pulmonary Growth and Brain Dissemination of Virulent Cryptococcus Neoformans in Mice. *PLOS ONE* **2012**, *7* (10), e47853. https://doi.org/10.1371/journal.pone.0047853.

(30)   O'Meara, T. R.; Alspaugh, J. A. The Cryptococcus Neoformans Capsule: A Sword and a Shield. *Clinical Microbiology Reviews* **2012**, *25* (3), 387–408. https://doi.org/10.1128/CMR.00001-12.

(31)   Okagaki, L. H.; Strain, A. K.; Nielsen, J. N.; Charlier, C.; Baltes, N. J.; Chrétien, F.; Heitman, J.; Dromer, F.; Nielsen, K. Cryptococcal Cell Morphology Affects Host Cell Interactions and Pathogenicity. *PLOS Pathogens* **2010**, *6* (6), e1000953. https://doi.org/10.1371/journal.ppat.1000953.

(32)   Artavanis-Tsakonas, K.; Love, J. C.; Ploegh, H. L.; Vyas, J. M. Recruitment of CD63 to Cryptococcus Neoformans Phagosomes Requires Acidification. *Proceedings of the National Academy of Sciences* **2006**, *103* (43), 15945–15950.

(33)   Levitz, S. M.; Nong, S.-H.; Seetoo, K. F.; Harrison, T. S.; Speizer, R. A.; Simons, E. R. Cryptococcus Neoformans Resides in an Acidic Phagolysosome of Human Macrophages. *Infection and Immunity* **1999**, *67* (2), 885–890. https://doi.org/10.1128/IAI.67.2.885-890.1999.

(34)   Smith, L. M.; Dixon, E. F.; May, R. C. The Fungal Pathogen Cryptococcus Neoformans Manipulates Macrophage Phagosome Maturation. *Cellular Microbiology* **2015**, *17* (5), 702–713. https://doi.org/10.1111/cmi.12394.

(35)   Leon-Rodriguez, C. M. D.; Fu, M. S.; Çorbali, M. O.; Cordero, R. J. B.; Casadevall, A. The Capsule of Cryptococcus Neoformans Modulates Phagosomal PH through Its Acid-Base Properties. *mSphere* **2018**. https://doi.org/10.1128/mSphere.00437-18.

(36)   Leon-Rodriguez, C. M. D.; Rossi, D. C. P.; Fu, M. S.; Dragotakes, Q.; Coelho, C.; Ros, I. G.; Caballero, B.; Nolan, S. J.; Casadevall, A. The Outcome of the Cryptococcus Neoformans–Macrophage Interaction Depends on Phagolysosomal Membrane Integrity. *The Journal of Immunology* **2018**, *201* (2), 583–603. https://doi.org/10.4049/jimmunol.1700958.

(37)   Burch, K. H.; Fine, G.; Quinn, E. L.; Eisses, J. F. Cryptococcus Neoformans as a Cause of Lytic Bone Lesions. *JAMA* **1975**, *231* (10), 1057–1059. https://doi.org/10.1001/jama.1975.03240220037017.

(38)   Hommel, B.; Mukaremera, L.; Cordero, R. J. B.; Coelho, C.; Desjardins, C. A.; Sturny-Leclère, A.; Janbon, G.; Perfect, J. R.; Fraser, J. A.; Casadevall, A.; Cuomo, C. A.; Dromer, F.; Nielsen, K.; Alanio, A. Titan Cells Formation in Cryptococcus Neoformans Is Finely Tuned by Environmental Conditions and Modulated by Positive and Negative Genetic Regulators. *PLOS Pathogens* **2018**, *14* (5), e1006982. https://doi.org/10.1371/journal.ppat.1006982.

(39)   Zaragoza, O.; García-Rodas, R.; Nosanchuk, J. D.; Cuenca-Estrella, M.; Rodríguez-Tudela, J. L.; Casadevall, A. Fungal Cell Gigantism during

Mammalian Infection. *PLOS Pathogens* **2010**, *6* (6), e1000945.

https://doi.org/10.1371/journal.ppat.1000945.

(40) Ben-Abdallah, M.; Sturny-Leclère, A.; Avé, P.; Louise, A.; Moyrand, F.; Weih, F.;

Janbon, G.; Mémet, S. Fungal-Induced Cell Cycle Impairment, Chromosome

Instability and Apoptosis via Differential Activation of NF-KB. *PLOS Pathogens*

2012, *8* (3), e1002555. https://doi.org/10.1371/journal.ppat.1002555.

(41) Ma, H.; Croudace, J. E.; Lammas, D. A.; May, R. C. Expulsion of Live

Pathogenic Yeast by Macrophages. *Current Biology* **2006**, *16* (21), 2156–2160.

https://doi.org/10.1016/j.cub.2006.09.032.

(42) Hybiske, K.; Stephens, R. S. Mechanisms of Host Cell Exit by the Intracellular

Bacterium Chlamydia. *Proceedings of the National Academy of Sciences* **2007**,

104 (27), 11430–11435. https://doi.org/10.1073/pnas.0703218104.

(43) Chu, H.; Lee, J.-H.; Han, S.-H.; Kim, S.-Y.; Cho, N.-H.; Kim, I.-S.; Choi, M.-S.

Exploitation of the Endocytic Pathway by Orientia Tsutsugamushi in

Nonprofessional Phagocytes. *Infection and Immunity* **2006**, *74* (7), 4246–4253.

https://doi.org/10.1128/IAI.01620-05.

(44) Leopold Wager, C. M.; Hole, C. R.; Wozniak, K. L.; Wormley, F. L. Cryptococcus

and Phagocytes: Complex Interactions That Influence Disease Outcome.

Frontiers in Microbiology **2016**, *7*.

(45) Wozniak, K. L.; Olszewski, M. A.; Wormley, F. L. Molecules at the Interface of

Cryptococcus and the Host That Determine Disease Susceptibility. *Fungal*

Genetics and Biology **2015**, *78*, 87–92. https://doi.org/10.1016/j.fgb.2014.10.013.

(46)   Johnston, S. A.; May, R. C. The Human Fungal Pathogen Cryptococcus
        Neoformans Escapes Macrophages by a Phagosome Emptying Mechanism That
        Is Inhibited by Arp2/3 Complex-Mediated Actin Polymerisation. *PLOS Pathogens*
        2010, *6* (8), e1001041. https://doi.org/10.1371/journal.ppat.1001041.

(47)   Alvarez, M.; Saylor, C.; Casadevall, A. Antibody Action after Phagocytosis
        Promotes Cryptococcus Neoformans and Cryptococcus Gattii Macrophage
        Exocytosis with Biofilm-like Microcolony Formation. *Cellular Microbiology* **2008**,
        10 (8), 1622–1633. https://doi.org/10.1111/j.1462-5822.2008.01152.x.

(48)   Dragotakes, Q.; Fu, M. S.; Casadevall, A. Dragotcytosis: Elucidation of the
        Mechanism for Cryptococcus Neoformans Macrophage-to-Macrophage Transfer.
        The Journal of Immunology **2019**. https://doi.org/10.4049/jimmunol.1801118.

(49)   Voelz, K.; Lammas, D. A.; May, R. C. Cytokine Signaling Regulates the Outcome
        of Intracellular Macrophage Parasitism by Cryptococcus Neoformans. *Infection
        and Immunity* **2009**. https://doi.org/10.1128/IAI.00297-09.

(50)   Diamond, R. D.; Bennett, J. E. Growth of Cryptococcus Neoformans Within
        Human Macrophages In Vitro. *Infection and Immunity* **1973**, *7* (2), 231–236.
        https://doi.org/10.1128/iai.7.2.231-236.1973.

(51)   Davis, M. J.; Eastman, A. J.; Qiu, Y.; Gregorka, B.; Kozel, T. R.; Osterholzer, J.
        J.; Curtis, J. L.; Swanson, J. A.; Olszewski, M. A. Cryptococcus Neoformans–
        Induced Macrophage Lysosome Damage Crucially Contributes to Fungal
        Virulence. *The Journal of Immunology* **2015**, *194* (5), 2219–2231.
        https://doi.org/10.4049/jimmunol.1402376.

(52) Liu, T.-B.; Perlin, D. S.; Xue, C. Molecular Mechanisms of Cryptococcal

Meningitis. *Virulence* **2012**, *3* (2), 173–181. https://doi.org/10.4161/viru.18685.

(53) Charlier, C.; Chrétien, F.; Baudrimont, M.; Mordelet, E.; Lortholary, O.; Dromer,

F. Capsule Structure Changes Associated with Cryptococcus Neoformans

Crossing of the Blood-Brain Barrier. *The American Journal of Pathology* **2005**,

166 (2), 421–432. https://doi.org/10.1016/S0002-9440(10)62265-1.

(54) Chang, Y.-C.; Wang, Z.; Flax, L. A.; Xu, D.; Esko, J. D.; Nizet, V.; Baron, M. J.

Glycosaminoglycan Binding Facilitates Entry of a Bacterial Pathogen into Central

Nervous Systems. *PLOS Pathogens* **2011**, *7* (6), e1002082.

https://doi.org/10.1371/journal.ppat.1002082.

(55) Vu, K.; Eigenheer, R. A.; Phinney, B. S.; Gelli, A. Cryptococcus Neoformans

Promotes Its Transmigration into the Central Nervous System by Inducing

Molecular and Cellular Changes in Brain Endothelial Cells. *Infection and

Immunity* **2013**, *81* (9), 3139–3147. https://doi.org/10.1128/IAI.00554-13.

(56) Vu, K.; Weksler, B.; Romero, I.; Couraud, P.-O.; Gelli, A. Immortalized Human

Brain Endothelial Cell Line HCMEC/D3 as a Model of the Blood-Brain Barrier

Facilitates In Vitro Studies of Central Nervous System Infection by Cryptococcus

Neoformans. *Eukaryotic Cell* **2009**, *8* (11), 1803–1807.

https://doi.org/10.1128/EC.00240-09.

(57) Chen, S. H. M.; Stins, M. F.; Huang, S.-H.; Chen, Y. H.; Kwon-Chung, K. J.;

Chang, Y.; Kim, K. S.; Suzuki, K.; Jong, A. Y. Y. 2003. Cryptococcus

Neoformans Induces Alterations in the Cytoskeleton of Human Brain

Microvascular Endothelial Cells. *Journal of Medical Microbiology 52* (11), 961–970. https://doi.org/10.1099/jmm.0.05230-0.

(58)   Aaron, P. A.; Jamklang, M.; Uhrig, J. P.; Gelli, A. The Blood–Brain Barrier Internalises Cryptococcus Neoformans via the EphA2-Tyrosine Kinase Receptor. *Cellular Microbiology* **2018**, *20* (3), e12811. https://doi.org/10.1111/cmi.12811.

(59)   Guerra, C. R.; Seabra, S. H.; Souza, W. de; Rozental, S. Cryptococcus Neoformans Is Internalized by Receptor-Mediated or 'Triggered' Phagocytosis, Dependent on Actin Recruitment. *PLOS ONE* **2014**, *9* (2), e89250. https://doi.org/10.1371/journal.pone.0089250.

(60)   Kjos, I.; Vestre, K.; Guadagno, N. A.; Borg Distefano, M.; Progida, C. Rab and Arf Proteins at the Crossroad between Membrane Transport and Cytoskeleton Dynamics. *Biochimica et Biophysica Acta (BBA) - Molecular Cell Research* **2018**, *1865* (10), 1397–1409. https://doi.org/10.1016/j.bbamcr.2018.07.009.

(61)   Pauwels, A.-M.; Trost, M.; Beyaert, R.; Hoffmann, E. Patterns, Receptors, and Signals: Regulation of Phagosome Maturation. *Trends in Immunology* **2017**, *38* (6), 407–422. https://doi.org/10.1016/j.it.2017.03.006.

(62)   Drew, B. A.; Burow, M. E.; Beckman, B. S. MEK5/ERK5 Pathway: The First Fifteen Years. *Biochimica et Biophysica Acta (BBA) - Reviews on Cancer* **2012**, *1825* (1), 37–48. https://doi.org/10.1016/j.bbcan.2011.10.002.

(63)   Wang, X.; Pesakhov, S.; Harrison, J. S.; Kafka, M.; Danilenko, M.; Studzinski, G. P. The MAPK ERK5, but Not ERK1/2, Inhibits the Progression of Monocytic Phenotype to the Functioning Macrophage. *Experimental Cell Research* **2015**, *330* (1), 199–211. https://doi.org/10.1016/j.yexcr.2014.10.003.

(64) Gilbert, A. S.; Seoane, P. I.; Sephton-Clark, P.; Bojarczuk, A.; Hotham, R.; Giurisato, E.; Sarhan, A. R.; Hillen, A.; Velde, G. V.; Gray, N. S.; Alessi, D. R.; Cunningham, D. L.; Tournier, C.; Johnston, S. A.; May, R. C. Vomocytosis of Live Pathogens from Macrophages Is Regulated by the Atypical MAP Kinase ERK5. *Science Advances 3* (8), e1700898. https://doi.org/10.1126/sciadv.1700898.

(65) Heo, K.-S.; Cushman, H. J.; Akaike, M.; Woo, C.-H.; Wang, X.; Qiu, X.; Fujiwara, K.; Abe, J. ERK5 Activation in Macrophages Promotes Efferocytosis and Inhibits Atherosclerosis. *Circulation* **2014**, *130* (2), 180–191. https://doi.org/10.1161/CIRCULATIONAHA.113.005991.

(66) Franchi, L.; Muñoz-Planillo, R.; Núñez, G. Sensing and Reacting to Microbes through the Inflammasomes. *Nat Immunol* **2012**, *13* (4), 325–332. https://doi.org/10.1038/ni.2231.

(67) Lei, G.; Chen, M.; Li, H.; Niu, J.-L.; Wu, S.; Mao, L.; Lu, A.; Wang, H.; Chen, W.; Xu, B.; Leng, Q.; Xu, C.; Yang, G.; An, L.; Zhu, L.-P.; Meng, G. Biofilm from a Clinical Strain of Cryptococcus Neoformans Activates the NLRP3 Inflammasome. *Cell Res* **2013**, *23* (7), 965–968. https://doi.org/10.1038/cr.2013.49.

(68) Stukes, S.; Coelho, C.; Rivera, J.; Jedlicka, A. E.; Hajjar, K. A.; Casadevall, A. The Membrane Phospholipid Binding Protein Annexin A2 Promotes Phagocytosis and Nonlytic Exocytosis of Cryptococcus Neoformans and Impacts Survival in Fungal Infection. *The Journal of Immunology* **2016**, *197* (4), 1252–1261. https://doi.org/10.4049/jimmunol.1501855.

(69) Bryan, R. A.; Zaragoza, O.; Zhang, T.; Ortiz, G.; Casadevall, A.; Dadachova, E. Radiological Studies Reveal Radial Differences in the Architecture of the Polysaccharide Capsule of Cryptococcus Neoformans. *Eukaryotic Cell* **2005**, *4* (2), 465–475. https://doi.org/10.1128/EC.4.2.465-475.2005.

(70) Wang, P.; Chintagari, N. R.; Gou, D.; Su, L.; Liu, L. Physical and Functional Interactions of SNAP-23 with Annexin A2. *Am J Respir Cell Mol Biol* **2007**, *37* (4), 467–476. https://doi.org/10.1165/rcmb.2006-0447OC.

(71) Yates, R. M.; Hermetter, A.; Russell, D. G. The Kinetics of Phagosome Maturation as a Function of Phagosome/Lysosome Fusion and Acquisition of Hydrolytic Activity. *Traffic* **2005**, *6* (5), 413–420. https://doi.org/10.1111/j.1600-0854.2005.00284.x.

(72) Russell, D. G.; VanderVen, B. C.; Glennie, S.; Mwandumba, H.; Heyderman, R. S. The Macrophage Marches on Its Phagosome: Dynamic Assays of Phagosome Function. *Nat Rev Immunol* **2009**, *9* (8), 594–600. https://doi.org/10.1038/nri2591.

(73) Nicola, A. M.; Robertson, E. J.; Albuquerque, P.; Derengowski, L. da S.; Casadevall, A. Nonlytic Exocytosis of Cryptococcus Neoformans from Macrophages Occurs In Vivo and Is Influenced by Phagosomal PH. *mBio* **2011**. https://doi.org/10.1128/mBio.00167-11.

(74) Fu, M. S.; Coelho, C.; Leon-Rodriguez, C. M. D.; Rossi, D. C. P.; Camacho, E.; Jung, E. H.; Kulkarni, M.; Casadevall, A. Cryptococcus Neoformans Urease Affects the Outcome of Intracellular Pathogenesis by Modulating

Phagolysosomal PH. *PLOS Pathogens* **2018**, *14* (6), e1007144.

https://doi.org/10.1371/journal.ppat.1007144.

(75)   Denham, S. T.; Brown, J. C. S. Mechanisms of Pulmonary Escape and

Dissemination by Cryptococcus Neoformans. *Journal of Fungi* **2018**, *4* (1), 25.

https://doi.org/10.3390/jof4010025.

(76)   Cox, G. M.; Mukherjee, J.; Cole, G. T.; Casadevall, A.; Perfect, J. R. Urease as a

Virulence Factor in Experimental Cryptococcosis. *Infection and Immunity* **2000**,

68 (2), 443–448. https://doi.org/10.1128/IAI.68.2.443-448.2000.

(77)   Yoshida, S.; Ohkusu, M.; Hata, K.; Yarita, K.; Fujii, T.; Takeo, K. Early Death at

Medium Acidification and Survival after Low PH Adaptation in Cryptococcus

Neoformans. *Mycoscience* **2001**, *42* (6), 535–541.

https://doi.org/10.1007/BF02460951.

(78)   Feldmesser, M.; Kress, Y.; Novikoff, P.; Casadevall, A. Cryptococcus

Neoformans Is a Facultative Intracellular Pathogen in Murine Pulmonary

Infection. *Infection and Immunity* **2000**, *68* (7), 4225–4237.

https://doi.org/10.1128/IAI.68.7.4225-4237.2000.

(79)   Tucker, S. C.; Casadevall, A. Replication of Cryptococcus Neoformans in

Macrophages Is Accompanied by Phagosomal Permeabilization and

Accumulation of Vesicles Containing Polysaccharide in the Cytoplasm.

Proceedings of the National Academy of Sciences **2002**, *99* (5), 3165–3170.

https://doi.org/10.1073/pnas.052702799.

(80)   Boya, P.; Andreau, K.; Poncet, D.; Zamzami, N.; Perfettini, J.-L.; Metivier, D.;

Ojcius, D. M.; Jäättelä, M.; Kroemer, G. Lysosomal Membrane Permeabilization

Induces Cell Death in a Mitochondrion-Dependent Fashion. *Journal of Experimental Medicine* **2003**, *197* (10), 1323–1334. https://doi.org/10.1084/jem.20021952.

(81)   Circu, M.; Cardelli, J.; Barr, M.; O'Byrne, K.; Mills, G.; El-Osta, H. Modulating Lysosomal Function through Lysosome Membrane Permeabilization or Autophagy Suppression Restores Sensitivity to Cisplatin in Refractory Non-Small-Cell Lung Cancer Cells. *PLOS ONE* **2017**, *12* (9), e0184922. https://doi.org/10.1371/journal.pone.0184922.

(82)   Stukes, S. A.; Cohen, H. W.; Casadevall, A. Temporal Kinetics and Quantitative Analysis of Cryptococcus Neoformans Nonlytic Exocytosis. *Infection and Immunity* **2014**, *82* (5), 2059–2067. https://doi.org/10.1128/IAI.01503-14.

(83)   Kusner, D. J.; Barton, J. A. ATP Stimulates Human Macrophages to Kill Intracellular Virulent Mycobacterium Tuberculosis Via Calcium-Dependent Phagosome-Lysosome Fusion. *The Journal of Immunology* **2001**, *167* (6), 3308–3315. https://doi.org/10.4049/jimmunol.167.6.3308.

(84)   Nunes, P.; Demaurex, N. The Role of Calcium Signaling in Phagocytosis. *Journal of Leukocyte Biology* **2010**, *88* (1), 57–68. https://doi.org/10.1189/jlb.0110028.

(85)   Kruskal, B. A.; Maxfield, F. R. Cytosolic Free Calcium Increases before and Oscillates during Frustrated Phagocytosis in Macrophages. *Journal of Cell Biology* **1987**, *105* (6), 2685–2693. https://doi.org/10.1083/jcb.105.6.2685.

(86) Myers, J. T.; Swanson, J. A. Calcium Spikes in Activated Macrophages during Fcγ Receptor-Mediated Phagocytosis. *Journal of Leukocyte Biology* **2002**, *72* (4), 677–684. https://doi.org/10.1189/jlb.72.4.677.

(87) Lévêque, M.; Penna, A.; Le Trionnaire, S.; Belleguic, C.; Desrues, B.; Brinchault, G.; Jouneau, S.; Lagadic-Gossmann, D.; Martin-Chouly, C. Phagocytosis Depends on TRPV2-Mediated Calcium Influx and Requires TRPV2 in Lipids Rafts: Alteration in Macrophages from Patients with Cystic Fibrosis. *Sci Rep* **2018**, *8* (1), 4310. https://doi.org/10.1038/s41598-018-22558-5.

(88) Vashi, N.; Andrabi, S. B. A.; Ghanwat, S.; Suar, M.; Kumar, D. Ca2+-Dependent Focal Exocytosis of Golgi-Derived Vesicles Helps Phagocytic Uptake in Macrophages *. *Journal of Biological Chemistry* **2017**, *292* (13), 5144–5165. https://doi.org/10.1074/jbc.M116.743047.

(89) Swisher, J. F. A.; Burton, N.; Bacot, S. M.; Vogel, S. N.; Feldman, G. M. Annexin A2 Tetramer Activates Human and Murine Macrophages through TLR4. *Blood* **2010**, *115* (3), 549–558. https://doi.org/10.1182/blood-2009-06-226944.

(90) Samantaray, S.; Correia, J. N.; Garelnabi, M.; Voelz, K.; May, R. C.; Hall, R. A. Novel Cell-Based in Vitro Screen to Identify Small-Molecule Inhibitors against Intracellular Replication of Cryptococcus Neoformans in Macrophages. *International Journal of Antimicrobial Agents* **2016**, *48* (1), 69–77. https://doi.org/10.1016/j.ijantimicag.2016.04.018.

(91) Huang, C.; Huang, C.; Cheng, J.; Liu, S.; Chen, I.; Tsai, J.; Chou, C.; Tseng, P.; Jan, C. Fendiline-Evoked [Ca2+]i Rises and Non-Ca2+-Triggered Cell Death in

Human Oral Cancer Cells. *Hum Exp Toxicol* **2009**, *28* (1), 41–48.

https://doi.org/10.1177/0960327108097436.

(92)   Cheng, J.-S.; Wang, J.-L.; Lo, Y.-K.; Chou, K.-J.; Lee, K.-C.; Liu, C.-P.; Chang,

H.-T.; Jan, C.-R. Effects of the Antianginal Drug Fendiline on Ca2+ Movement in

Hepatoma Cells. *Hum Exp Toxicol* **2001**, *20* (7), 359–364.

https://doi.org/10.1191/096032701680350523.

(93)   Seoane, P. I.; Taylor-Smith, L. M.; Stirling, D.; Bell, L. C. K.; Noursadeghi, M.;

Bailey, D.; May, R. C. Viral Infection Triggers Interferon-Induced Expulsion of

Live Cryptococcus Neoformans by Macrophages. *PLoS Pathog* **2020**, *16* (2),

e1008240. https://doi.org/10.1371/journal.ppat.1008240.

(94)   Wormley, F. L.; Perfect, J. R.; Steele, C.; Cox, G. M. Protection against

Cryptococcosis by Using a Murine Gamma Interferon-Producing Cryptococcus

Neoformans Strain. *Infection and Immunity* **2007**, *75* (3), 1453–1462.

https://doi.org/10.1128/IAI.00274-06.

(95)   Hoag, K. A.; Lipscomb, M. F.; Izzo, A. A.; Street, N. E. IL-12 and IFN- γ Are

Required for Initiating the Protective Th1 Response to Pulmonary

Cryptococcosis in Resistant C.B-17 Mice. *Am J Respir Cell Mol Biol* **1997**, *17* (6),

733–739. https://doi.org/10.1165/ajrcmb.17.6.2879.

(96)   Milam, J. E.; Herring-Palmer, A. C.; Pandrangi, R.; McDonald, R. A.; Huffnagle,

G. B.; Toews, G. B. Modulation of the Pulmonary Type 2 T-Cell Response to

Cryptococcus Neoformans by Intratracheal Delivery of a Tumor Necrosis Factor

Alpha-Expressing Adenoviral Vector. *Infection and Immunity* **2007**, *75* (10),

4951–4958. https://doi.org/10.1128/IAI.00176-07.

(97)   Murdock, B. J.; Huffnagle, G. B.; Olszewski, M. A.; Osterholzer, J. J. Interleukin-

17A Enhances Host Defense against Cryptococcal Lung Infection through

Effects Mediated by Leukocyte Recruitment, Activation, and Gamma Interferon

Production. *Infection and Immunity* **2014**, *82* (3), 937–948.

https://doi.org/10.1128/IAI.01477-13.

(98)   Kleinschek, M. A.; Muller, U.; Brodie, S. J.; Stenzel, W.; Kohler, G.;

Blumenschein, W. M.; Straubinger, R. K.; McClanahan, T.; Kastelein, R. A.;

Alber, G. IL-23 Enhances the Inflammatory Cell Response in Cryptococcus

Neoformans Infection and Induces a Cytokine Pattern Distinct from IL-12. *The

Journal of Immunology* **2006**, *176* (2), 1098–1106.

https://doi.org/10.4049/jimmunol.176.2.1098.

(99)   Blackstock, R.; Murphy, J. W. Role of Interleukin-4 in Resistance to

Cryptococcus Neoformans Infection. *Am J Respir Cell Mol Biol* **2004**, *30* (1),

109–117. https://doi.org/10.1165/rcmb.2003-0156OC.

(100)   Müller, U.; Stenzel, W.; Köhler, G.; Werner, C.; Polte, T.; Hansen, G.; Schütze,

N.; Straubinger, R. K.; Blessing, M.; McKenzie, A. N. J.; Brombacher, F.; Alber,

G. IL-13 Induces Disease-Promoting Type 2 Cytokines, Alternatively Activated

Macrophages and Allergic Inflammation during Pulmonary Infection of Mice with

Cryptococcus Neoformans. *The Journal of Immunology* **2007**, *179* (8), 5367–

5377. https://doi.org/10.4049/jimmunol.179.8.5367.

(101)   Weiss, G.; Bogdan, C.; Hentze, M. W. Pathways for the Regulation of

Macrophage Iron Metabolism by the Anti-Inflammatory Cytokines IL-4 and IL-13.

The Journal of Immunology **1997**, *158* (1), 420–425.

(102) Lewis, J. S.; Keselowsky, B. G. *Immunomimetic Materials*; Wiley Hoboken, NJ, 2014.

CHAPTER 2: VOMOCYTOSIS OF *CRYPTOCOCCUS NEOFORMANS* CELLS FROM MURINE, BONE MARROW-DERIVED DENDRITIC CELLS

2.1 Abstract

Cryptococcus neoformans (CN) cells survive within the acidic phagolysosome of macrophages for extended times, then escape without impacting the viability of the host cell via a phenomenon that has been coined 'vomocytosis'. Through this mechanism, CN disseminate throughout the body, sometimes resulting in a potentially fatal condition - Cryptococcal Meningitis (CM). Justifiably, vomocytosis studies have focused primarily on macrophages, as alveolar macrophages within the lung act as first responders that ultimately expel this fungal pathogen. Herein, we hypothesize that dendritic cells (DCs), an innate immune cell with attributes that include phagocytosis and antigen presentation, can also act as 'vomocytes'. Presciently, this report shows that vomocytosis of CN indeed occurs from DCs. Primarily through time-lapse microscopy imaging, we show that rates of vomocytosis events from DCs are comparable to those seen from macrophages and further, are independent of the presence of the CN capsule and infection ratios. Moreover, phagosome-altering drugs such as chloroquine and bafilomycin A, as well as the actin-modifying drug, cytochalasin B inhibit this phenomenon from DCs. Although DC immunophenotype does not affect the total number of vomocytic events, we observed differences in the numbers of CN per phagosome and expulsion times. Interestingly, these observations were similar in primary, murine macrophages. Understanding the vomocytic behavior of different phagocytes and their phenotypic subtypes is needed to help elucidate the full picture of the dynamic interplay between CN and the immune system. Critically, deeper insight

into vomocytosis could reveal novel approaches to treat CM, as well as other immune-related conditions.

2.2 Introduction

Pathogens have evolved over time to develop means for persistence, dissemination, and infection within their mammalian hosts. The fungal species *Cryptococcus neoformans* (CN) is an opportunistic pathogen that causes an infectious disease called 'Cryptococcosis' that predominantly affects immunocompromised patients—primarily those afflicted with HIV/AIDS[1–3]. This infection can deteriorate into a condition called Cryptococcal Meningitis (CM), where CN establishes an infection in the central nervous system (CNS). Globally, there are estimated to be 223,100 CM cases and 181,000 deaths annually[1].

Cryptococcus neoformans spores typically enter the host through the lung via inhalation. Subsequently, the fungal pathogen disseminates from the lung into other tissues, including the CNS[2,4]. The three proposed mechanisms that facilitate CN entry into the CNS are paracytosis, transcytosis, and hitchhiking. In the latter, CN are suggested to cross the blood brain barrier (BBB) by 'hitchhiking' within host phagocytes[5,6]. This is known as the 'Trojan Horse' hypothesis. *Kechichian et al*. showed that depletion of alveolar macrophages in mice significantly reduces cryptococcal dissemination to the CNS[7]. Later, *Charlier et al*. showed that infecting naïve hosts with CN-infected monocytes significantly increases CN accumulation in the brain, compared to infecting with CNs directly[8].

Further, Cryptococcal cells have been shown to escape from macrophages (MΦs) by inducing expulsion whilst leaving the phagocyte unharmed through a phenomenon called 'vomocytosis' (non-lytic exocytosis)[3,9–11].

Like most cell types, macrophages regularly perform exocytosis to recycle membrane components and excrete various factors[12–14]. However, vomocytosis is a unique form of exocytosis whereby these immune cells slowly (over 5 to 20 hours) expel large pathogenic particulates that they are otherwise programmed to be retained and digested. Studies have identified intracellular, physicochemical, and immunological cues in CN-infected MΦs that are linked to this mechanism. As MΦs perform vomocytosis, actin rapidly and transiently polymerizes in a cage-like structure around the phagosome, which then fuses with the plasma membrane[15]. These cages may be a post-phagosome permeabilization attempt by the MΦ to inhibit CNs' escape, as inhibiting actin polymerization has been shown to increase vomocytosis occurrence. In addition, CN disrupts phagolysosomal maturation, as characterized by the rapid removal of the early phagosome markers Rab5 and Rab11[16]. Some reports have suggested that there is alkalinization of, and abnormal calcium ion levels in phagosomal compartments that contain the live pathogen[16–20]. Furthermore, the addition of weak bases to CN-infected macrophages has been shown to modulate vomocytosis occurrence from macrophages[17,20]. Moreover, *Gilbert et al*. showed that pharmacological inhibition of ERK5 increases vomocytosis occurrence[21].

Further, the immune state of infected MΦs has been suggested to also influence this phenomenon. A recent study by *Seoane et al*. discovered that viral exposure to either measles or human immunodeficiency virus (HIV) were both shown to significantly

boost expulsion rates of CN cells from MΦs[22]. Moreover, other factors known to elicit an antiviral response—the TLR3 agonist poly(I·C) and type I interferons, IFN-α and IFN-β—all similarly increase MΦ vomocytosis events. Another study investigated how different T cell effector-induced phenotypes can impact the expulsion rates of infected J774 MΦs[23]. Prior to infection, these cells were treated with cytokines inducing T effector cell-induced phenotypes Th1 (IFN-γ and TNF-α), Th2 (IL-4 and IL-13), or Th17 (IL-17). The Th1 and Th17 subtypes of J774 cells showed diminished intracellular CN proliferation and increased vomocytosis rates, whilst the Th2 group displayed increased intracellular CN proliferation and reduced vomocytosis occurrence.

Taken altogether, studies have given some clarity on the influence of intracellular, physicochemical, and immune states on vomocytosis. However, they focus entirely on MΦs, which are only a single cell type in an army of immune cells. Moreover, *Yang et al*. recently discovered the occurrence of this phenomenon in neutrophils[24].

Like macrophages and neutrophils, dendritic cells (DCs) have the unique ability to phagocytose particulates, including pathogens. More importantly, DCs link the innate and adaptive arms of the immune system. These innate immune cells are key for maintaining a balance between the host defense against pathogens and protection of "self" antigens of host cells and tissues[25–27]. Dendritic cells detect invading pathogens due to their constituent sensors (e.g. Toll-like receptors [TLRs])[28,29]. They communicate the presence of pathogens to the adaptive immune system, thereby initiating long lasting, antigen-specific responses. Migration of DCs to T cell-rich regions is critical here and is mainly regulated by the chemokine receptor CCR7[30–32] and CCL21[33–35]. Following DC migration to secondary lymphoid organs, lymphocytes are subsequently

activated and induced to proliferate and become potent effector cells (e.g. helper T cells)[25]. Interestingly, other innate immune cell types can traffick via lymphatics[32,36] and perform antigen presentation[37–39]. While these cell types have some promising capability in lymphatic migration and antigen presentation, their abilities are limited in comparison to DCs, which are recognized as the primary antigen presenting cell type whose dominant function is to traffick to the LNs to present foreign material to LN-resident T cells.

During cryptococcal infections, DCs are known interact with CN cells and have been demonstrated to phagocytose CN cells following opsonization with complement or antibody[40]. *Hole et al*. demonstrated the ability of DC lysosomal extract to cause morphological changes in CN and kill the pathogen *in vitro* via oxidative and non-oxidative mechanisms[41]. *Artavanis-Tsakonas et al*. showed that CN-containing DC phagosomes have an impaired CD63 recruitment, indicative of a distinct phagosomal compartment composition that may affect the outcome of antigen processing and presentation[42]. However, to the best of our knowledge, the ability of DCs to expel CN from their phagosome via vomocytosis has not been investigated thus far.

We hypothesized that DCs could perform vomocytosis, especially given that they share much of the same vacuolar machinery as their phagocytic relatives, MΦs and neutrophils. Herein, we endeavored to document vomocytosis from DCs— a key player in bridging the innate and adaptive immune response. Further, we investigated the effect of CN infection ratio, presence of CN capsule, drug manipulation of the phagosome conditions and actin polymerization on vomocytosis from DCs. The overall effect of the immune state on vomocytosis from both DCs and MΦs was also assessed.

Finally, we characterized vomocytosis based on multiple outcomes— rate of vomocytosis occurrence, timing of expulsion, and number of internalized CN prior to expulsion. We believe that further investigation of CN's complex interactions with different phagocytic cell types will act as a step towards elucidating the complex story of cryptococcal infections and underlying mechanisms of vomocytosis.

2.3 Materials and Methods

Bone marrow-derived Dendritic Cell and Macrophage (MΦ) Culture

Primary DCs and MΦs were obtained from the bone marrow of C57BL/6 mice as described in previous studies[43–45]. Growth media consisted of DMEM/F-12 1:1 with L-glutamine (Cellgro, Herndon, VA), 10% fetal bovine serum, 1% sodium pyruvate (Lonza, Walkersville, MD), 1% nonessential amino acids (Lonza, Walkersville, MD), 1% penicillin/streptomycin (Cytiva, Marlborough, MA) and 20 ng/mL GM-CSF (R&D Systems, Minneapolis, MN) (DC media) or L929 conditioned media (MΦ media) and incubated at 37°C and 5% CO_2. For conciseness, media containing all necessary growth factors and added reagents for the necessary cell type will be denoted as 'complete media'. Unless otherwise noted we used DC and MΦ on day 10 of their respective cultures.

Cell Phenotype Validation via Flow Cytometry

On day 6 of DC or MΦ culture, cells were characterized by measuring the presence of phenotype-specific surface markers, with antibodies against F4/80 [APC, BM8 Clone] (eBioscience, San Diego, CA) and CD11c [PE-Cy7, HL3 Clone] (BD

Pharmingen, San Diego, CA) via an Attune Nxt Flow Cytometer (Life Technologies, Carlsbad, CA).

Cell Phenotype Validation via RNA Analysis

On day 10 or 11 of DC or MΦ culture, the contents of cells were extracted via application of TRIzol (Thermo Fisher Scientific, Waltham, MA). To isolate RNA from samples, a chloroform solvent extraction was performed according to manufacturer instructions. Next, RNA was purified using a kit, RNA Clean & Concentrator with DNAse (Zymo Research, Irvine, CA). The DNA Technologies Core at UC Davis assessed RNA quality (score>7.0), performed Batch 3'Tag-Seq library preparation, and sequenced using an Illumina NextSeq sequencer (Illumina, San Diego, CA). For analysis, reads were trimmed, aligned, and quantified for gene counts using OmicSoft software (Qiagen, Hilden, Germany). Dimensional reduction for principal component analysis (PCA) plots was also performed in the OmicSoft software.

Dendritic Cell and MΦ Polarization Validation

Dendritic cells and MΦs were seeded on 12 well plates (0.5 million cells/ well [DCs] and 0.25 million cells/ well [MΦs]) in complete media containing polarizing agents. The difference in seeding density was due to spreading ability, with MΦs being much more elongated than DCs and therefore taking up more surface area per cell. For inflammatory activation, cells were treated with LPS (100 ng/ml) from *Escherichia coli* O111:B4 (Sigma, St. Louis, MO). For anti-inflammatory polarization DCs were treated with 1uM of dexamethasone (DEX; Alfa Aesar, Tweksbury, MA) and MΦs with IL-4

51

(20ng/ml) and IL-13 (20ng/ml; denoted 'IL4/13' for brevity; R&D Systems) in MΦ media. After a 48-hour incubation period, the expressions of cell surface markers were determined via flow cytometry using antibodies against F4/80, CD38 [PerCP-eFluor 710, 90 Clone] (eBioscience), Arginase 1 [PE, A1exF5 Clone] (eBioscience), and iNOS [PE-Cy7, CXNFT Clone] (eBioscience) for MΦs and antibodies against CD11c, MHCII [Alexa-Fluor 488, M5/114.15.2 Clone] (BD Pharmingen), CD80 [APC, 16-10A1 Clone] (BioLegend, San Diego, CA), and CD86 [PE, GL1 Clone] (BD Pharmingen) for DCs. Additionally, an LPS activation resistance test was performed by adding LPS (100 ng/ml) to DCs and MΦs previously treated with tolerogenic polarization agents for an additional 48 hours. Subsequently, the expressions of the same cell surface markers were quantified using flow cytometry.

Effect of infection rate on vomocytosis

Dendritic cells and MΦs were seeded on 24 well plates (75,000 cells/ well [DCs] and 50,000 cells/ well [MΦs]) in complete media and incubated at 37°C and 5% CO_2. Infections with CNs and subsequent time-lapse imaging studies were performed between day 11-15. Wildtype CN H99 and the acapsular mutant *cap59* CN (both generously gifted by Dr. Angie Gelli, UC Davis, CA) were grown first on yeast extract peptone dextrose (YPD) agar (Thermo Fisher Scientific) followed by transferring a single colony to YPD broth (Thermo Fisher Scientific) shaking at 30°C overnight. The next day, CNs were washed with PBS (x3) via centrifugation. The heat-killed (HK) CN negative control group was prepared by incubating CNs at 70°C on a heat block for 1 hour. Both live and HK CNs were opsonized with 10 ug/ml of the anti-capsular IgG1

monoclonal antibody 18B7 (supplied from both Sigma and the Casadevall Lab, Johns Hopkins University, MD) and 50% human AB serum (Sigma). Opsonized pathogen was co-incubated with phagocytes at a 1:1 or 5:1 CN:phagocyte ratio (c.p.r.) for 2 hours in media with 10% human AB serum. Next, infected culture wells were washed with complete media (x5) to ensure all extracellular CNs were removed. Lastly, complete media was added, and time-lapse imaging was performed on infected cells for 14 hours.

Effect of Drugs on Vomocytosis

For drug-treated experimental groups, DCs were infected with CN at a 5:1 c.p.r. using identical methods outlined previously. After the 2-hour phagocytosis and washing step, the wells were treated with DC media containing either 10uM of chloroquine [CQ] (Thermo Fisher Scientific), 100 nM of cytochalasin B from *Drechslera dematioidea* [CYT low] (Sigma), 4uM of cytochalasin B (CYT hi), or 100 nM of bafilomycin A1 [BFA] (Sigma). These parameters were selected based on the range of drug concentrations used in prior vomocytosis studies[15,17,24,46]. This step was followed by time-lapse imaging for 14 hours whilst in drug-containing media.

Effect of Polarizing Agents on Vomocytosis

For experiments studying the effect of phagocyte polarization on vomocytic frequency, DEX or LPS were added to DCs at 48 hours prior to CN infection. For MΦs, IL4/13 or LPS was added to the cells 48 hours prior CN infection. Polarizing agent-containing media was replaced with fresh complete media prior to infection with CN. The infection then proceeded using identical methods as previously outlined.

Time-lapse Imaging

Infected cells were kept at 37°C and 5% CO_2 in the imaging chamber of the BZ-X Fluorescence Microscope (Keyence, Itasca, IL). Images were taken every 4 minutes for a period of 14 hours and compiled into a single movie file using BZ-X software. Movies were blinded by a third party before manual tracking of CNs and scoring for vomocytosis events by an independent technician.

Confocal Time-Lapse and High-Resolution Imaging

Before infection, DCs were stained with 1,1'-Dioctadecyl-3,3,3',3'-Tetramethylindodicarbocyanine, 4-Chlorobenzenesulfonate Salt (DiD; 1µM; Thermo Fisher Scientific) and CN were stained with Calcofluor White (CFW; 1mg/ml; Sigma). After 2 hours of infection at a 1:1 c.p.r., the cells were washed 5 times with DC media. Next, 4 hours after washing, the sample was fixed with 2% paraformaldehyde and vomocytosing cells were imaged using the Olympus FV3000 confocal (Olympus Corporation, Westborough, MA) at 60x magnification.

DC viability

Dendritic cells were seeded on 24-well plates (75,000 cells/ well) in DC media and incubated at 37°C and 5% CO_2. Cells were co-incubated with CNs opsonized using previously mentioned methods. Extracellular CNs were washed with DC media and 14 hours later cell viability was measured using the CyQUANT lactate dehydrogenase (LDH) cytotoxicity assay (Thermo Fisher Scientific) according to manufacturer's

instructions. Additional details on the viability assays are provided in the Supplementary Information.

Data and Statistical Analysis

In each experimental group replicate, 300 randomly selected CNs from multiple viewing regions were observed and vomocytosis manually quantified. All statistical analyses were performed using GraphPad Prism 9. Categorical data of vomocytosis frequency in the different conditions was assessed by one-way ANOVA corrected for multiple comparisons by false discovery rate (FDR) using a two-stage linear step-up procedure of Benjamini, Krieger and Yekutieli (GraphPad® Prism). This same statistical analysis procedure was used to evaluate flow cytometry marker expression data, number of CN cells per phagosome data, and timing of expulsion data. For F4/80 and CD11c expression comparison, an unpaired t-test was used as there were only two groups to compare. All data shown include at least three independent experiments. Original time-lapse movies, upon which manual scoring was performed, are freely available upon request. All column graphs, generated on GraphPad Prism 9, display the individual data points, mean, and standard error mean (SEM). All violin plots, generated on R, visualize the individual event data points, mean (red dot), and box plot containing median and interquartile range. All p-values for significant comparisons are listed in **Table 2.S1**.

2.4 Results

DC and MΦ phenotype validation

      The phenotypes of the bone-marrow derived DCs and MΦs were characterized via flow cytometry to confirm that the cell cultures generated with these protocols were authentic. The protocols used were derived from robust techniques from prior literature for generation of murine, bone marrow derived DCs and MΦs using GM-CSF[45] and M-CSF[44] respectively. These methods have been widely used in prior studies requiring MΦs for vomocytosis experiments[17,20,21] and DCs for Cryptococcal infection experiments[40,47–49], in which the resultant cultures are accepted to be relatively pure in the correct phagocyte phenotype. For our study, the cells grown were characterized for the DC marker - CD11c, and the MΦ marker - F4/80, via flow cytometry. (**Figure 2.1A**) The purity of MΦ and DC cultures based on presence or lack of F4/80 and CD11c markers are visualized via bar graphs. Dendritic cell cultures exhibit low F4/80 mean fluorescence intensity (MFI) and high CD11c MFI cell populations, while MΦ cultures display high F4/80 MFI and low CD11c MFI cell populations. (**Figure 2.1B**) Furthermore, RNA sequencing analysis of each cell type display notable clustering and separation by PCA plotting. (**Figure 2.1C**). These results confirm that the cultures grown are genuine bone marrow-derived DCs and MΦs in line with prior literature[50,51].
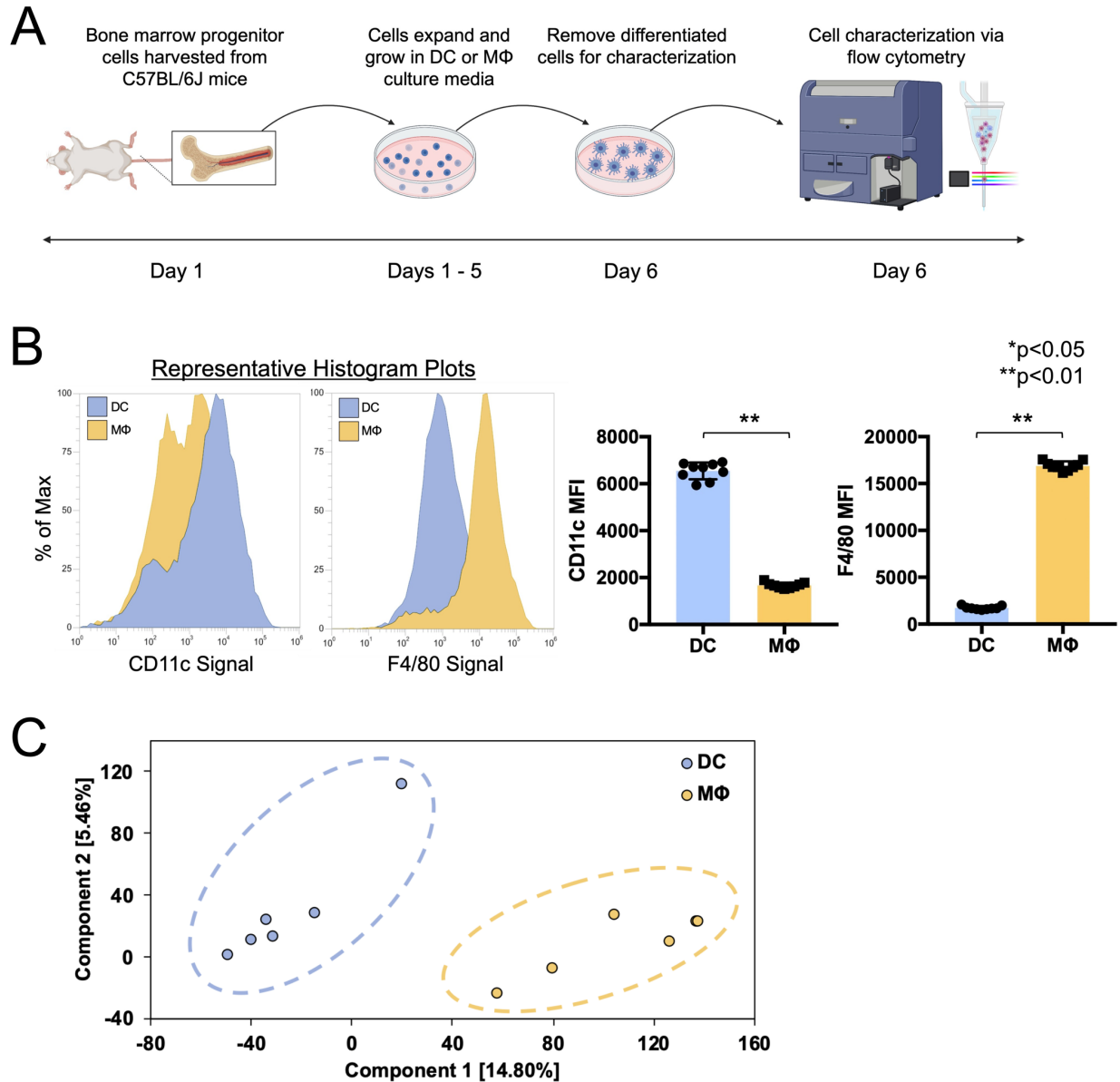
Figure 2.1. Verification of DC and MΦ phenotypes via F4/80 (MΦ marker) and CD11c (DC marker) flow cytometric analysis and RNA expression analysis. (**A**) Schematic of flow cytometry experiment. Bone marrow progenitor cells were obtained from C57BL/6J mice and grown in either DC differentiation media (GM-CSF supplemented) or MΦ differentiation media (M-CSF supplemented via L929). On day 6, these cells were stained and analyzed via flow cytometry. (**B**) Flow cytometry data for

F4/80 and CD11c identification markers. Representative histogram plots are shown for fluorescence intensity of F4/80 and CD11c markets. The flow populations were assessed by MFI for each marker. Column graphs of full flow cytometry data show the MFI for F4/80 and CD11c for DC-differentiated and MΦ-differentiated cultures (N=3, n=9, statistical analysis performed using an unpaired t-test). (**C**) PCA plot analysis displaying clustering and separation of DC and MΦ cultures by RNA expression data. (N=6, n=6, dimensional reduction performed on OmicSoft software).

Vomocytosis from DCs is independent of CN capsule and infection rates, and is comparable to vomocytosis from MΦs

We quantified vomocytic events using time-lapse microscopy and verified their non-lytic nature via cell viability assays. After 2-hour phagocytosis of CN, phagocytic cells were washed for the removal of extracellular CN, and time-lapse imaging experiments were performed during a period of 14 hours (**Figure 2.2A**). Vomocytosis events, defined as expulsions of CN from host cell while both remain intact, were observed at both CN:phagocyte ratios (c.p.r.) of 1:1 and 5:1, as shown in representative time lapse images (**Figure 2.2B-C**). Confocal time-lapse microscopy videos confirmed vomocytosis events by visually verifying instances of increased CN (green) fluorescent intensity upon uncoupling between DC and CN cells over the course of 8 hours (**Figure 2.S1**). Overall, vomocytosis occurred at a rate of 17% for MΦs infected at a 1:1 c.p.r., 18% for MΦs infected at a 5:1 c.p.r., 11% for DCs infected at a 1:1 c.p.r., 13% for DCs infected at a 5:1 c.p.r., and 13% for DCs infected with *cap59* CN at a 5:1 c.p.r. (**Figure 2.2D-E**). For the HK CN control groups, an expulsion rate of only 2% or less was

observed for both DC and MΦ groups infected at 1:1 and 5:1 c.p.r. To confirm that these events were indeed non-lytic, DC viability was tested via an LDH assay. We observed no increased toxicity due to CN infection (**Figure 2.S2**). Notably, the vomocytosis rates observed from DCs were not significantly different from those observed from MΦs at 1:1 and 5:1 c.p.r. (**Figure 2.2F**). For conclusive visual confirmation of vomocytosis, high resolution confocal microscopy was used to observe two fixed DC cells mid-vomocytosis at 6 hours after infection with CN (**Figure 2.2G**).
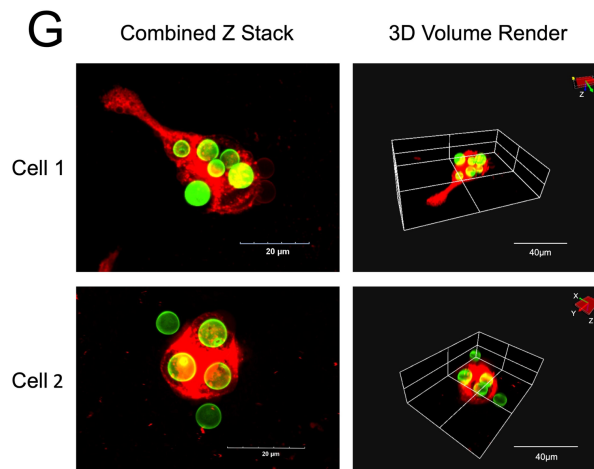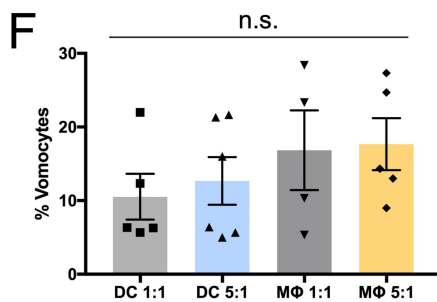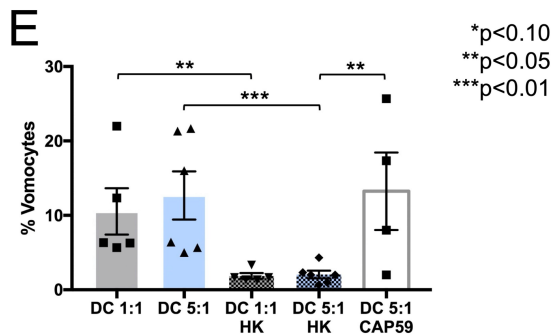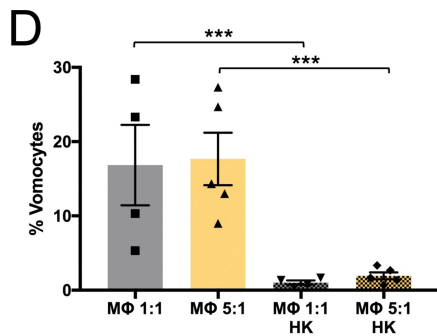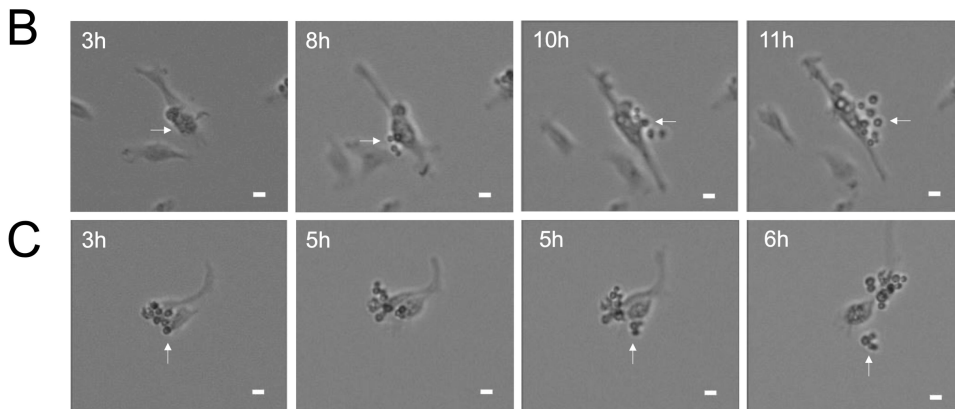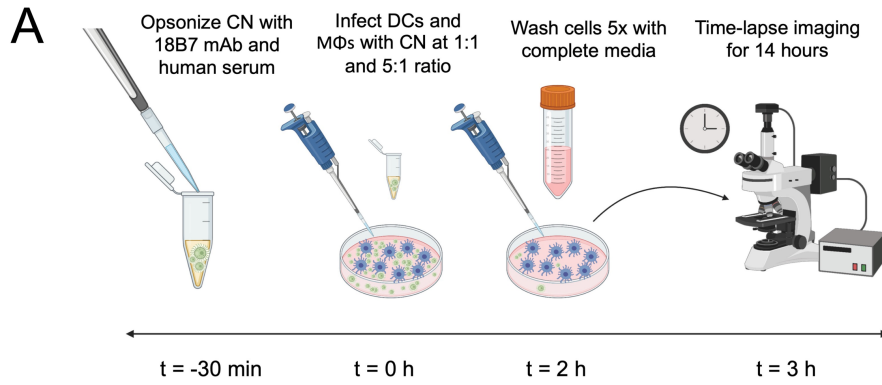
Figure 2.2. Time-lapse analysis of vomocytosis from DCs. (**A**) Schematic of time-lapse experiment. CN was prepared for phagocytosis by opsonizing with 18B7 mAb and human serum. DCs or MΦs were infected with opsonized CN either at a 1:1 or 5:1 c.p.r. for 2 hours. Following infection, the phagocytes were washed 5x and time-lapse imaged for 14 hours. Representative time-lapse images of DCs performing vomocytosis at (**B**) 1:1, or (**C**) 5:1 c.p.r. (scale bar = 10µm). (**D-F**) Graphs of vomocytosis rates of MΦs and DCs are shown at 1:1 and 5:1 c.p.r., compared to a HK CN control and acapsular *cap59* CN (N≥4 for each condition, statistical analysis performed using one-way ANOVA corrected for multiple comparisons by FDR using a two-stage linear step-up procedure of Benjamini, Krieger and Yekutieli). **(G)** Confocal images showing instances of DCs (DiD, red) expelling CN (CFW, green).

Drugs that disrupt phagolysosomal maturation and actin polymerization inhibit vomocytosis

Next, DCs were treated with drugs previously documented to affect phagolysosomal maturation, and vomocytosis from MΦs. Namely, CQ, CYT, and BFA were used for these experiments (**Figure 2.3A**). After assessing potential toxicity to DCs and CNs at the desired concentrations (**Figure 2.S2**), the individual drugs were added to wells containing CN-infected DCs at a 5:1 c.p.r., just prior time-lapse imaging. All drugs (at the selected concentrations) reduced vomocytosis rates (**Figure 2.3B**). For DCs, we observed vomocytosis rates of 4%, 5%, 6%, and 6% for CQ, CYT hi, CYT lo, and BFA respectively. We confirmed that these inhibited rates were not due to the

impact of the drugs on immune cell and CN cell viability (**Figure 2.S3**). Furthermore, in CN-infected DC cultures treated with these drugs, there were no observed increases in toxicity to extracellular or intracellular CNs (**Figure 2.S4**).
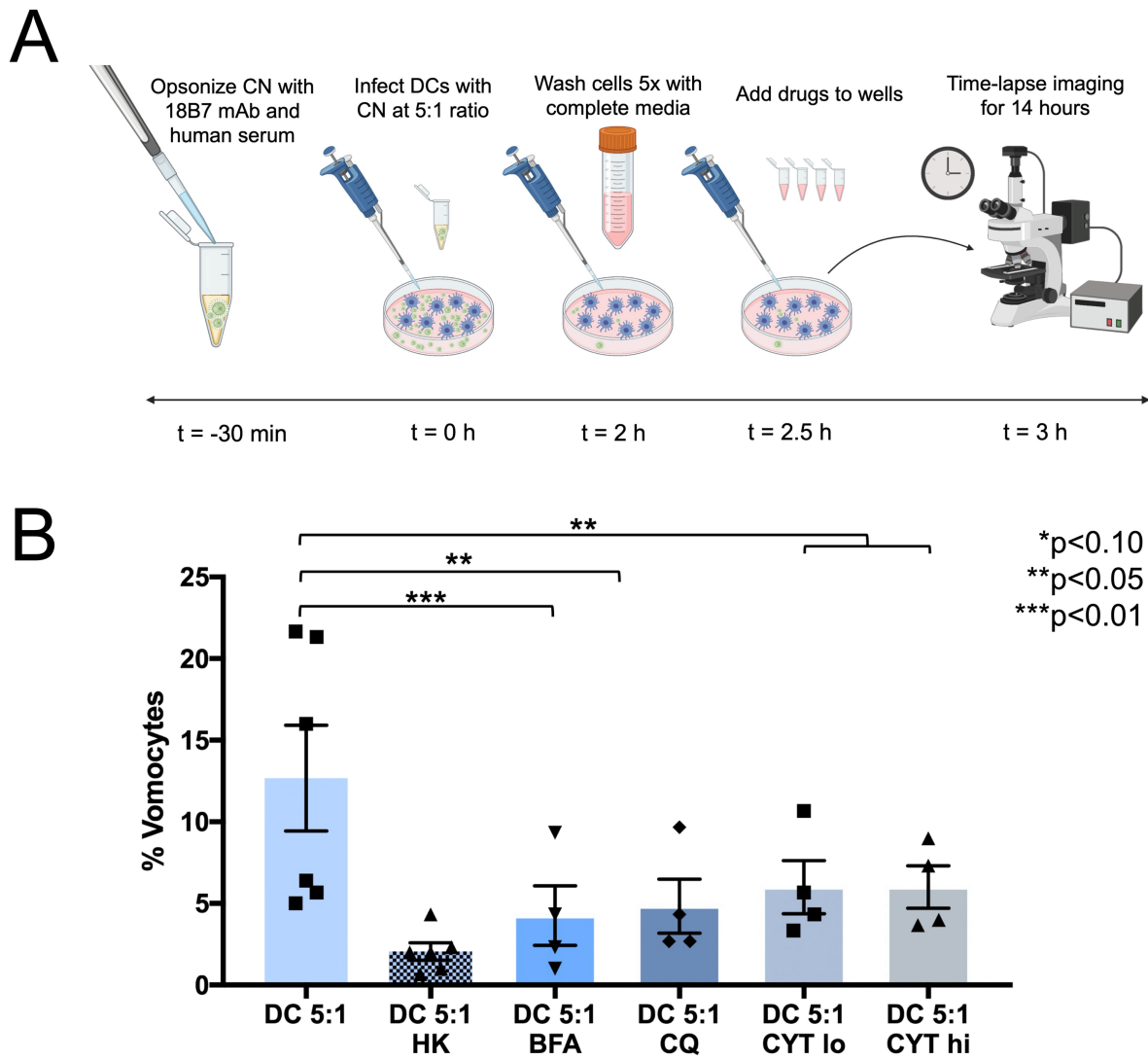
Figure 2.3. Time-lapse analysis of DC vomocytosis rates under exposure to vomocytosis-modulating drugs. (**A**) Schematic of time-lapse experiment. CN cells were prepared for phagocytosis by opsonizing with 18B7 mAb and human serum. DCs were infected with opsonized CN at a 5:1 c.p.r. for 2 hours. Following infection, the wells

were washed 5x, replaced with drug-containing media, and time-lapse imaged for 14 hours. (**B**) Vomocytosis rates of DCs, at a 5:1 infection ratio, are shown in untreated, HK CN, and drug-treated conditions—either BFA, CQ, CYT lo, or CYT hi (N≥4 for each condition, statistical analysis performed using one-way ANOVA corrected for multiple comparisons by FDR using a two-stage linear step-up procedure of Benjamini, Krieger and Yekutieli).

Treatment of MΦs and DCs with polarization agents alters their immune phenotype

Prior to testing the effect of immune state on vomocytosis, verification of the immunophenotype of MΦs and DCs was performed (**Figure 2.4A**). In these experiments, the immature MΦ (iMΦ; Control), activated (LPS), anti-inflammatory (IL4/13), and tolerized then challenged (IL4/13 + LPS) conditions were probed (**Figure 2.4B**). The LPS-treated group displayed significantly higher inflammatory marker expression of CD38 and iNOS compared to the immature, untreated group. Interestingly, the tolerogenic marker Arg1 was also increased on the LPS-treated MΦs; this finding may be due to an inhibitory feedback loop following earlier inflammation in this group. On the other hand, the IL4/13-treated group showed no significant differences for CD38 and iNOS, compared to the immature group, whilst exhibiting higher Arg1 expression than the untreated and LPS groups. Additionally, the tolerogenic group challenged with LPS displayed similarly high levels of Arg1. Additionally, this group had similar expression of CD38 and iNOS markers to the LPS-treated cells.

For DCs, the inflammatory markers MHCII, CD80, and CD86 were analyzed via flow cytometry on CD11c+ gated cells. The immature DC (iDC; Control), activated

(LPS), and tolerized (DEX) conditions were analyzed. Additionally, an added DEX-treated DC group was challenged with LPS (DEX + LPS) for an additional 48 hours to test resistance to inflammatory activation. The LPS-treated group displayed significantly higher MHCII, CD80, and CD86 expression compared to the immature untreated group (**Figure 2.4C**). Meanwhile, the DEX group displayed no significant difference to the immature group on the basis of these inflammatory markers. Furthermore, when tested with LPS after DEX treatment, these tolerogenic DCs displayed significantly lower activation of MHCII and CD86 expressions compared to the LPS-treated group, indicating resistance toward maturation.

Immune polarization of MΦs and DCs does not affect vomocytosis rate

Next, the vomocytosis rates of polarized MΦs and DCs were tested (**Figure 2.4D**). For MΦs, the anti-inflammatory (IL4/13) and pro-inflammatory (LPS) conditions showed significantly higher vomocytosis rates than the heat killed control. However, there were no significant differences in rates between the untreated (18%), anti-inflammatory (13%), or pro-inflammatory (20%) MΦs (**Figure 2.4E, left**). Similarly, DCs polarized to tolerogenic (DEX) and inflammatory (LPS) phenotypes displayed a higher vomocytosis rate than that of the HK CN group. However, the DC vomocytosis rates of the tolerogenic (12%) and inflammatory (19%) groups were not significantly different to each other or the untreated group (13%) (**Figure 2.4E, right**).
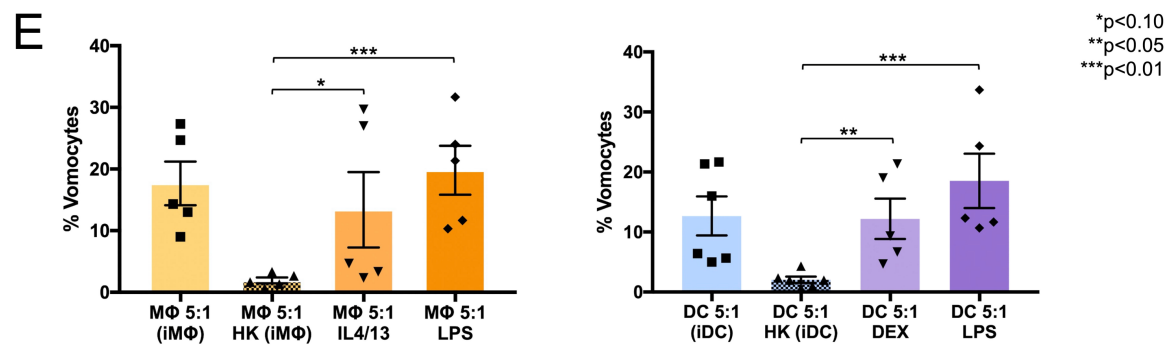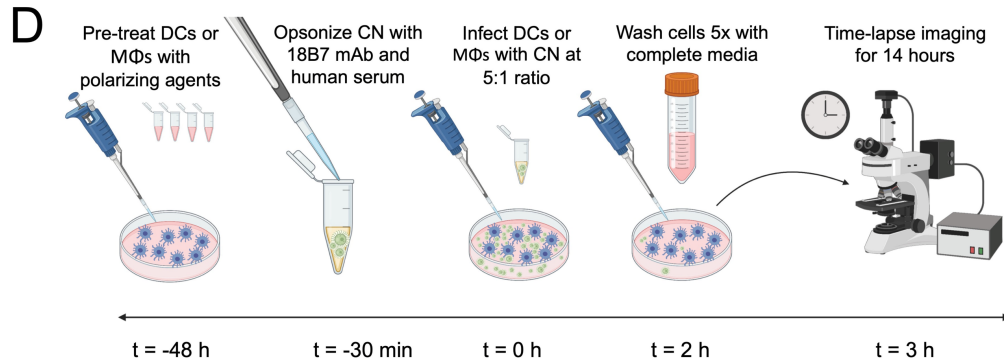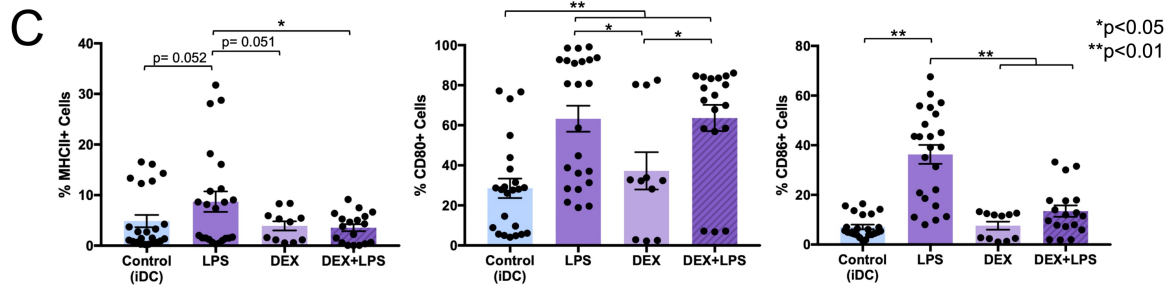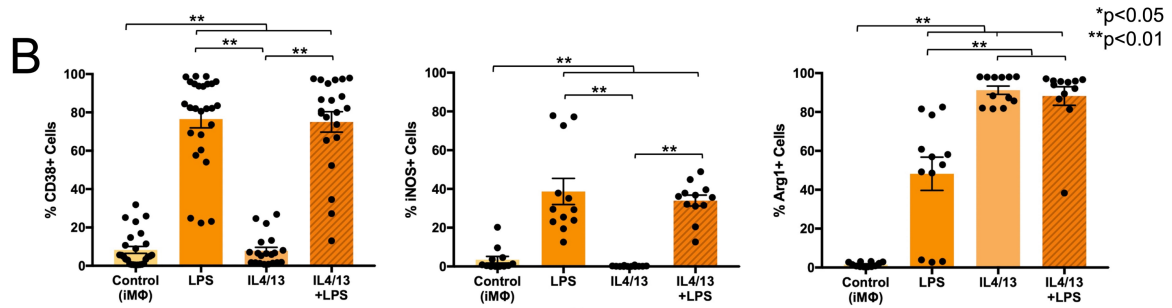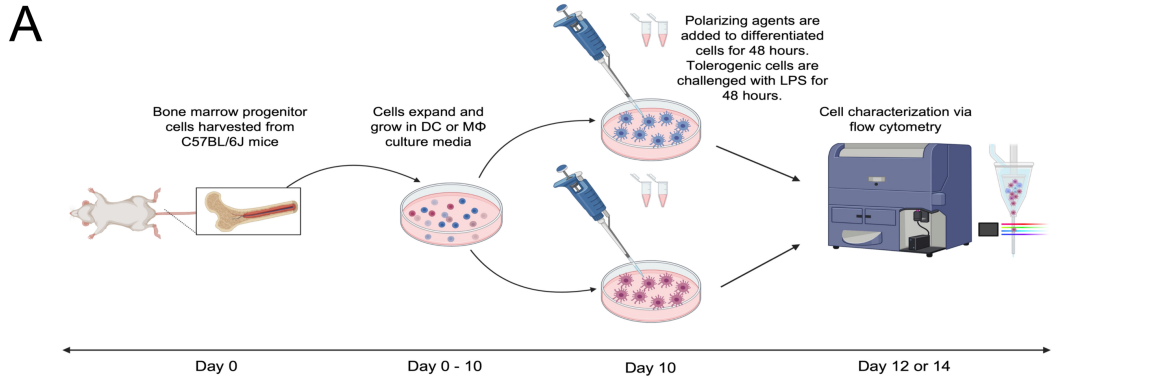
Figure 2.4. DC and MΦ vomocytosis rates following immune polarization. (**A**) Schematic of flow cytometry experiment. Dendritic cells and MΦs were incubated with polarization agents for 48 hours. Dendritic cells were polarized using dexamethasone, or LPS for tolerized or inflammatory phenotypes, respectively. Macrophages were polarized using agents LPS or IL4/13 for inflammatory (M1) or tolerogenic (M2) phenotypes, respectively. Also, an additional experimental group of tolerized DC and MΦ were challenged with LPS for another 48 hours. These groups were stained for DC immunophenotype markers (MHCII, CD80, and CD86) or MΦ immunophenotype markers (CD38, iNOS, and Arg1) and analyzed via flow cytometry. (**B**) Confirmation of DC immunophenotype characterization by flow cytometry readout of maturation markers MHCII, CD80, and CD86. (**C**) Confirmation of MΦ immune phenotype characterization by flow cytometry readout of inflammatory activation markers CD38 and iNOS, as well as the M2 marker Arg1. (**D**) Schematic of time-lapse experimental design. Briefly, prior to infection, DCs and MΦs were incubated with polarization agents for 48 hours. Then, CN was prepared for phagocytosis by opsonizing with 18B7 mAb and human serum. Polarized DCs and MΦ were infected with opsonized CN at a 5:1 c.p.r. for 2 hours. Following infection, the phagocytes were washed 5 times and time-lapse imaged for 14 hours. (**E**) Vomocytosis rates of DCs and MΦs at a 5:1 infection ratio are shown for immature (untreated), HK CN, tolerized, and inflammatory states. (N≥4, n≥11 for each condition, statistical analysis performed using one-way ANOVA corrected for multiple comparisons by FDR using a two-stage linear step-up procedure of Benjamini, Krieger and Yekutieli).

Infection Ratio, Drug treatments, and Immune Polarization affect Vomocytosis Kinetics

We used time-lapse videos to measure of exact time of expulsion for each vomocytic event. There was no difference in vomocytosis timing for DCs infected with CN at a 1:1 and 5:1 c.p.r., and no difference compared to DCs infected with the *cap59* CN (**Figure 2.5A**). For MΦs, the 5:1 c.p.r. condition displayed significantly lower average time to expulsion compared to the 1:1 c.p.r. group (**Figure 2.5B**). Comparing DCs and MΦs, the MΦ 1:1 c.p.r. condition showed a higher time to expulsion than both the DC 1:1 and DC 5:1 c.p.r. conditions (**Figure 2.5C**). For the drug-treated DC groups, both the CQ and CYT hi treatments performed vomocytosis faster than the DC 5:1 untreated control (**Figure 2.5D**). Further, both immune-polarized DCs showed significantly lower time of expulsion than the unpolarized control, with the LPS-treated group having faster expulsion times than the DEX-treated group (**Figure 2.5E**). In MΦs, both polarized conditions displayed differences in timing that were not significantly different compared to the control. However, the LPS-treated condition had a significantly faster time of expulsion than the IL4/13-treated group (**Figure 2.5F**).
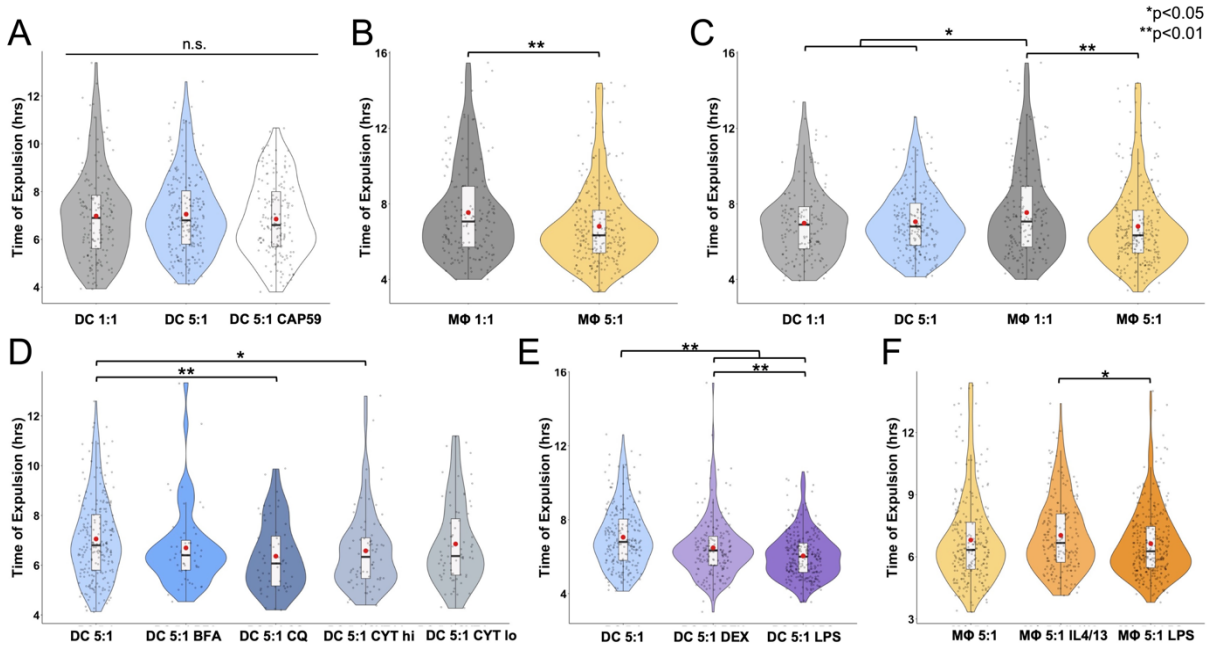
Figure 2.5. **Vomocytosis event timing analysis**. Results are displayed in violin box plots with individual dots representing each timing event. The red circle in each plot represents the mean timing occurrence and the black line in the box plot represents the median. (**A**) Violin plot displaying timing of DC vomocytosis events compared between 1:1 and 5:1 c.p.r., as well as 5:1 c.p.r. with *cap59* CN. (**B**) Violin plot of MΦ vomocytosis timing between 1:1 and 5:1 c.p.r. (**C**) violin plot comparing vomocytosis timing between DC and MΦ at different CN infection ratios. D) Violin plot of DC vomocytosis expulsion timing under a 5:1 infection ratio of CN under different drug treated conditions (BFA, CQ, CYT lo, or CYT hi) compared to an untreated control. (**E**) Violin plot of DC vomocytosis timing under a 5:1 CN infection as an immature phenotype (untreated), tolerogenic phenotype (DEX treated), and inflammatory phenotype (LPS treated). (**F**) Graph of MΦ vomocytosis timing under a 5:1 CN infection as an immature M0 phenotype (untreated), tolerogenic M2 phenotype (IL4/13), and inflammatory M1 phenotype (LPS treated) (N≥4, n≥51 for each condition, statistical analyses were

performed using one-way ANOVA corrected for multiple comparisons by FDR using a two-stage linear step-up procedure of Benjamini, Krieger and Yekutieli).

Different treatments affect number of CN per vomosome

In addition to characterizing the vomocytosis rates and timing of different conditions, the number of CN located in the phagosome before a vomocytosis event, or 'vomosome', was also documented and analyzed. Under different infection ratios, the 5:1 condition had a significantly higher average number of CN per vomosome compared to the 1:1 infection ratio for DCs. Additionally, the 5:1 c.p.r. *cap59* CN mutant condition displayed a higher number of CN per vomosome than both the 5:1 and DC 1:1 c.p.r. for DCs. (**Figure 2.6A**) However, in MΦs there was no significant difference in CN per vomosome between the 1:1 and 5:1 infection ratios (**Figure 2.6B**). Notably, both the 1:1 and 5:1 c.p.r. MΦ groups showed higher number of CN located in their vomosomes than both DC 1:1 and DC 5:1 c.p.r. groups (**Figure 2.6C**). When analyzing drug-treated conditions, the DC 5:1 c.p.r. groups treated with CQ, CYT hi, or CYT lo had a significantly higher number of CN per vomosome than the control. The BFA-treated DC group showed no significant difference in CN per vomosome compared to the untreated control (**Figure 2.6D**). Finally, immune polarized groups were analyzed for differences in number of CN per vomosome. Both DEX-treated and LPS-treated DCs were observed to have a higher number of CN located in the phagosome prior to a vomocytosis event compared to the unpolarized control. Additionally, the LPS-treated DC group had a higher CN per vomosome count than the DEX-treated group (**Figure 2.6E**). For polarized MΦs, IL4/13-treated cells displayed a lower CN per vomosome

count to the control. Conversely, the LPS-treated group had a higher CN per vomosome average than the control, as well as IL4/13-treated groups. (**Figure 2.6F**).
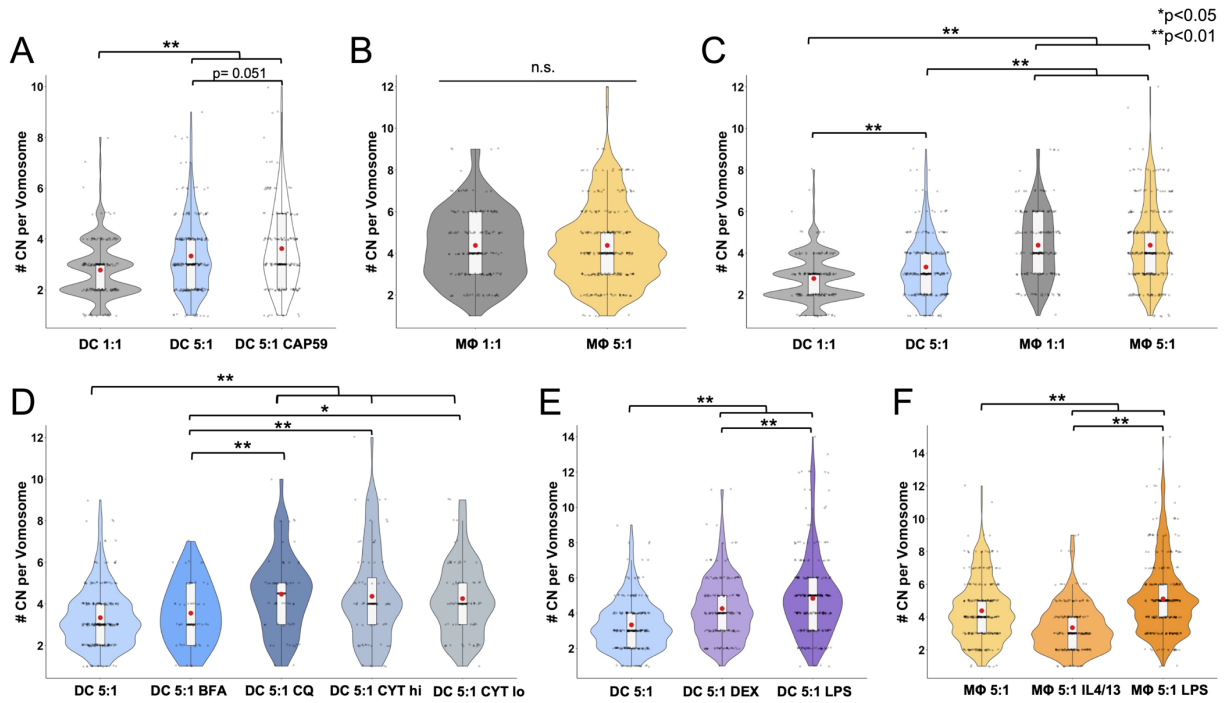
Figure 2.6. **Number of CN per vomosome**. Results are displayed in violin box plots with individual dots representing # CN per vomosome for each event. The red circle in each plot represents the mean timing occurrence and the black line in the box plot represents the median. (**A**) Violin plot displaying # CN per DC vomosome compared between 1:1 and 5:1 CN infection ratios, as well as 5:1 infection with a *cap59* CN. (**B**) Violin plot of # CN per MФ vomosome compared between 1:1 and 5:1 CN infection ratios. (**C**) Violin plot comparing # CN per vomosome between DC and MФ at different CN infection ratios. (**D**) Violin plot of # CN per vomosome for DCs with a 5:1 CN infection ratio under different drug treated conditions (BFA, CQ, CYT lo, or CYT hi) compared to an untreated control. (**E**) Violin plot of # CN per vomosome for DCs with a

5:1 CN infection as an immature phenotype (untreated), tolerogenic phenotype (DEX treated), and inflammatory phenotype (LPS treated). (**F**) Graph of # CN per vomosome for MΦs with a 5:1 CN infection as an immature M0 phenotype (untreated), tolerogenic M2 phenotype (IL4/13-treated), and inflammatory M1 phenotype (LPS treated) (N≥4, n≥51 for each condition, statistical analyses were performed using one-way ANOVA corrected for multiple comparisons by FDR using a two-stage linear step-up procedure of Benjamini, Krieger and Yekutieli).

2.5 Discussion and Conclusion

Our novel results show that live CN can perform vomocytosis from DCs, to a similar extent exhibited by both MΦs and neutrophils. Here, the occurrence of this phenomenon from DCs was rigorously verified by time-lapse microscopy, confocal imaging, and viability assays. Additionally, the average rate and timing of vomocytosis events from DCs were the same as those from MΦs. On the basis of CD11c MFI, F4/80 MFI, and RNA PCA analysis, the results confidently support the phenotype and purity of DC cultures in comparison to MΦ cultures; this is further confirmed by other literature that describe use of non-adherent progenitors treated GM-CSF for differentiation and CD11c to assess purity[52,53]. As mentioned previously, prior CN-related studies have assumed the bone marrow progenitor differentiation methods used to be considered pure for both DCs and MΦs[17,20,21,40,47–49]. Flow cytometry gating techniques show the DC cell culture's CD11c purity is over 75% (data not shown). Notably, even if the DC cultures are not fully pure, the rates seen in this study are high enough to still confirm the occurrence of vomocytosis in the DC population. Given our results on DC

vomocytosis and those published on MΦs and neutrophils, it is likely that some components of this mechanism may be conserved across these cell types derived from common myeloid progenitor cells.

Vomocytosis rates from DCs were observed to have no significant correlation to infection rate or presence of CN capsule. However, DCs infected with *cap59* CN contained a significantly higher number of CN per vomosome compared to DCs infected with the wildtype strain (H99). This is not surprising, as the CN capsule is known to be a potent anti-phagocytic agent that plays a role in reducing uptake by MΦs[54–56] and DCs[57]. Additionally, DCs infected at a 5:1 ratio showed higher amount of CN per vomosome than DCs 1:1 infected, which may be attributed to the larger number of CN that the DCs encountered during the experiment.

When treated with drugs to modify the phagosome (CQ, BFA) or actin polymerization (CYT lo, CYT hi), DCs displayed substantially lower rates of vomocytosis compared to the untreated control. Chloroquine is a weak base that passively diffuses into acidic organelles in the cytoplasm, becomes protonated and prevents maturation and fusion of endosomes and lysosomes[58,59]. Cytochalasin B is an actin polymerization inhibitor that has been demonstrated to induce a release of lysosomal enzymes, modulating lysosomal fusion with phagosomes[60,61]. Lastly, BFA is involved in the inhibition of the vacuolar ATPase in lysosomes[62]. With respect to CQ, our findings conflict with previous studies that have successfully demonstrated this drug to increase vomocytosis from J774 MΦ cell lines[10,17]. However, *Yang et al* showed that CQ decreases vomocytosis rates from primary murine neutrophils[24]. These discrepancies could be attributed to differences in cell type, as well as source (cell line vs. primary

murine cells). Interestingly, the decreased BFA-treated vomocytosis rates we observed from DCs align with observations by *Nicola et al* (from J774 macrophage cells), that this drug treatment reduces vomocytosis rates[17]. On the other hand, neutrophils were shown to have no change in vomocytosis rates after BFA treatment[24]. Again, these differences could be due to cell type, as well as cell source. Overall, our findings indicate that vomocytosis from DCs is indeed inhibited by phagosomal alkalinization—by either the weak base CQ or the ATPase inhibitor BFA. Pertaining to CYT treatment, again there is some disagreement within literature on the effect of this drug on vomocytosis. *Dragotakes et al* observed a decrease in vomocytosis rates of J774 MΦs following treatment with either cytochalasin B or D[46]. Conversely, *Alvarez et al*. saw increased rates of expulsion in the same cell type following cytochalasin D treatment[9]. In neutrophils, cytochalasin D was also seen to increase vomocytosis rates in a study by *Yang et al*[24]. Our observations for DCs align with those published by *Dragotakes et al*., but are in conflict with the other two studies. It is possible that cytochalasin B may cause lysosomal fusion in the infected DCs and cripple the CN's ability to thrive in the phagosome, although our viability data suggests that intracellular CN are still intact during this treatment. The role of CYT in inhibiting actin polymerization may play a more significant role in limiting the phagocyte's machinery and preventing CN from inducing an expulsion. In investigating average timing of vomocytosis, the CQ-treated and CYT hi-treated vomocytosis events displayed a statistically shorter length of time before expulsion compared to the untreated group. Chloroquine and CYT both reduce expulsion rates, but the CN are released relatively quicker compared to untreated cells. These events may be due to alternate mechanisms such as endosome recycling

pathways[63]. Interestingly, within the drug treated groups, the average number of CNs per vomosome were all significantly higher than the untreated group with the exception of the BFA-treated group. It is possible that BFA alkalinization of the phagosome reduces CN dividing ability, as CN has been observed to replicate faster in acidic environments[18,64].

Treatment of MΦs and DCs with polarization agents did not affect the vomocytosis rates compared to the unpolarized control. This result is contrary to some documented literature for MΦs, as *Gilbert et al.* found that inflammatory-polarized MΦs (via ERK5 inhibition) displayed a higher rate of expulsion than untreated MΦs, shown in both primary human MΦs and J774 cells[21]. Other conflicts exist where *Voelz et al.* showed that anti-inflammatory IL-4 or IL-13 treated MΦs perform a lower rate of vomocytosis compared to an untreated control, also in both primary human MΦs and J774 cells[23]. However, the same study showed that the pro-inflammatory IFN-γ, TNF-α, or IL-17 treated human and J774 MΦs did not have a significantly different vomocytosis rate than unpolarized MΦs, which aligns with our observations. Interestingly, a recent study by *Zhang et al.* found that primary murine MΦs treated with inflammatory extracellular vesicles displayed lower vomocytosis rates[65]— this result contradicts both this study and previous studies. Overall, investigation of the effect of immune phenotype on vomocytosis has been inconclusive. This may be attributed to differences in cell types, polarization procedures, phenotype validation and vomocytosis observation methods. Our results suggest that immune polarization is not a significant influence on vomocytosis rates from MΦs or DCs. However, there was a significant difference in the average time for vomocytosis occurrence for these groups. Cryptococcal cells

performed vomocytosis in a significantly shorter time from LPS-treated DCs compared to DEX-treated DCs. Similarly, the average non-lytic exocytosis time of CNs in LPS-treated MΦs was significantly longer in time length compared to that of IL4/13-treated MΦs. This observation is likely due to the differences in molecular and physicochemical characteristics involved in phagolysosomal maturation between activated and tolerogenic phenotypes. For instance, M2 macrophages have been shown to undergo rapid and profound phagosomal acidification relative to M1 macrophages[66]. Moreover, the same study demonstrates that reactive oxygen species (ROS) production is much greater and more sustained in M1 than in M2 phagosomes. Perhaps the mature, ROS and cathepsin-rich phagosome of LPS-treated phagocytes creates an inhospitable environment for CNs, prompting them to escape at a faster rate than in the less harsh anti-inflammatory polarized phagosomes. Additionally, for both DCs and MΦs, the LPS-treated groups displayed higher numbers of CN per vomosome compared to the tolerogenic group. The higher number of CN per vomosome and faster ejection from LPS-treated DCs compared to DEX-treated DCs could suggest a direct correlation between number of CN and ejection time— this same trend was observed from DCs treated with CQ and CYT hi.

In summary, this study documents the first recorded observation of DCs performing vomocytosis of CN. Moreover, multiple parameters were tested for their effects on vomocytosis including the infection ratio, presence of CN capsule, treatment with drugs, and polarization of phagocyte immune state. Vomocytosis from DCs is independent of infection ratio, CN capsule, or immune polarization phenotype. However, application of drugs that disrupt phagolysosome and actin processes significantly inhibit

the DC vomocytosis. Interestingly, infection ratio, drug treatments, and immune polarization influence the timing of vomocytosis, as well as the number of CN present in the DC vomosome prior to expulsion. Overall, the capability of DCs to expel CNs following ingestion appears similar to that of MΦs based on occurrence rate, timing, and number of CN per vomosome. This finding could help to further elucidate infection dissemination mechanisms in immunocompromised patients, as this phenomenon is clearly conserved between multiple types of phagocytes, including DCs. Finally, more studies are needed to understand the mechanisms involved in vomocytosis from DCs, and moreover determine if there is commonality of processes across all the phagocytic cells that are implicated to perform this behavior. Further, CN is not the only pathogen that has been shown to induce vomocytosis. Therefore, questions on the cohesion of mechanisms across pathogens and phagocytes should be addressed in future investigations.

2.6 Acknowledgements

2.7 Supplementary Methods

Confocal Time-Lapse

Prior to the experiment, DCs were stained with DiD (1µM) and CN cells were stained with FITC-NHS (1mg/ml). Three hours after infection, cells were placed in the imaging chamber of Olympus FV3000 confocal at 37°C and 5% CO_2. Images were taken every 10 minutes for the period of 5 hours at 20x magnification and analyzed for vomocytosis events.

Effect of drugs on CN viability

To assess the toxicity of drugs, CFW-stained CN cells (250,000 cells/mL in DC media) were incubated with CQ, CYT hi, CYT lo, or BFA for 14 hours. Next, they were washed (x3) with DC media, stained with Propidium Iodide (PI; Sigma) at 2µg/ml in 0.1% BSA in PBS solution for 15 minutes and assessed via flow cytometry.

Effect of drugs on DC viability

Dendritic cells were seeded on 96-well plates (15,000 cells/ well) in DC media and incubated at 37°C and 5% CO_2. The next day, cells were treated with CQ, CYT hi, CYT lo, or BFA for 14 hours, and washed (x3) with DC media. Subsequently, an LDH assay was performed to assess viability.

Effect of infection with drug treatments on extracellular and intracellular CN viability

Dendritic cells and MΦs were seeded on 24 well plates (75,000 cells/ well [DCs] and 50,000 cells/ well [MΦs], respectively) in complete media and incubated at 37°C and 5% CO_2. On day 11, phagocytes were infected at a 5:1 ratio with opsonized, CFW-stained CN. Following 2 hours of phagocytosis, wells were washed with complete media (x5) to remove external CN. After14 hours, external CN were isolated by removing the supernatant and washing (x5). Then, intracellular CN were isolated by lysing the washed phagocytes with ice cold sterile water for 60 minutes. All samples were subsequently washed with PBS and stained with PI for 15 minutes. Finally, the viability was evaluated via flow cytometry.

2.8 Supplemental Figures

Graph	Comparison	Statistical Method Used	p-value
Figure 1B, left	DC vs. MΦ	Unpaired t-test	<0.0001
Figure 1B, right	DC vs. MΦ	Unpaired t-test	<0.0001
Figure 2D	MΦ 1:1 vs. MΦ 1:1 HK	Corrected one-way ANOVA	0.0043
	MΦ 5:1 vs. MΦ 5:1 HK	Corrected one-way ANOVA	0.002
Figure 2E	DC 1:1 vs. DC 1:1 HK	Corrected one-way ANOVA	0.0425
	DC 5:1 vs. DC 5:1 HK	Corrected one-way ANOVA	0.0085
	DC 5:1 HK vs. DC 5:1 CAP59	Corrected one-way ANOVA	0.0124
Figure 3B	DC 5:1 vs. DC 5:1 BFA	Corrected one-way ANOVA	0.0084
	DC 5:1 vs. DC 5:1 CQ	Corrected one-way ANOVA	0.0133
	DC 5:1 vs. DC 5:1 CYT lo	Corrected one-way ANOVA	0.0317
	DC 5:1 vs. DC 5:1 CYT hi	Corrected one-way ANOVA	0.0317
Figure 4B, left	Control (iMΦ) vs. LPS	Corrected one-way ANOVA	<0.0001
	Control (iMΦ) vs. IL4/13 + LPS	Corrected one-way ANOVA	<0.0001
	LPS vs. IL4/13	Corrected one-way ANOVA	<0.0001
	IL4/13 vs. IL4/13 + LPS	Corrected one-way ANOVA	<0.0001
Figure 4B, middle	Control (iMΦ) vs. LPS	Corrected one-way ANOVA	<0.0001
	Control (iMΦ) vs. IL4/13 + LPS	Corrected one-way ANOVA	<0.0001
	LPS vs. IL4/13	Corrected one-way ANOVA	<0.0001
	IL4/13 vs. IL4/13 + LPS	Corrected one-way ANOVA	<0.0001
Figure 4B, right	Control (iMΦ) vs. LPS	Corrected one-way ANOVA	<0.0001
	Control (iMΦ) vs. IL4/13	Corrected one-way ANOVA	<0.0001
	Control (iMΦ) vs. IL4/13 + LPS	Corrected one-way ANOVA	<0.0001
	LPS vs. IL4/13	Corrected one-way ANOVA	<0.0001
	LPS vs. IL4/13 + LPS	Corrected one-way ANOVA	<0.0001
Figure 4C, left	Control (iDC) vs. LPS	Corrected one-way ANOVA	0.0524
	LPS vs. DEX	Corrected one-way ANOVA	0.0513
	LPS vs. DEX + LPS	Corrected one-way ANOVA	0.0154
Figure 4C, middle	Control (iDC) vs. LPS	Corrected one-way ANOVA	<0.0001
	Control (iDC) vs. LPS + DEX	Corrected one-way ANOVA	0.0002
	LPS vs. DEX	Corrected one-way ANOVA	0.0136
	DEX vs. DEX + LPS	Corrected one-way ANOVA	0.0165
Figure 4C, right	Control (iDC) vs. LPS	Corrected one-way ANOVA	<0.0001
	LPS vs. DEX	Corrected one-way ANOVA	<0.0001
	LPS vs. DEX + LPS	Corrected one-way ANOVA	<0.0001

Graph (cont.)	Comparison	Statistical Method Used	p-value
Figure 4E, left	MΦ 5:1 HK (iMΦ) vs. MΦ 5:1 IL4/13	Corrected one-way ANOVA	0.0634
	MΦ 5:1 HK (iMΦ) vs. MΦ 5:1 LPS	Corrected one-way ANOVA	0.0068
Figure 4E, right	DC 5:1 HK (iDC) vs. DC 5:1 DEX	Corrected one-way ANOVA	0.0338
	DC 5:1 HK (iDC) vs. DC 5:1 LPS	Corrected one-way ANOVA	0.0015
Figure 5B	MΦ 1:1 vs. MΦ 5:1	Unpaired t-test	0.0009
Figure 5C	DC 1:1 vs. MΦ 1:1	Corrected one-way ANOVA	0.0122
	DC 5:1 vs. MΦ 1:1	Corrected one-way ANOVA	0.0183
	MΦ 1:1 vs. MΦ 5:1	Corrected one-way ANOVA	0.0002
Figure 5D	DC 5:1 vs. DC 5:1 CQ	Corrected one-way ANOVA	0.0036
	DC 5:1 vs. DC 5:1 CYT hi	Corrected one-way ANOVA	0.0292
Figure 5E	DC 5:1 vs. DC 5:1 DEX	Corrected one-way ANOVA	0.0001
	DC 5:1 vs. DC 5:1 LPS	Corrected one-way ANOVA	<0.0001
	DC 5:1 DEX vs. DC 5:1 LPS	Corrected one-way ANOVA	0.0021
Figure 5F	MΦ 5:1 IL4/13 vs. MΦ 5:1 LPS	Corrected one-way ANOVA	0.0186
Figure 6A	DC 1:1 vs. DC 5:1	Corrected one-way ANOVA	0.0003
	DC 1:1 vs DC 5:1 CAP59	Corrected one-way ANOVA	<0.0001
	DC 5:1 vs DC 5:1 CAP59	Corrected one-way ANOVA	0.0511
Figure 6C	DC 1:1 vs. DC 5:1	Corrected one-way ANOVA	0.001
	DC 1:1 vs MΦ 1:1	Corrected one-way ANOVA	<0.0001
	DC 1:1 vs MΦ 5:1	Corrected one-way ANOVA	<0.0001
	DC 5:1 vs. MΦ 1:1	Corrected one-way ANOVA	<0.0001
	DC 5:1 vs. MΦ 5:1	Corrected one-way ANOVA	<0.0001
Figure 6D	DC 5:1 vs. DC 5:1 CQ	Corrected one-way ANOVA	<0.0001
	DC 5:1 vs. DC 5:1 CYT hi	Corrected one-way ANOVA	<0.0001
	DC 5:1 vs. DC 5:1 CYT lo	Corrected one-way ANOVA	<0.0001
	DC 5:1 BFA vs. DC 5:1 CQ	Corrected one-way ANOVA	0.0055
	DC 5:1 BFA vs. DC 5:1 CYT hi	Corrected one-way ANOVA	0.0099
	DC 5:1 BFA vs. DC 5:1 CYT lo	Corrected one-way ANOVA	0.0258
Figure 6E	DC 5:1 vs. DC 5:1 DEX	Corrected one-way ANOVA	<0.0001
	DC 5:1 vs. DC 5:1 LPS	Corrected one-way ANOVA	<0.0001
	DC 5:1 DEX vs. DC 5:1 LPS	Corrected one-way ANOVA	0.0014
Figure 6F	MΦ 5:1 vs. MΦ 5:1 IL4/13	Corrected one-way ANOVA	<0.0001
	MΦ 5:1 vs. MΦ 5:1 LPS	Corrected one-way ANOVA	<0.0001
	MΦ 5:1 IL4/13 vs. MΦ 5:1 LPS	Corrected one-way ANOVA	<0.0001

Table S1. All significant p-values and statistical methods used for comparisons made in Figures S.1-6.
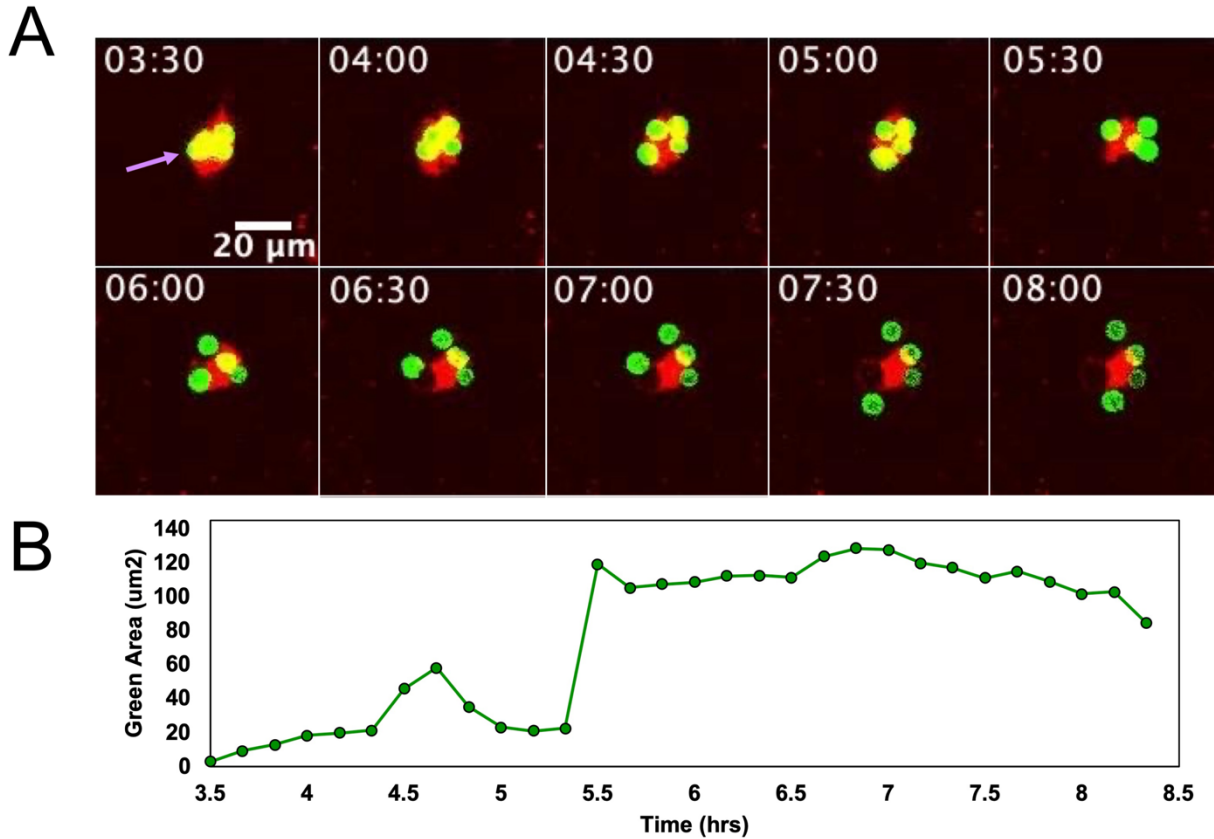
Figure 2.S1. (**A**) Confocal time-lapse microscopy was used to image an instance of a DC (DiD, red) expelling multiple CN (FITC-NHS, green) via vomocytosis. The representative images are shown 30 minutes apart, starting 3.5 hours after infection, with the exocytosis event occurring at 5.5 hours. (**B**) The amount of green fluorescence (not overlapped with red) over time calculated using ImageJ shows a sharp increase at 5.5 hours when the vomocytosis event occurs.
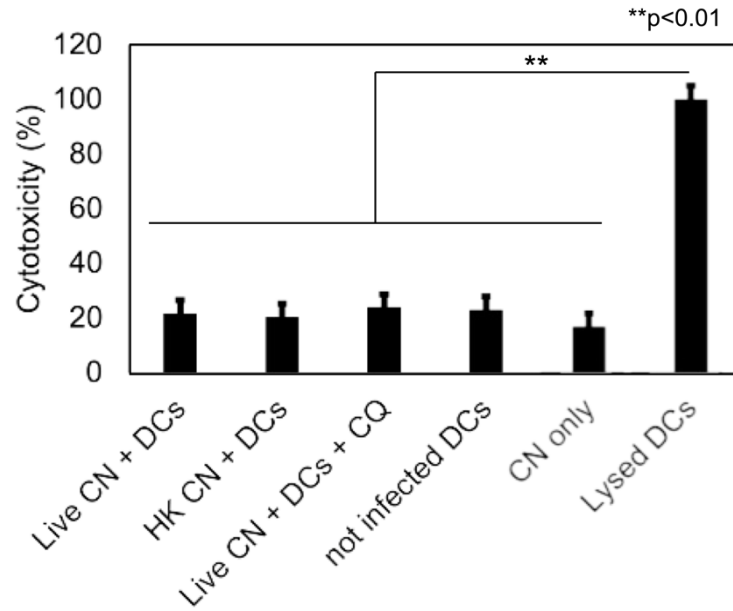
Figure 2.S2. Viability of CN-infected DCs after 14-hour co-incubation with CNs. Dendritic cells and opsonized CNs were co-incubated and extracellular CNs were removed via warm DC media washes after 2 hours. An LDH assay was performed after 14 hours co-incubation (N=3, n=12, statistical analyses were performed using one-way ANOVA corrected for multiple comparisons by FDR using a two-stage linear step-up procedure of Benjamini, Krieger and Yekutieli).
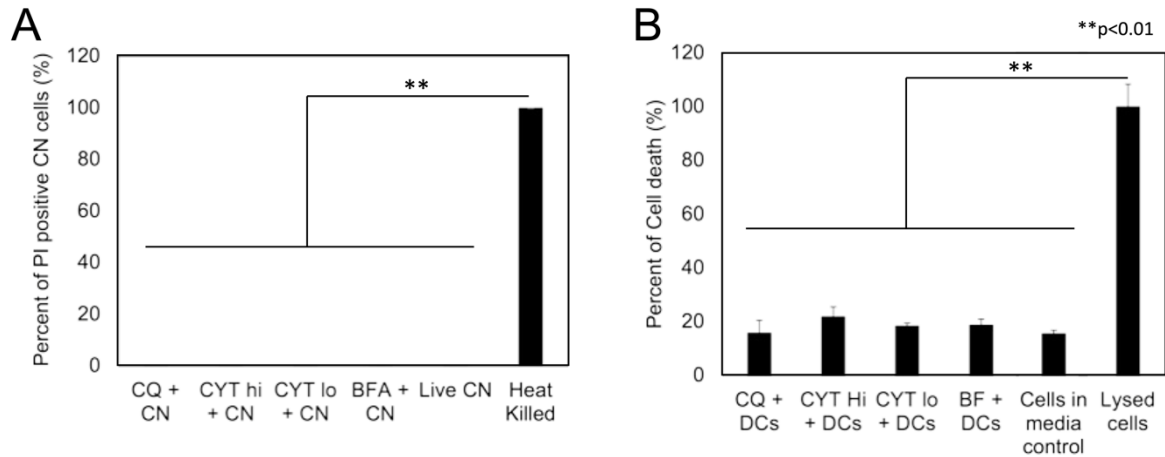
Figure 2.S3. Toxicity evaluation of lysosomal maturation and actin polymerization disruptor drugs on CN and DCs. (**A**) Opsonized and CFW stained *C. neoformans* cells were exposed to drugs for 14 hours in DC media. Viability of CN was measured via PI staining on a flow cytometer. (**B**) Dendritic cells were exposed to drugs for 14 hours in DC media. Cytotoxic evaluation was performed via LDH assay 14 hours after co-incubation with drugs (N=3, n=12, statistical analyses were performed using one-way ANOVA corrected for multiple comparisons by FDR using a two-stage linear step-up procedure of Benjamini, Krieger and Yekutieli).
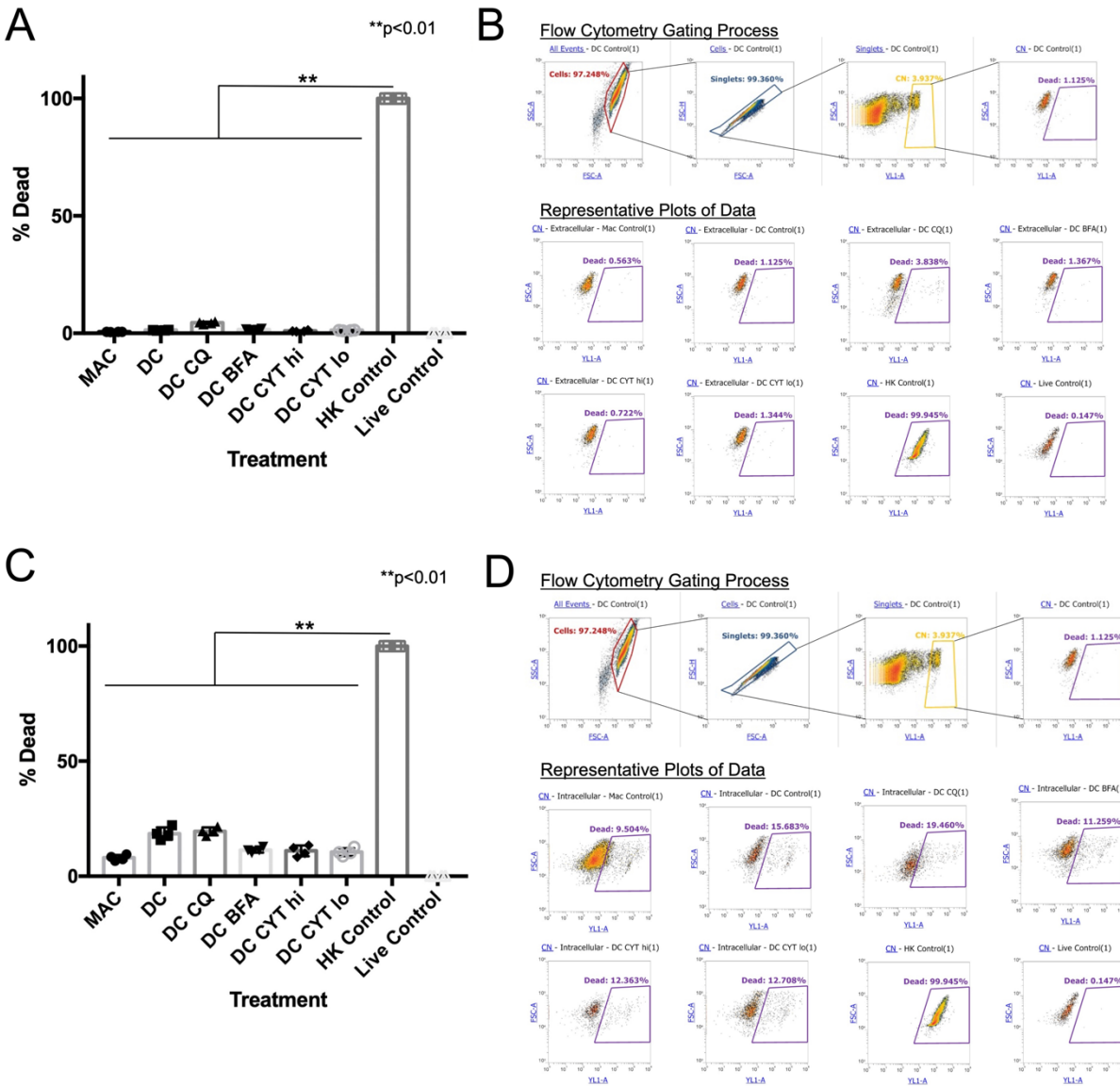
Figure 2.S4. Viability of CN during infection with MΦs or DCs treated with drugs. Opsonized and CFW stained CN cells were co-incubated with MΦs and DCs at a 5:1 CN:phagocyte ratio for 2 hours, washed, then DC groups were exposed to drug treatments for 14 hours. After incubation, extracellular CN were isolated via collection of supernatant and washes, while intracellular CN were collected via sterile H_2O lysis. Additionally, heat-killed and live CN groups were used as controls. (**A**) Column graph of

extracellular CN viability measured by PI staining via flow cytometry. (**B**) Gating process to select cells, singlets, CFW-stained CN, and dead CN is shown as well as representative plots for each condition. (**C**) Column graph of intracellular CN viability measured by PI staining via flow cytometry. (**D**) Gating process to select cells, singlets, CFW-stained CN, and dead CN is shown as well as representative plots for each condition (N=1, n=4, statistical analyses were performed using one-way ANOVA corrected for multiple comparisons by FDR using a two-stage linear step-up procedure of Benjamini, Krieger and Yekutieli).

2.9 References

(1) Rajasingham, R.; Smith, R. M.; Park, B. J.; Jarvis, J. N.; Govender, N. P.; Chiller, T. M.; Denning, D. W.; Loyse, A.; Boulware, D. R. Global Burden of Disease of HIV-Associated Cryptococcal Meningitis: An Updated Analysis. *The Lancet Infectious Diseases* **2017**, *17* (8), 873–881. https://doi.org/10.1016/S1473-3099(17)30243-8.

(2) May, R. C.; Stone, N. R. H.; Wiesner, D. L.; Bicanic, T.; Nielsen, K. Cryptococcus: From Environmental Saprophyte to Global Pathogen. *Nat Rev Microbiol* **2016**, *14* (2), 106–117. https://doi.org/10.1038/nrmicro.2015.6.

(3) Cruz-Acuña, M.; Pacifici, N.; Lewis, J. S. Vomocytosis: Too Much Booze, Base, or Calcium? *mBio* **2019**. https://doi.org/10.1128/mBio.02526-19.

(4) Denham, S. T.; Brown, J. C. S. Mechanisms of Pulmonary Escape and Dissemination by Cryptococcus Neoformans. *Journal of Fungi* **2018**, *4* (1), 25. https://doi.org/10.3390/jof4010025.

(5)   Sorrell, T. C.; Juillard, P.-G.; Djordjevic, J. T.; Kaufman-Francis, K.; Dietmann, A.; Milonig, A.; Combes, V.; Grau, G. E. R. Cryptococcal Transmigration across a Model Brain Blood-Barrier: Evidence of the Trojan Horse Mechanism and Differences between Cryptococcus Neoformans Var. Grubii Strain H99 and Cryptococcus Gattii Strain R265. *Microbes and Infection* **2016**, *18* (1), 57–67. https://doi.org/10.1016/j.micinf.2015.08.017.

(6)   Santiago-Tirado, F. H.; Onken, M. D.; Cooper, J. A.; Klein, R. S.; Doering, T. L. Trojan Horse Transit Contributes to Blood-Brain Barrier Crossing of a Eukaryotic Pathogen. *mBio* **2017**. https://doi.org/10.1128/mBio.02183-16.

(7)   Kechichian, T. B.; Shea, J.; Poeta, M. D. Depletion of Alveolar Macrophages Decreases the Dissemination of a Glucosylceramide-Deficient Mutant of Cryptococcus Neoformans in Immunodeficient Mice. *Infection and Immunity* **2007**. https://doi.org/10.1128/IAI.00587-07.

(8)   Charlier, C.; Nielsen, K.; Daou, S.; Brigitte, M.; Chretien, F.; Dromer, F. Evidence of a Role for Monocytes in Dissemination and Brain Invasion by Cryptococcus Neoformans. *Infection and Immunity* **2009**. https://doi.org/10.1128/IAI.01065-08.

(9)   Alvarez, M.; Casadevall, A. Phagosome Extrusion and Host-Cell Survival after Cryptococcus Neoformans Phagocytosis by Macrophages. *Current Biology* **2006**, *16* (21), 2161–2165. https://doi.org/10.1016/j.cub.2006.09.061.

(10) Ma, H.; Croudace, J. E.; Lammas, D. A.; May, R. C. Expulsion of Live Pathogenic Yeast by Macrophages. *Current Biology* **2006**, *16* (21), 2156–2160. https://doi.org/10.1016/j.cub.2006.09.032.

(11) Seoane, P. I.; May, R. C. Vomocytosis: What We Know so Far. *Cell Microbiol* **2020**, *22* (2), e13145. https://doi.org/10.1111/cmi.13145.

(12) Thorn, P.; Zorec, R.; Rettig, J.; Keating, D. J. Exocytosis in Non-Neuronal Cells. *Journal of Neurochemistry* **2016**, *137* (6), 849–859. https://doi.org/10.1111/jnc.13602.

(13) Tran, D. T.; Ten Hagen, K. G. Real-Time Insights into Regulated Exocytosis. *Journal of Cell Science* **2017**, *130* (8), 1355–1363. https://doi.org/10.1242/jcs.193425.

(14) Wu, L.-G.; Hamid, E.; Shin, W.; Chiang, H.-C. Exocytosis and Endocytosis: Modes, Functions, and Coupling Mechanisms. *Annual Review of Physiology* **2014**, *76* (1), 301–331. https://doi.org/10.1146/annurev-physiol-021113-170305.

(15) Johnston, S. A.; May, R. C. The Human Fungal Pathogen Cryptococcus Neoformans Escapes Macrophages by a Phagosome Emptying Mechanism That Is Inhibited by Arp2/3 Complex-Mediated Actin Polymerisation. *PLOS Pathogens* **2010**, *6* (8), e1001041. https://doi.org/10.1371/journal.ppat.1001041.

(16) Smith, L. M.; Dixon, E. F.; May, R. C. The Fungal Pathogen Cryptococcus Neoformans Manipulates Macrophage Phagosome Maturation. *Cellular Microbiology* **2015**, *17* (5), 702–713. https://doi.org/10.1111/cmi.12394.

(17) Nicola, A. M.; Robertson, E. J.; Albuquerque, P.; Derengowski, L. da S.; Casadevall, A. Nonlytic Exocytosis of Cryptococcus Neoformans from Macrophages Occurs In Vivo and Is Influenced by Phagosomal PH. *mBio* **2011**. https://doi.org/10.1128/mBio.00167-11.

(18) Leon-Rodriguez, C. M. D.; Fu, M. S.; Çorbali, M. O.; Cordero, R. J. B.; Casadevall, A. The Capsule of Cryptococcus Neoformans Modulates Phagosomal PH through Its Acid-Base Properties. *mSphere* **2018**. https://doi.org/10.1128/mSphere.00437-18.

(19) Samantaray, S.; Correia, J. N.; Garelnabi, M.; Voelz, K.; May, R. C.; Hall, R. A. Novel Cell-Based in Vitro Screen to Identify Small-Molecule Inhibitors against Intracellular Replication of Cryptococcus Neoformans in Macrophages. *International Journal of Antimicrobial Agents* **2016**, *48* (1), 69–77. https://doi.org/10.1016/j.ijantimicag.2016.04.018.

(20) Fu, M. S.; Coelho, C.; Leon-Rodriguez, C. M. D.; Rossi, D. C. P.; Camacho, E.; Jung, E. H.; Kulkarni, M.; Casadevall, A. Cryptococcus Neoformans Urease Affects the Outcome of Intracellular Pathogenesis by Modulating Phagolysosomal PH. *PLOS Pathogens* **2018**, *14* (6), e1007144. https://doi.org/10.1371/journal.ppat.1007144.

(21) Gilbert, A. S.; Seoane, P. I.; Sephton-Clark, P.; Bojarczuk, A.; Hotham, R.; Giurisato, E.; Sarhan, A. R.; Hillen, A.; Velde, G. V.; Gray, N. S.; Alessi, D. R.; Cunningham, D. L.; Tournier, C.; Johnston, S. A.; May, R. C. Vomocytosis of Live Pathogens from Macrophages Is Regulated by the Atypical MAP Kinase ERK5. *Science Advances 3* (8), e1700898. https://doi.org/10.1126/sciadv.1700898.

(22) Seoane, P. I.; Taylor-Smith, L. M.; Stirling, D.; Bell, L. C. K.; Noursadeghi, M.; Bailey, D.; May, R. C. Viral Infection Triggers Interferon-Induced Expulsion of Live Cryptococcus Neoformans by Macrophages. *PLoS Pathog* **2020**, *16* (2), e1008240. https://doi.org/10.1371/journal.ppat.1008240.

(23) Voelz, K.; Lammas, D. A.; May, R. C. Cytokine Signaling Regulates the Outcome of Intracellular Macrophage Parasitism by Cryptococcus Neoformans. *Infection and Immunity* **2009**. https://doi.org/10.1128/IAI.00297-09.

(24) Yang, X.; Wang, H.; Hu, F.; Chen, X.; Zhang, M. Nonlytic Exocytosis of Cryptococcus Neoformans from Neutrophils in the Brain Vasculature. *Cell Communication and Signaling* **2019**, *17* (1), 117. https://doi.org/10.1186/s12964-019-0429-0.

(25) Merad, M.; Sathe, P.; Helft, J.; Miller, J.; Mortha, A. The Dendritic Cell Lineage: Ontogeny and Function of Dendritic Cells and Their Subsets in the Steady State and the Inflamed Setting. *Annual Review of Immunology* **2013**, *31* (1), 563–604. https://doi.org/10.1146/annurev-immunol-020711-074950.

(26) Steinman, R. M.; Banchereau, J. Taking Dendritic Cells into Medicine. *Nature* **2007**, *449* (7161), 419–426. https://doi.org/10.1038/nature06175.

(27) Cabeza-Cabrerizo, M.; Cardoso, A.; Minutti, C. M.; Pereira da Costa, M.; Reis e Sousa, C. Dendritic Cells Revisited. *Annual Review of Immunology* **2021**, *39* (1), 131–166. https://doi.org/10.1146/annurev-immunol-061020-053707.

(28) Krishnaswamy, J. K.; Chu, T.; Eisenbarth, S. C. Beyond Pattern Recognition: NOD-like Receptors in Dendritic Cells. *Trends in Immunology* **2013**, *34* (5), 224–233. https://doi.org/10.1016/j.it.2012.12.003.

(29) Hemmi, H.; Akira, S. TLR Signalling and the Function of Dendritic Cells. *Chem Immunol Allergy* **2005**, *86*, 120–135. https://doi.org/10.1159/000086657.

(30) Förster, R.; Schubel, A.; Breitfeld, D.; Kremmer, E.; Renner-Müller, I.; Wolf, E.; Lipp, M. CCR7 Coordinates the Primary Immune Response by Establishing

Functional Microenvironments in Secondary Lymphoid Organs. *Cell* **1999**, *99* (1), 23–33. https://doi.org/10.1016/S0092-8674(00)80059-8.

(31) Clatworthy, M. R.; Aronin, C. E. P.; Mathews, R. J.; Morgan, N. Y.; Smith, K. G. C.; Germain, R. N. Immune Complexes Stimulate CCR7-Dependent Dendritic Cell Migration to Lymph Nodes. *Nat Med* **2014**, *20* (12), 1458–1463. https://doi.org/10.1038/nm.3709.

(32) Hampton, H. R.; Chtanova, T. Lymphatic Migration of Immune Cells. *Frontiers in Immunology* **2019**, *10*.

(33) Tal, O.; Lim, H. Y.; Gurevich, I.; Milo, I.; Shipony, Z.; Ng, L. G.; Angeli, V.; Shakhar, G. DC Mobilization from the Skin Requires Docking to Immobilized CCL21 on Lymphatic Endothelium and Intralymphatic Crawling. *Journal of Experimental Medicine* **2011**, *208* (10), 2141–2153. https://doi.org/10.1084/jem.20102392.

(34) Russo, E.; Teijeira, A.; Vaahtomeri, K.; Willrodt, A.-H.; Bloch, J. S.; Nitschké, M.; Santambrogio, L.; Kerjaschki, D.; Sixt, M.; Halin, C. Intralymphatic CCL21 Promotes Tissue Egress of Dendritic Cells through Afferent Lymphatic Vessels. *Cell Reports* **2016**, *14* (7), 1723–1734. https://doi.org/10.1016/j.celrep.2016.01.048.

(35) Russo, E.; Nitschké, M.; Halin, C. Dendritic Cell Interactions with Lymphatic Endothelium. *Lymphatic Research and Biology* **2013**, *11* (3), 172–182. https://doi.org/10.1089/lrb.2013.0008.

(36) TAKEDA, A.; SASAKI, N.; MIYASAKA, M. The Molecular Cues Regulating Immune Cell Trafficking. *Proc Jpn Acad Ser B Phys Biol Sci* **2017**, *93* (4), 183–195. https://doi.org/10.2183/pjab.93.012.

(37) Vono, M.; Lin, A.; Norrby-Teglund, A.; Koup, R. A.; Liang, F.; Loré, K. Neutrophils Acquire the Capacity for Antigen Presentation to Memory CD4+ T Cells in Vitro and Ex Vivo. *Blood* **2017**, *129* (14), 1991–2001. https://doi.org/10.1182/blood-2016-10-744441.

(38) BARKER, R. N.; ERWIG, L.-P.; HILL, K. S. K.; DEVINE, A.; PEARCE, W. P.; REES, A. J. Antigen Presentation by Macrophages Is Enhanced by the Uptake of Necrotic, but Not Apoptotic, Cells. *Clin Exp Immunol* **2002**, *127* (2), 220–225. https://doi.org/10.1046/j.1365-2249.2002.01774.x.

(39) Randolph, G. J.; Jakubzick, C.; Qu, C. Antigen Presentation by Monocytes and Monocyte-Derived Cells. *Curr Opin Immunol* **2008**, *20* (1), 52–60. https://doi.org/10.1016/j.coi.2007.10.010.

(40) Kelly, R. M.; Chen, J.; Yauch, L. E.; Levitz, S. M. Opsonic Requirements for Dendritic Cell-Mediated Responses to Cryptococcus Neoformans. *Infection and Immunity* **2005**, *73* (1), 592–598. https://doi.org/10.1128/IAI.73.1.592-598.2005.

(41) Hole, C. R.; Bui, H.; Wormley, F. L.; Wozniak, K. L. Mechanisms of Dendritic Cell Lysosomal Killing of Cryptococcus. *Scientific reports* **2012**, *2* (1), 1–9.

(42) Artavanis-Tsakonas, K.; Love, J. C.; Ploegh, H. L.; Vyas, J. M. Recruitment of CD63 to Cryptococcus Neoformans Phagosomes Requires Acidification. *Proceedings of the National Academy of Sciences* **2006**, *103* (43), 15945–15950.

(43) Allen, R. P.; Bolandparvaz, A.; Ma, J. A.; Manickam, V. A.; Lewis, J. S. Latent, Immunosuppressive Nature of Poly(Lactic-Co-Glycolic Acid) Microparticles. *ACS Biomater. Sci. Eng.* **2018**, *4* (3), 900–918. https://doi.org/10.1021/acsbiomaterials.7b00831.

(44) Zhang, X.; Goncalves, R.; Mosser, D. M. The Isolation and Characterization of Murine Macrophages. *Current Protocols in Immunology* **2008**, *83* (1), 14.1.1-14.1.14. https://doi.org/10.1002/0471142735.im1401s83.

(45) Lutz, M. B.; Kukutsch, N.; Ogilvie, A. L. J.; Rößner, S.; Koch, F.; Romani, N.; Schuler, G. An Advanced Culture Method for Generating Large Quantities of Highly Pure Dendritic Cells from Mouse Bone Marrow. *Journal of Immunological Methods* **1999**, *223* (1), 77–92. https://doi.org/10.1016/S0022-1759(98)00204-X.

(46) Dragotakes, Q.; Fu, M. S.; Casadevall, A. Dragotcytosis: Elucidation of the Mechanism for Cryptococcus Neoformans Macrophage-to-Macrophage Transfer. *The Journal of Immunology* **2019**. https://doi.org/10.4049/jimmunol.1801118.

(47) Tanaka, M.; Ishii, K.; Nakamura, Y.; Miyazato, A.; Maki, A.; Abe, Y.; Miyasaka, T.; Yamamoto, H.; Akahori, Y.; Fue, M.; Takahashi, Y.; Kanno, E.; Maruyama, R.; Kawakami, K. Toll-Like Receptor 9-Dependent Activation of Bone Marrow-Derived Dendritic Cells by URA5 DNA from Cryptococcus Neoformans. *Infect Immun* **2012**, *80* (2), 778–786. https://doi.org/10.1128/IAI.05570-11.

(48) Nakamura, K.; Miyazato, A.; Xiao, G.; Hatta, M.; Inden, K.; Aoyagi, T.; Shiratori, K.; Takeda, K.; Akira, S.; Saijo, S.; Iwakura, Y.; Adachi, Y.; Ohno, N.; Suzuki, K.; Fujita, J.; Kaku, M.; Kawakami, K. Deoxynucleic Acids from Cryptococcus Neoformans Activate Myeloid Dendritic Cells via a TLR9-Dependent Pathway. *The Journal of Immunology* **2008**, *180* (6), 4067–4074. https://doi.org/10.4049/jimmunol.180.6.4067.

(49) Grahnert, A.; Richter, T.; Piehler, D.; Eschke, M.; Schulze, B.; Müller, U.; Protschka, M.; Köhler, G.; Sabat, R.; Brombacher, F.; Alber, G. IL-4 Receptor-

Alpha-Dependent Control of Cryptococcus Neoformans in the Early Phase of Pulmonary Infection. *PLoS One* **2014**, *9* (1), e87341. https://doi.org/10.1371/journal.pone.0087341.

(50) dos Anjos Cassado, A. F4/80 as a Major Macrophage Marker: The Case of the Peritoneum and Spleen. *Macrophages* **2017**, 161–179.

(51) Pépin, E.; Goutet, M.; Ban, M. Murine Bone Marrow-Derived Dendritic Cells as a Potential in Vitro Model for Predictive Identification of Chemical Sensitizers. *Toxicology letters* **2007**, *175* (1–3), 89–101.

(52) Wan, H.; Dupasquier, M. Dendritic Cells in Vivo and in Vitro. *Cellular & Molecular Immunology* **2005**.

(53) Rogers, P. B.; Driessnack, M. G.; Schwartz, E. H. Analysis of the Developmental Stages, Kinetics, and Phenotypes Exhibited by Myeloid Cells Driven by GM-CSF in Vitro. *PLOS ONE* **2017**, *12* (7), e0181985. https://doi.org/10.1371/journal.pone.0181985.

(54) Bolaños, B.; Mitchell, T. G. Phagocytosis of Cryptococcus Neoformans by Rat Alveolar Macrophages. *Journal of Medical and Veterinary Mycology* **1989**, *27* (4), 203–217. https://doi.org/10.1080/02681218980000291.

(55) Levitz, S. M.; DiBenedetto, D. J. Paradoxical Role of Capsule in Murine Bronchoalveolar Macrophage-Mediated Killing of Cryptococcus Neoformans. *J Immunol* **1989**, *142* (2), 659–665.

(56) Granger, D. L.; Perfect, J. R.; Durack, D. T. Virulence of Cryptococcus Neoformans. Regulation of Capsule Synthesis by Carbon Dioxide. *J Clin Invest* **1985**, *76* (2), 508–516. https://doi.org/10.1172/JCI112000.

(57) Vecchiarelli, A.; Pietrella, D.; Lupo, P.; Bistoni, F.; McFadden, D. C.; Casadevall, A. The Polysaccharide Capsule of Cryptococcus Neoformans Interferes with Human Dendritic Cell Maturation and Activation. *Journal of Leukocyte Biology* **2003**, *74* (3), 370–378. https://doi.org/10.1189/jlb.1002476.

(58) Halcrow, P. W.; Geiger, J. D.; Chen, X. Overcoming Chemoresistance: Altering PH of Cellular Compartments by Chloroquine and Hydroxychloroquine. *Frontiers in Cell and Developmental Biology* **2021**, *9*, 170.

(59) Xia, M.-C.; Cai, L.; Zhang, S.; Zhang, X. A Cell-Penetrating Ratiometric Probe for Simultaneous Measurement of Lysosomal and Cytosolic PH Change. *Talanta* **2018**, *178*, 355–361.

(60) Zurier, R. B.; Hoffstein, S.; Weissmann, G. Cytochalasin B: Effect on Lysosomal Enzyme Release from Human Leukocytes. *Proceedings of the National Academy of Sciences* **1973**, *70* (3), 844–848.

(61) Koza, E. P.; Wright, T. E.; Becker, E. L. Lysosomal Enzyme Secretion and Volume Contraction Induced in Neutrophils by Cytochalasin B, Chemotactic Factor and A23187. *Proceedings of the Society for Experimental Biology and Medicine* **1975**, *149* (2), 476–479.

(62) Tapper, H.; Sundler, R. Bafilomycin A1 Inhibits Lysosomal, Phagosomal, and Plasma Membrane H+-ATPase and Induces Lysosomal Enzyme Secretion in Macrophages. *Journal of cellular physiology* **1995**, *163* (1), 137–144.

(63) Hsu, V. W.; Prekeris, R. Transport at the Recycling Endosome. *Current Opinion in Cell Biology* **2010**, *22* (4), 528–534. https://doi.org/10.1016/j.ceb.2010.05.008.

(64) DeLeon-Rodriguez, C. M.; Casadevall, A. Cryptococcus Neoformans: Tripping on Acid in the Phagolysosome. *Frontiers in Microbiology* **2016**, *7*.

(65) Zhang, L.; Zhang, K.; Li, H.; Coelho, C.; de Souza Gonçalves, D.; Fu, M. S.; Li, X.; Nakayasu, E. S.; Kim, Y.-M.; Liao, W.; Pan, W.; Casadevall, A. Cryptococcus Neoformans-Infected Macrophages Release Proinflammatory Extracellular Vesicles: Insight into Their Components by Multi-Omics. *mBio 12* (2), e00279-21. https://doi.org/10.1128/mBio.00279-21.

(66) Canton, J.; Khezri, R.; Glogauer, M.; Grinstein, S. Contrasting Phagosome PH Regulation and Maturation in Human M1 and M2 Macrophages. *Mol Biol Cell* **2014**, *25* (21), 3330–3341. https://doi.org/10.1091/mbc.E14-05-0967.

CHAPTER 3: A MULTI-FLUOROPHORE STAINING SCHEME FOR IDENTIFICATION AND QUANTIFICATION OF VOMOCYTOSIS

3.1 Abstract:

Vomocytosis is a process by which fungal pathogens, primarily *Cryptococcus neoformans*, escape from the digestive phagosome compartment of phagocytic immune cells after ingestion. Interestingly, this expulsion leaves both the pathogen and phagocyte unharmed and is believed to be an important mechanism by which CNs disseminate throughout infected hosts. This phenomenon was relatively recently discovered in 2006, and research to date has relied almost entirely on quantification via manual counting of vomocytosis events in time-lapse microscopy videos. This archaic method has the significant disadvantages of requiring excessive labor in manual analysis, limited through-put capabilities, and low accuracy due to subjectivity. Here, we present a superior alternative method to measure vomocytosis rates using a novel, multi-fluorophore reporter system comprised of two in-tube staining steps during infection and a flow cytometry readout. This approach overcomes the limitations of conventional time lapse microscopy methods, with key advantages of high throughput capability, simple procedural steps, and accurate objective readouts. This study rigorously characterizes this vomocytosis reporter system in CN-infected MΦ and DC cultures, and further translates the staining scheme to measure potential expulsion of biomaterial particles. Ultimately, the fluorescent reporter system presented here provides a universal tool for vomocytosis rate measurement of phagocytosed material. This facile approach opens the door to new types of vomocytosis-related studies such

as high throughput treatment mechanistic screening and downstream characterization of expelled material.

3.2 Introduction

Pathogens have evolved over time to evade the host immune system in various ways. The fungal species, *Cryptococcus neoformans* (CN), is equipped with numerous mechanisms to resist and avoid the innate immune system. One primary example is CN's ability to persist within the acidic phagolysosome following engulfment by phagocytes, and escape through a process called vomocytosis, or nonlytic exocytosis, while leaving the host and pathogen cells unharmed[1–4]. This unique attribute is highly relevant to mechanisms of fungal dissemination within infected hosts. After entering a host via inhalation, these fungal cells first encounter alveolar macrophages (MΦ) within the lung that ingest the invading CN. However, rather than digesting and killing the pathogens, these immune cells instead are modulated to act as a shuttle to transport infection throughout the body. This is possible due to the ability of CN to survive within the digestive phagosome and trigger vomocytic escape after several hours[5]. Through this 'Trojan Horse' mechanism of dissemination, infection can even cross the highly guarded blood brain barrier into the central nervous system of the host in a condition called cryptococcal meningitis (CM). Primarily affecting immunocompromised individuals, including an estimated 220,000 HIV/AIDS patients, CM causes ~181,000 deaths/ year worldwide[6]. Crucially, greater understanding of vomocytosis could lead to the development of new CM treatments for patients.

Due to the relevance of MΦs in CM infections, vomocytosis studies thus far have primarily focused on the occurrence of this event in this one cell type. However, other phagocytic cell types— neutrophils[7] and dendritic cells (DCs)[8]— have recently been documented to perform vomocytosis of CN during infection. However, the underlying mechanisms of this phenomenon are mostly unknown, with only a small handful of phagosomal properties, proteins, and immunological phenotypes known to affect expulsion rates[3,4].

To efficiently study vomocytosis, a robust method for quantifying phagocytosis and expulsion rates is needed. However, there is currently a deficiency in availability of effective techniques for measuring the occurrence of these expulsion events. Present studies rely primarily on manual counting of vomocytic events via time lapse microscopy of unstained or fluorescently stained phagocyte infections with CN. While straightforward, time lapse microscopy quantification of vomocytosis is a highly time consuming and labor-intensive option, as hundreds of hours of cell culture footage must be stored and analyzed manually for just a limited number of data replicates. Another limitation of this technique is the necessity for access to or ownership of expensive time lapse microscopy and in-stage cell incubation equipment. Lastly, a crucial drawback of time lapse microscopy is that video analysis is highly subjective; even when analyzed in a blinded manner, the accuracy of such measurements is highly unreliable, especially when attempting to distinguish marginal differences in vomocytosis rates between treatment groups. Other than time lapse microcopy, there is another method developed by *Nicola et al.* that uses a fluorescence-activated cell sorting (FACS) centered approach for detecting expulsion of CN from phagocytes[9]. The process involves using

staining and FACS to isolate live phagocytes with internalized CNs, then incubating this subpopulation for a given period and analyzing via flow cytometry at the end point to determine which intact phagocytes no longer contain CN. The approach has advantages over time lapse microscopy in allowing for objective quantification of expulsion in a systematic manner, and has been used in multiple studies to measure vomocytosis rates[7,9–11]. However, this method also displays significant limitations. In a similar drawback to time lapse microscopy, the Nicola et al. protocol requires use of expensive FACS equipment which may not be available or accessible to most labs. Importantly, another key limitation of this staining protocol is its narrow use-case, only being compatible with capsular fungal cells such as CN. The technique does not have the capability to measure expulsion rates of other microbes or non-biological particulates due to its required use of the fungal extracellular stain, Uvitex 2B, which is only applicable for fungal cells. In its current state, the field of vomocytosis research is in need for new methodologies of quantifying expulsions that can overcome the long-standing limitations of conventional approaches.
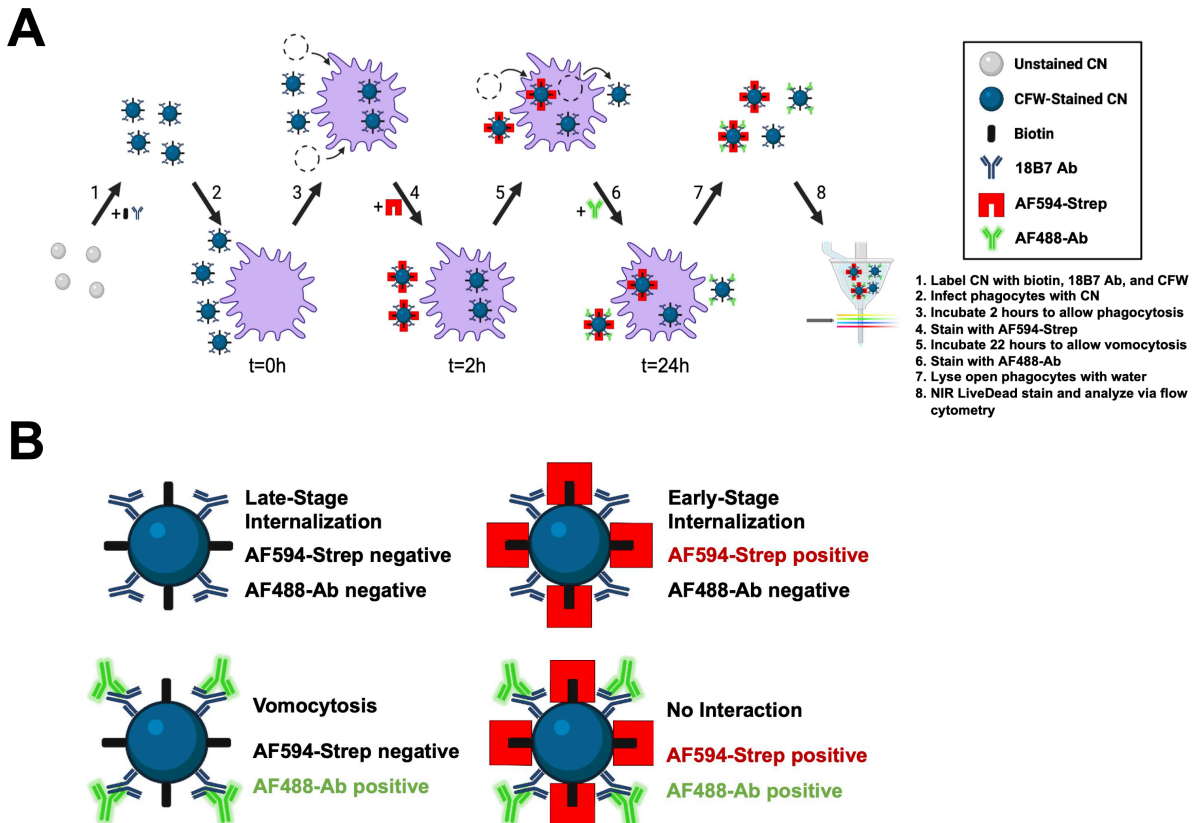
Figure 3.1. Schematic illustrating the design of the vomocytosis reporter system. (**A**) The experimental steps of the reporter system consist of (1) conjugating biotin to CN via NHS chemistry, opsonizing with 18B7 Ab, and labeling with CFW fungal stain; (2) infect CN with phagocytes at a 2:1 CN:phagocyte ratio; (3) incubate for 2 hours to allow for phagocytosis of CN; (4) apply AF594-Strep to culture to stain only extracellular CN at this timepoint and confirm internalization; (5) incubate for 22 more hours to allow for vomocytosis events to occur; (6) apply AF488-Ab to culture to stain only extracellular CN at this timepoint and confirm expulsion; (7) lyse open phagocytes using sterile water to release any internalized CN; (8) apply NIR LiveDead stain on CN to identify and remove non-live fungal cells, and run flow cytometry analysis of CN fluorescence. (**B**) Based primarily on the two key reporter fluorescent stains of AF594-Strep and AF488-

Ab, there are 4 different scenarios for CN outcome of incubation with phagocytes. Either double negative (phagocytosed prior to AF594-Strep stain, and remains internalized: "late-stage internalization"), single positive AF594-Strep (phagocytosed after AF594-Strep stain, and remains internalized: "early-stage internalization"), single positive AF488-Ab (vomocytosed), and double positive (no interaction with phagocytes during experiment).

This study outlines a novel, multi-fluorescent reporter system staining scheme that enables precise monitoring of phagocytic entry and vomocytic expulsion of CN from phagocytes during infection. This system is composed of a pre-labeling step of CN followed by two extracellular stains during infection, and finally flow cytometry analysis of stained CN (**Figure 3.1A**). Prior to infection, the CN are coated with biotin using NHS chemistry. Additionally, the CN are pre-labeled with a fungal tracking dye Calcofluor White (CFW) and opsonized with an anti-capsule 18B7 antibody (18B7 Ab). Following a 2-hour phagosomal ingestion incubation period, a fluorescent AlexaFluor (AF) 594-conjugate of streptavidin (AF594-Strep) is applied to targeting biotin on the surface of external CN located outside of the phagosome. This step is used to distinguish phagocytosed from non-phagocytosed CN at this time point. Next, at an ending time point of 24 hours after initial infection, any external CNs are stained using a fluorescent AF488 secondary antibody (AF488-Ab) targeting the 18B7 Ab present on the surface of external CN. This second stain is used to determine which CNs have been exocytosed; while some CN may enter and exit during this period, those cases are minimized by removing the opsonizing 18B7 Ab following the phagocytosis period to reduce further

internalization. These selective extracellular stains are achievable due to the bulky nature of AF594-Strep and AF488-Ab. Finally, phagocytes are lysed via sterile water to free any internalized CN, and a Near-IR Dead Cell Stain Kit (NIR LiveDead) is applied to identify between live and killed fungal cells. Through assessing each fungal cell via flow cytometry, the fluorescence of these two key reporter stains (AF594-Strep and AF488-Ab) are able to distinguish between the 4 outcome scenarios of CN following incubation with phagocytes— (i) phagocytosis prior to AF594-Strep labeling: "late-stage internalization", (ii) phagocytosis after AF594-Strep labeling: "early-stage internalization", (iii) phagocytosis prior to AF594-Strep labeling, then expulsion and labeling with AF488-Ab: "vomocytosis", and (iv) remaining extracellular for both AF594-Strep and AF488-Ab labeling: "no interaction" (**Figure 3.1B**). In this study, the functionalities of the reporter system components are demonstrated through fluorescence microscopy, flow cytometry, and confocal microscopy. Then, the full reporter staining protocol is used to detect real vomocytosis rates of CN following incubation with either MΦ or DC phagocyte types. The reporter system is shown to also distinguish differences in vomocytosis occurrence of CN-infected cultures treated with drugs that modify the phagosomal physicochemical environment and actin polymerization. Additionally, single cell Raman scattering of FACS-sorted reporter-stained CN cells is used to confirm that these fungal populations indeed have distinct biochemical compositions depending on outcome of phagocyte interaction for either infection of MΦ or DC. Finally, the reporter system protocol is adapted to detect expulsion rates of poly(lactic-co-glycolic) (PLGA) microparticles (MPs) phagocyted by

MΦs or DCs to demonstrate the flexibility of this universal system to objectively quantify phagocytic expulsion of both pathogenic fungi and biomaterial particles.

3.3 Materials & Methods

Bone marrow-derived MΦ and DC Culture

Phagocytes were grown via differentiating bone marrow progenitor cells from 8 to 12 week old C57BL/6 mice as described in previous studies[12]. Cell media used was DMEM/F-12 1:1 with L-glutamine (Cellgro, Herndon, VA) and contained 10% fetal bovine serum (R&D Systems, Minneapolis, MN), 1% nonessential amino acids (Lonza, Walkersville, MD), 1% sodium pyruvate (Lonza), 1% penicillin/streptomycin (Cytiva, Marlborough, MA), and a differentiation factor. For MΦ media, the differentiation factor was M-CSF supplied by 20% L929-treated media. The differentiation factor for DC media was 20ng/mL GM-CSF (R&D Systems). Cells were plated on day 6 of culture and used for experiments between day 8-12.

Cryptococcus Neoformans *Culture*

A *Cdc24* mutant strain of CN (generously gifted by Dr. Angie Gelli, UC Davis, CA) was used for the entirety of this study due to its phenotype of not being able to replicate at 37°C[13]. We avoided using wildtype CN that has the natural ability to divide at 37°C within hosts[14] during infections which may reduce the accuracy of the reporter system. Prior to infection, CN were grown first by streaking a frozen culture on yeast peptone dextrose (YPD) agar (Thermo Fisher Scientific, Waltham, MA) at 30°C. Once

visible colonies formed, a single colony of CN was transferred to YPD broth (Thermo Fisher Scientific) and left shaking overnight at 30°C.

Pre-Labeling of CN For Reporter Staining

Before infection or reporter staining, CN were first labeled with biotin. Biotin was conjugated to the surface of the fungal cells using N-Hydroxysuccinimide (NHS) chemistry; 10 million CN per ml were incubated with 2mg/ml NHS-dPEG®12-biotin (Sigma, St. Louis, MO) for 45 minutes. Following this labeling, excess reagents were washed 3x with PBS via centrifugation. Next, CN were stained with a fluorescently active fungal dye CFW (Sigma) at a concentration of 1mg/ml for 15 minutes, then washed 3x using 1% w/v of bovine serum albumin (BSA, Sigma) in PBS (hereby referred to as 'protein buffer') via centrifugation. Finally, the fungal cells were coated with 10µg/ml of anti-capsular 18B7 Ab (supplied from both Sigma and the Casadevall Lab, Johns Hopkins University, MD) for 30 minutes. For brevity, CN labeled with biotin, CFW, and 18B7 Ab are simply referred to as 'pre-labeled CN'.

Fluorescence Microscopy of Reporter-Stained CN Infections

Fluorescence microscopy was utilized for visual assessment of CN reporter staining. Macrophages were seeded onto a 12 well culture plate at a density of 100k cells per well. Next, the phagocytes were infected with pre-labeled CN at a 2:1 CN:phagocyte ratio for 2 hours, then rinsed 3 times with warm PBS. Reporter stains of either 5µg/ml AF594-Strep (Biolegend, San Diego, CA) or 10µg/ml AF488-Ab (polyclonal goat anti-mouse IgG, Thermo Fisher Scientific) were applied to the adherent

infected culture for 30 minutes in protein buffer. Cells were then gently rinsed with warm PBS 3x and imaged using a BZ-X Fluorescence Microscope (Keyence, Itasca, IL) for CFW fluorescence (DAPI filter cube, Keyence) AF594-Strep signal (TxRed filter cube, Keyence), and AF488-Ab signal (GFP filter cube, Keyence).

Confocal Fluorescence Microscopy of Reporter-Stained CN Infections

Reporter staining was also assessed via confocal microscopy for z-stack resolution of CN localization. Prior to infection, MΦs were stained with 1μM of 1,1'-Dioctadecyl-3,3,3',3'-Tetramethylindodicarbocyanine, 4-Chlorobenzenesulfonate Salt (DiD, Thermo Fisher Scientific) as a lipophilic dye tracer and seeded onto a glass chamber slide. Phagocytes were infected 2:1 phagocyte:CN with pre-labeled CN. After a 2-hour incubation to allow for phagocytosis, the culture was rinsed 3x with PBS and stained with either 5μg/ml AF594-Strep or 10μg/ml AF488-Ab in protein buffer. After 3 additional washes, cells were fixed with 2% paraformaldehyde diluted with PBS and imaged using the Olympus FV3000 confocal (Olympus Corporation, Westborough, MA) at 60x magnification.

Reporter System Measurement of CN Vomocytosis Events Via Flow Cytometry

To test the performance of the reporter system, CN-infected phagocyte cultures were assessed for vomocytosis occurrence. First, adherent phagocytes (MΦ or DC) that were grown on a 6 well culture plate at ~1 million cells per well were lifted into suspension via incubation with warm PBS with 2.5mM ethylenediaminetetraacetic acid (EDTA) and 2.5mM dextrose, then scraped after 10 minutes. Macrophages or DCs in

media were infected with pre-labeled CN at a 2:1 CN:phagocyte ratio while in suspension; these cultures were kept within individual tubes and incubated at 37°C with lids open while loosely covered with aluminum foil to allow air exchange. Following 2 hours to allow for phagocytosis, the cultures were rinsed once with protein buffer via centrifugation. The cultures were then stained with AF594-Strep at a 5μg/ml concentration for 30 minutes, rinsed with protein buffer, and resuspended in warm fresh media. After 22 hours, or 24 hours after phagocytosis, 10μg/ml fluorescent AF488-Ab was applied to the infected cultures for 30 minutes and subsequently rinsed with protein buffer. Next, the phagocytes within the tubes were lysed via incubation in cold sterile water for 30 minutes. To assess the viability of the CN, a Near-IR Dead Cell Stain Kit (NIR LiveDead, Thermo Fisher Scientific) was applied according to the manufacturer's instructions. The LiveDead selectively labels dead cells by staining the intracellular proteins of those cells with compromised membranes. Finally, the stained CN were fluorescently analyzed via flow cytometry on an Attune NxT Flow Cytometer (Thermo Fisher Scientific). Refrigerated controls were treated identically to Live CN-infected groups, except after AF594-Strep staining the cultures were kept in 4°C for the remainder of the experiment. For heat-killed (HK) CN controls, the CN were placed in a heat block at 70°C for 1 hour prior to labeling and infection; the methods are otherwise identical to that of live CN. For flow cytometry analysis, vomocytosis events were categorized as CFW positive, AF594-Strep negative, and AF488-Ab positive, with dead cell events removed from the final statistic (NIR LiveDead positive cells removed). Vomocytosis percentage was calculated by dividing the vomocytosis events by the phagocytosed population (CFW positive and AF594-Strep negative events).

Flow Cytometry Evaluation of Phagocyte Viability Following CN Infection

To assess the viability of phagocytes during infection conditions, DCs or MΦs were first stained with 1μM DiD as a tracking label. Then, the phagocytes were either left uninfected or were infected with live or HK CN at a 2:1 CN:phagocyte ratio (200k CN, 100k phagocyte) for 24 hours in suspension. The cells were then stained with Propidium Iodide (PI, Sigma) at a concentration of 2μg/ml in 0.1% BSA in PBS buffer for 30 minutes. Via flow cytometry, phagocyte viability was assessed by first gating on DiD positive cells, then assessing the percent positive gated for PI (dead) signal.

Measurement of Vomocytosis Rates Using Reporter System for Drug-Treated Phagocyte Cultures Infected With CN

The reporter staining procedure for drug-treated experimental groups was identical to non-drug treated groups as outlined previously. For drug-treated groups, the phagocytes were first infected with CN in drug-free media. However, following AF594-Strep staining, these groups were then incubated with the relevant drug-containing media for the remainder of infection. Cells were treated with 100nM of bafilomycin A1 (BFA, Sigma), 4μM cytochalasin B (CYT hi, Sigma), 100nM cytochalasin B (CYT lo), or 10μM chloroquine (CQ, Thermo Fisher Scientific). These drugs and their concentrations were selected based on relevant reference experiments from vomocytosis studies[7–9,15,16].

Reporter-Stained CN FACS Sorting and Post-Sort Purity Analysis

Prior to FACS sorting, phagocytes (MΦ or DC) were infected with live pre-labeled CN in suspension as previously outlined. Throughout the 24-hour infection, the culture was stained with the reporter components, lysed to liberate intracellular CN, and NIR LiveDead stained using identical methods outlined for prior reporter experiments. The resulting stained CN were kept on ice and sorted using an Astrios EQ (Beckman Coulter, Brea, CA) by the UC Davis Flow Core. Events were first gated for positive CFW and negative NIR LiveDead signal, then sorted by AF594-Strep and AF488-Ab signal into 4 separate tubes with a minimum of 1000 events each for both MΦ and DC (8 sorted tubes total). Small allocations of each sorted sample were then run on the Attune NxT Flow Cytometer to assess post sort purity, again gated on positive CFW and negative LiveDead.

Single cell laser trap Raman scattering (LTRS) analysis of reported-sorted CN during infection

The LTRS spectra were acquired using a custom-built inverted Raman scanning confocal microscope with an excitation wavelength of 785 nm and a 60×, 1.2 NA water immersion objective on an inverted IX73 Olympus microscope. Raman spectra were recorded via an Andor Kymera-3281-C spectrophotometer and Newton DU920P-BR-DD CCD camera. Preliminary *in situ* data processing was performed using Solis v4.31.30005.0 software. The physical background of LTRS is based on using a tightly focused laser beam to form an optical trap[17–19]. The same beam is also used to excite Raman scattering from the irradiated samples of interest. This approach enables highly sensitive chemical manipulation and characterization single optically trapped particles such as CN in aqueous environment. The laser exposure time was set to 60 s per scan

(i.e. one single trapped cell was irradiated for 60 s), with a laser power of ~65 mW, and pinhole aperture set to 1 mm. At least 10 individual spectra were collected per each sample type (total 8 sample types). The post-collection spectra analysis was performed using custom scripts written in MATLAB v2021b (MathWorks, MA, USA). Spectral post-collection included cosmic ray removal, penalized least-squares (PLS) background correction, smoothing, and normalization. Since in biological samples the spectral fingerprint region ~800-1800 cm^{-1} is pertinent to downstream analyses, the spectra were cropped to contain this region. Subsequently, the processed spectral sets were subjected to principal component analysis (PCA) and hierarchical clustering analysis based on the corresponding MATLAB built-in functions[20,21]. The custom MATLAB scripts and the associated in-house spectra processing software can be provided on request.

Fabrication and Preparation of PLGA MPs for Reporter System Experiments

Phagocytosable PLGA MPs were created using an oil-in-water emulsion using a Tissuemiser homogenizer (OMNI, Kennesaw, GA) as described in previous studies[12]. A 1:1 blend of acid-terminated PLGA (PURASORB PDLG 5004A from Corbion, Amsterdam, Netherlands) and 8-arm PLGA-Azide (Nanosoft Polymers, Winston-Salem, NC) were used, both with 50:50 lactic-to-glycolic acid ratio and 20kDa molecular weight parameters.

To functionalize the PLGA MPs for reporter experiments, the particles were first conjugated with biotin using click chemistry via incubation with 100µM Biotin-dPEG®12-DBCO (Sigma) for 30 minutes. The MPs were then washed with PBS and stained with FITC again utilizing click chemistry via incubation with 100µM DBCO-PEG2000-

fluorescein (Nanocs, New York City, NY) for 30 minutes. Finally, the functionalized PLGA MPs were rinsed with protein buffer via centrifugation to remove remaining reagents. For conciseness, these PLGA MPs with conjugated biotin and FITC are hereby referred to as 'pre-labeled PLGA MPs'.

Fluorescence Microscopy Visualization of Reporter-Stained PLGA MP Following Phagocytosis by MΦs

For fluorescence microscopy experiments, MΦs were seeded onto a 12 well plate at a density of 100k cells per well. Then, pre-labeled PLGA MPs were incubated with the MΦs at a 10:1 MP:phagocyte ratio. After a 1-hour phagocytosis period, excess MPs were washed off via rinsing with PBS three times. Cultures were either left unstained, stained with 5µg/ml AF594-Strep, or stained with 20µg/ml allophycocyanin (APC) conjugate of anti-FITC antibody (APC-Ab, FIT-22 Mouse Clone, Biolegend) in protein buffer for 30 minutes. Excess dye was rinsed off using protein buffer and the *in vitro* cultures were imaged using a BZ-X Fluorescence Microscope for FITC fluorescence (GFP filter cube) AF594-Strep signal (TxRed filter cube), and APC-Ab signal (Cy5 filter cube, Keyence).

Reporter Staining and Flow Cytometry Measurement of PLGA MP Pseudo Vomocytosis Rates After Incubation with Phagocytes

Pre-labeled PLGA MPs were incubated with MΦs or DCs at a 5:1 MP:phagocyte ratio for 1 hour in suspension to allow for phagocytosis. The resulting cultures were then stained with 5µg/ml AF594-Strep for 30 minutes. Then, one group was split into two

tubes, one of which was treated with sterile water for lysis, and the other left unlysed; then the two tubes were recombined and together this was called the 'partial lysis' condition. Next, the culture was stained with 20µg/ml APC-Ab for 30 minutes as an extracellular stain for the FITC tracker on the surface of the PLGA MPs. For the unlysed control, the culture was stained with APC-Ab without prior lysis. Following this stain, the groups were then fully lysed by sterile water and rinsed with protein buffer and analyzed via flow cytometry. Vomocytosis events were categorized as FITC positive, AF594-Strep negative, and APC-Ab positive. Vomocytosis percentage was calculated by dividing the vomocytosis events by the phagocytosed population (events positive for FITC and negative for AF594-Strep).

Data and Statistical Analysis

Statistical analyses were performed using GraphPad Prism 9. Comparison between reporter-measured vomocytosis rates were evaluated via one-way ANOVA corrected for multiple comparisons by false discovery rate (FDR) using a two-stage linear step-up procedure of Benjamini, Krieger and Yekutieli via GraphPad Prism 9. This same method was also used to statistically compare the viability of phagocytes under different infection conditions. For experiments comparing reporter measurements of PLGA MP expulsion from phagocytes, an unpaired t-test was used as there were only two groups (unlysed and partial lysis) to compare. All data shown include at least three independent experiments with phagocytes sourced from the bone marrow of separate mice. All column graphs, generated on GraphPad Prism 9, display the individual data points, mean, and standard deviation (SD).

3.4 Results

AF594-Strep and AF488-Ab Reporter Components Selectively Stain Extracellular CN During In Vitro *Phagocyte Infection*

For the reporter system to function properly, the AF594-Strep and AF488-Ab stains must selectively stain only extracellular CN during infection. To investigate the performance of the reporter stains, MΦs were infected with pre-labeled CN and stained with AF594-Strep or AF488-Ab following phagocytosis, then analyzed via fluorescence microscopy and flow cytometry (**Figure 3.2A**). Through fluorescence imaging, AF488-Ab (green) and AF594-Strep (red) labeling of CN (blue) show the selectivity of each stain for extracellular CN only, while phagocytosed CN remain unstained (**Figure 3.2B**). Additionally, following lysis of reporter-stained cultures, flow cytometry analysis of AF594-Strep and AF488-Ab signal can be used to create gates for internalized or externalized CN (**Figure 3.2C**). Additionally, through confocal imaging of fixed cultures following reporter staining, the selectivity of each stain for external CN can be clearly visualized for both AF594-Strep and AF488-Ab signal (**Figure 3.2D-E**). These results indicate that the reporter system components perform as expected with high enough signal resolution to be distinguishable via microscopy and flow cytometry.
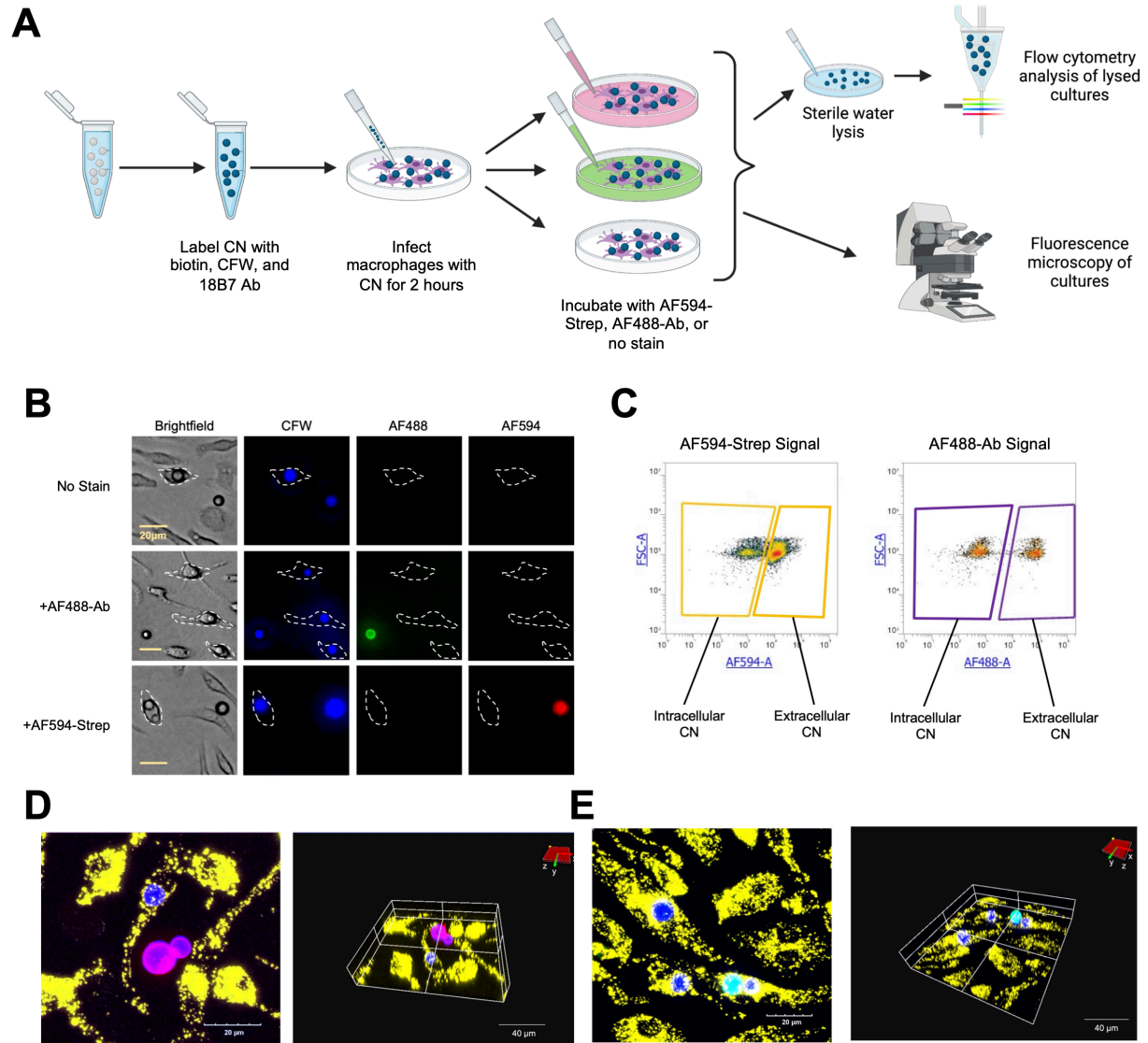
Figure 3.2. AF594-Strep and AF488-Ab extracellular staining ability confirmed via fluorescent microscopy, flow cytometry, and confocal microscopy. (**A**) Schematic of experimental design. Prior to infection, CN were labeled with biotin, CFW, and 18B7 Ab. Then, MΦs were infected with labeled CN and incubated for 2 hours. Cultures were then stained with AF594-Strep, AF488-Ab, or no stain and analyzed via microscopy or flow cytometry. (**B**) Fluorescence microscopy confirmation of extracellular staining. Pre-stain of CFW in blue is shown for all CN in the images. When AF488-Ab stain was applied, any extracellular CN were stained with green AF488 fluorescence. If incubated

with the AF594-Strep stain, cultures displayed red AF594 fluorescence signal only on extracellular CN. Both stains leave internalized CN unstained. (**C**) Flow cytometry confirmation of extracellular staining. Following either AF594-Strep or AF488-Ab staining, both lysed cultures displayed distinct gate-able flow cytometry populations by the respective fluorescence signal. (**D**) Confocal confirmation of AF594-Strep extracellular staining via a combined Z stack (left) and 3D volume render (right). In the images, stains are shown for MΦ (DiD, yellow), CN (CFW, blue), and AF594-Strep (AF594, red). As visualized in the images, only the extracellular CN was stained by AF594-Strep. (**E**) Confocal confirmation of AF488-Strep extracellular staining via a combined Z stack (left) and 3D volume render (right). Stains are shown for MΦ (DiD, yellow), CN (CFW, blue), and AF488-Ab (AF488, green).

Reporter System Quantifies Vomocytosis Rates of CN Following Phagocyte Infection

　　Next, the ability of the reporter system to measure vomocytosis events was assessed. Cultures of MΦs or DCs were infected with pre-labeled CN at a 2:1 CN:phagocyte ratio and stained with AF594-Strep after 2 hours and AF488-Ab after 24 hours. Then, the phagocytes were lysed using sterile water, a NIR LiveDead stain was applied, and the fluorescence of each CN was evaluated using flow cytometry (**Figure 3.3A**). The gating strategy involved first selecting CFW-positive (CN signal), then AF594-Strep negative (internalized at t=2h), then AF488-Ab positive events (exocytosed). Finally, the dead CN were removed from the final vomocytosis statistic based on NIR LiveDead signal gating. (**Figure 3.3B**) This gating strategy displayed a clear vomocytosed population of CN indicating that the reporter system could indeed

112

measure vomocytosis rates. This reporter staining was performed on CN-infected MΦ and DC cultures and compared to HK CN infected and refrigerated (after phagocytosis) negative controls (**Figure 3.3C-D**). For both MΦ and DC infections, the live CN groups displayed significantly higher vomocytosis occurrence than the refrigerated control, which was also significantly higher than the HK-infected control. To test if the vomocytosis events were due to phagocyte lysis during the experiment, the viability of MΦs and DCs during infection was assessed by PI staining and flow cytometry analysis. For both phagocyte types, the un-infected, live-infected, and HK-infected groups displayed minimal toxicity throughout a 24-hour period compared to the dead control (**Figure 3.3E-F**). Overall, these data indicate that the reporter system can be reliably used to measure vomocytosis events of CN-infected MΦs and DCs.
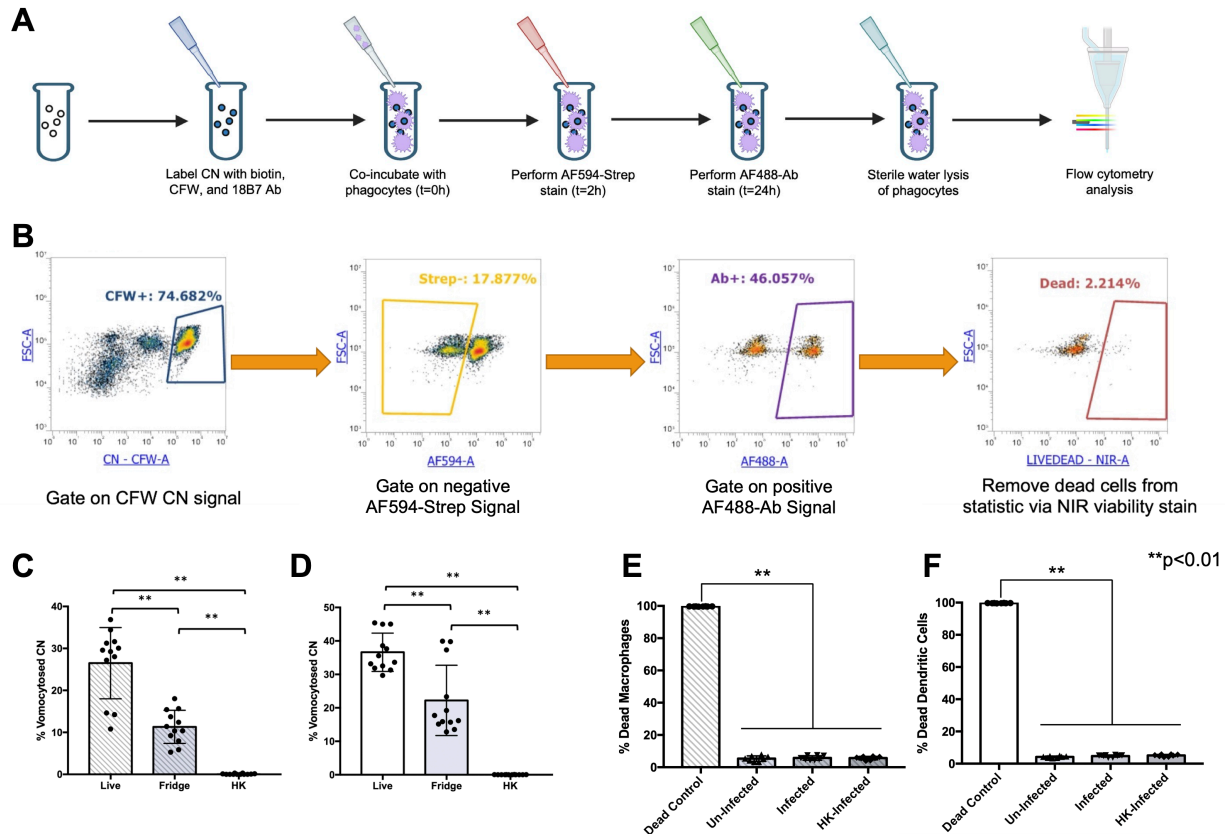
Figure 3.3. Reporter system capability to measure vomocytosis rates of MΦs and DCs. (**A**) Schematic of experimental design for reporter system staining. First, CN are coated with biotin, CFW, and 18B7 Ab. The fungal cells are next incubated with phagocytes (MΦ or DC) at a 2:1 CN:phagocyte for 2 hours to allow for phagocytosis. During the infection, the culture is stained with AF594-Strep at t=2h and AF488-Ab at t=24h. Then, the cultures are lysed using sterile water and analyzed for fluorescence via flow cytometry. (**B**) Gating process for analysis of flow cytometry data. First, only CFW positive events are gated to select CN from debris. Next, negative AF594-Strep signal events are gated to select only CN that were internalized at t=2h. From this population, positive AF488-Ab signal events are gating to measure the percentage of internalized CN that were expelled. Finally, NIR LiveDead signal is used to assess the viability of the

exocytosed CN to remove unviable cells from the final vomocytosis rate calculation. (**C**) Bar graph of reporter-measured CN vomocytosis rates during MΦ infection. Macrophages were infected with live CN or HK CN. Additionally, a refrigerated control was used to slow vomocytosis rates at 4°C during the incubation following AF594-Strep staining. (N=4, n=12) (**D**) Bar graph of reporter-measured CN vomocytosis rates during DC infection. Live CN vomocytosis rates were compared to HK CN and refrigerated controls. (N=4, n=12) (**E**) Bar graph of MΦ viability following CN infection. The viability of un-infected, live-infected, and HK-infected MΦs were assessed via PI staining and compared to a MΦ heat-treated control. (N=3, n=9) (**F**) Bar graph of DC viability following CN infection. The viability of un-infected, live-infected, and HK-infected MΦs were assessed via PI staining and compared to a MΦ heat-treated control. (N=3, n=9) All statistical analyses were one-way ANOVAs corrected for multiple comparisons by false discovery rate (FDR) using a two-stage linear step-up procedure of Benjamini, Krieger and Yekutieli via GraphPad Prism 9.
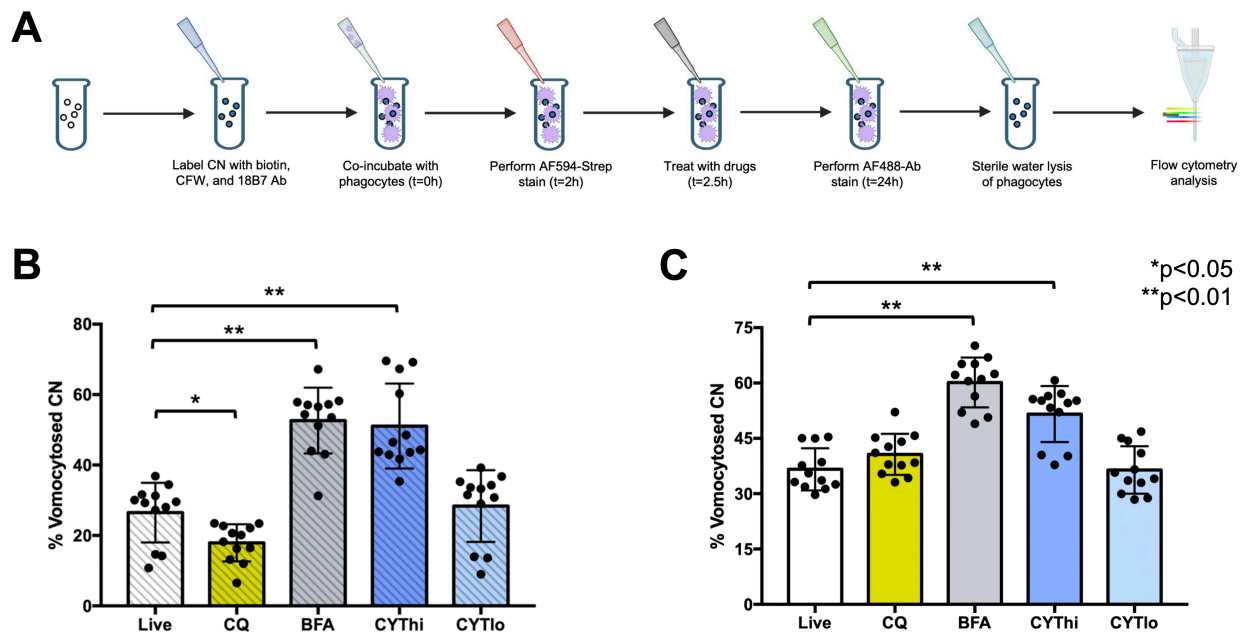
Figure 3.4. Reporter system used to measure differences in vomocytosis rates of phagocytes treated with phagosome or actin modifying drugs. (**A**) Schematic outlining the experimental design for drug-treated reporter system vomocytosis quantification. Briefly, like prior experiments CN were pre-labeled with biotin, CFW, and primary Ab, then incubated with phagocytes (MΦ or DC) for 2 hours. The AF594-Strep stain was then performed, followed by drug treatment. At the end time point of 24 hours, AF488-Ab staining was performed. Subsequently, phagocytes were lysed, and CN were analyzed via flow cytometry for vomocytosis rate assessment. (**B**) Bar graph of vomocytosis rates of CN during drug-treated MΦ infections. Macrophages infected with live CN were treated with CQ, BFA, CYT hi, or CYT lo drug incubations following phagocytosis and the vomocytosis rates of CN were measured using the reporter system. (N=4, n=12) (**C**) Bar graph of vomocytosis rates of CN during drug-treated DC infections. Dendritic cells were infected with live CN, then treated with CQ, BFA, CYT hi, or CYT lo drug incubations following phagocytosis. Vomocytosis rates of CN were

subsequently measured via reporter system. (N=4, n=12) All statistical analyses were one-way ANOVAs corrected for multiple comparisons by false discovery rate (FDR) using a two-stage linear step-up procedure of Benjamini, Krieger and Yekutieli via GraphPad Prism 9.

Reporter System Detects Differences in Vomocytosis Occurrence During Drug-Treated Conditions

Vomocytosis is known to involve modulation of the phagosomal environment including pH[9,22–24] and disruption of actin structure within the host phagocyte[15]. To further characterize the reporter system's ability to detect differences in vomocytosis rates, MΦs or DCs infected with CN were treated with phagosome and actin modifying drugs (**Figure 3.4A**). The drugs used were CQ (a weak base known to increase phagosomal pH[25,26]), BFA (an ATPase inhibitor that prevents acidification and lysosome fusion in phagosomes[27,28]), or CYT (an inhibitor of actin polymerization and modulator of lysosomal fusion[29,30]) (**Figure 3.4A**). Cytochalasin B was used at two different concentrations of CYT hi (4 µM) or CYT lo (100 nM) due to the variability in literature. In MΦ cultures, the CQ treated group displayed a significantly reduced vomocytosis rate while the BFA and CYT hi treated groups had higher expulsion occurrences (**Figure 3.4B**). For DC infected with CN, the BFA and CYT hi groups also recorded higher incidences of vomocytosis measured by the reporter system (**Figure 3.4C**). Interestingly, the finding that CQ reduces MΦ vomocytosis rates conflicts with prior studies investigating J774 MΦ cell lines by *Ma et al.* and *Nicola et al.* but is in agreement with other observations in neutrophils and DCs[2,7–9]. The significant increase

in vomocytosis rates in BFA-treated MΦ and DC infections differs from observations by *Nicola et al* (in J774 MΦ) and *Pacifici et al* (in primary DCs) that BFA-treatment decreases expulsion rates[8,9]. All these findings differ from *Yang et al*'s results showing that neutrophil vomocytosis rates are unaffected by BFA treatment[7]. Lastly, the observed increase in vomocytosis rates for CYT hi-treated MΦ and DC groups is in line with previous studies investigating J774 MΦs by *Alvarez et al* and neutrophils by *Yang et al*[7,9]. However, again there exists disagreement within literature, with decreases in CYT-modulated vomocytosis rates seen in J774 MΦs by *Dragotakes et al.* and DCs by *Pacifici et al*[8,16]. This inconsistency in prior studies may be due to the variety of cell types, cell sources, and vomocytosis measurement methodologies. Despite some differences compared to already conflicting literature, these findings indicate that the reporter system can measure differences in vomocytosis rates of drug-treated groups with high resolution and repeatability in our experimental settings.

Reporter System Detects Differences in Pre-Filtered Exocytosis Occurrence and the Viability of Exocytosed CN

In measuring the vomocytosis rates using the reporter system, the dead CN were filtered out of the final calculation due to vomocytosis being defined as both the host and pathogen remaining alive. However, we still presented the total exocytosed CN (dead included) data in **Figure 3.S1A,C** to gain further resolution on what is occurring during the infection with MΦs and DCs. When analyzing the unfiltered expulsion events, the HK CN and refrigerated groups still displayed lower rates than the live CN group for both MΦ and DC infections, although the HK CN group showed a non-zero number of

expulsions, unlike the vomocytosis statistics. For both CN-infected MΦs and DCs, still the BFA and CYT hi groups displayed higher unfiltered expulsions than the live control. However, infected DCs interestingly showed higher CN expulsions in the CQ-treated group. Unlike the vomocytosis statistic, the CN-infected MΦ group treated with CQ did not see any significant difference from the control group. (**Figure 3.S1A,C**) In investigating the viability of exocytosed CN, the percentage of killed CN was observed to be significantly higher in the CQ-treated group for both MΦ and DC infections. (**Figure 3.S1B,D**) This is in line with reports that CQ has some anti-fungal activity in phagocytes[31–33]. Interestingly the CN-infected DC refrigerated group displayed significantly higher % killed expelled CN compared to the control group, which indicates that potentially the CN are sensitive to temperature combined with intraphagosomal conditions.
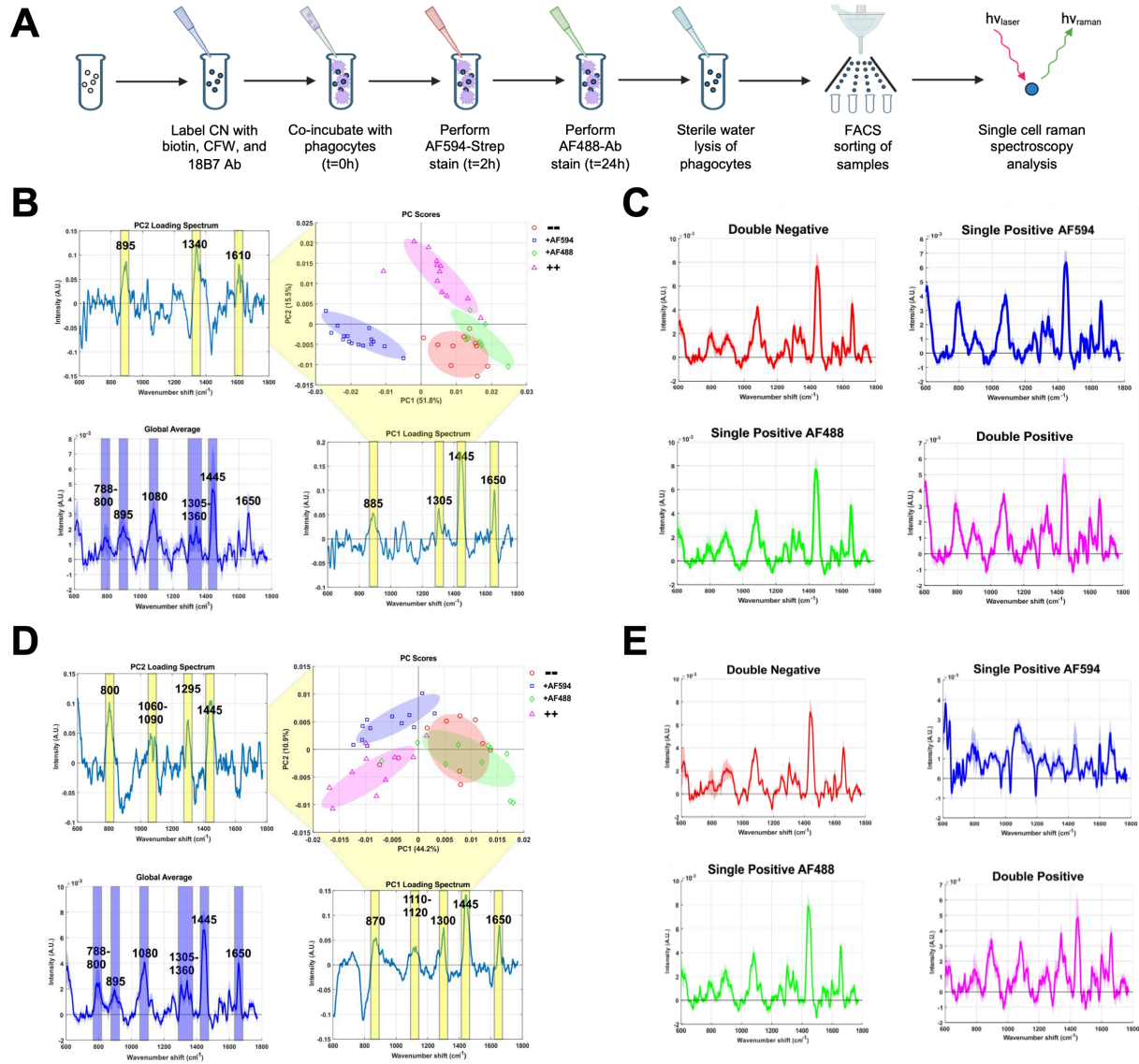
Figure 3.5. Single cell laser trap Raman scattering (LTRS) analysis of reporter system-sorted CN following infection with MΦs or DCs. (**A**) Schematic outlining experimental design for Raman analysis of reporter-sorted CN. Like prior experiments, MΦs or DCs were infected with pre-labeled CN and stained with AF594-Strep and AF488-Ab during infection. Following phagocyte lysis and NIR LiveDead staining, CN were sorted into 4 groups based on reporter fluorescent signals via FACS: double negative, single positive AF594-Strep, single positive AF488-Ab, and double positive groups. Multiple CN (n ≥

10) were evaluated from each of the four populations via single cell LTRS for both MΦ infection and DC infection cultures. (**B**) Principal component analysis of reporter-sorted CN from DC infection. PCA plot displays clustering and separation of the 4 reporter-sorted CN groups (double negative, red circle, late-stage internalization; single positive AF594-Strep, blue square, early-stage internalization; single positive AF488-Ab, green diamond, vomocytosis; double positive, purple triangle, no interaction). (**C**) Individual Raman fingerprints of reporter-sorted CN groups from DC infection. (**D**) Principal component analysis of reporter-sorted CN from MΦ infection. PCA plot displays clustering and separation of the 4 reporter-sorted CN groups. (**E**) Individual Raman fingerprints of reporter-sorted CN groups from MΦ infection.

Reporter-Stained FACS-Sorted CN Groups Display Distinct Compositional Differences Measured by Single Cell Laser Trap Raman Scattering Analysis

The reporter system staining scheme can not only be used to measure vomocytosis rates via analytical flow cytometry but can also be used to sort reporter-stained populations via FACS for downstream analysis purposes. We aimed to characterize the biochemical composition of each reporter-stained CN population scenario for both infected DC and MΦ cultures using single cell laser trap Raman scattering (LTRS) analysis. To achieve this, reporter-stained CN-infected MΦ and DC cultures were FACS sorted by AF594-Strep and AF488-Ab signal resulting in 4 sorted CN populations for each phagocyte type. Following FACS sorting, each population was assessed via flow cytometry showing high post-sort purity of 78% or higher (**Figure 3.S2**). Raman spectroscopy has proven an ideal tool for biochemical characterization of

a broad range of various samples types ranging through metabolites and other small molecules to extracellular vesicles and whole cell analyses[20,34–36]. In Raman scattering, as monochromatic photons from a laser light source are utilized to irradiate the sample of interest, a small proportion of these photons are inelastically scattered. These photons are detected with sensitive spectrometers, typically charge-coupled devices (CCD), and they report on various vibrating molecular structures within the sample. Thus, an acquired Raman spectrum can be considered as a chemical fingerprint of the sample, wherein every spectral peak and band correspond to certain chemical feature, for example nucleic acid or protein. In this study, the sorted CN populations were analyzed via single cell LTRS[17–19] to produce a unique fingerprint to be used for comparison of the chemical composition of each group (**Figure 3.5A**). To the best of our knowledge, this is the first report of LTRS analysis of CN. For DCs and MΦs, each reporter-sorted population of CN displayed unique Raman properties. These differences are visualized via cluster separation within principal component analysis (PCA) plots and group average spectra for double negative, single positive AF594, single positive AF488, and double positive CN. PCA is a widely-used multivariate analysis technique[37] to reduce the dimensionality of e.g. spectral data whereby the pertinent spectral features contributing the most to differences between the sample groups are difficult to discern by visual inspection but can be mapped out and visualized by the PCA. Important graphs include the PCA scores plot that displays each measured spectrum as a single marker in the plot. Whereas the PC loading spectra show the spectral peaks and bands the correspond to the majority of the variation within the given data set. For clarity, the global average spectra of CNs used to infect DCs and MΦs are shown in

Figure 3.5. as well. Lastly, the average Raman spectra of each measured group is shown in **Figure 3.5** panels **C** and **E**. (**Figure 3.5B-E**). As represented in **Figure 3.5B**, there is a distinct separation between the different groups. The principal component (PC) 1 and 2 correspond to 51.8% and 15.5 % of total variation within the data set. Essentially, by scrutinizing the PC scores plot and the associated PC1 loading spectrum, the double negative (red circles), AF488 single positive (green diamonds), and double positive (purple triangles) CNs express more carbohydrate, protein, and phospholipid related vibrations than the AF594 single positive CNs (**Table 3.1**). Also, by analyzing the PC2 loading spectrum, the double positive CNs exhibit more carbohydrate and protein associated spectral features than the three other CN groups. Although currently beyond the scope of this study, we cautiously hypothesize that especially the surface structures of CNs undergo chemical changes during the phagocytosis/vomocytosis processes while the double negative CNs (i.e. no interaction with the phagocytes) remain more unchanged. Intriguingly, the CNs that have interacted with MΦs (**Figure 3.5D**), show slightly different trend. Thereby, by first inspecting the PC scores plot with the PC1 loading spectrum, the double negative and AF488 single positive CNs express more carbohydrate, protein, and phospholipid associated spectral features than the AF594 single negative and double positive CNs. Moving forward to the interpretation of PC2 loading spectrum, especially the AF594 single positive group has more of these chemical features from the rest. However, since the PC1 corresponds to 44.2% and PC2 to 10.9% of total variation within this data set, the PC1 direction gives the predominant interpretation of the spectral data of CNs that have interacted with MΦs . Again, in order to avoid overinterpretation of this Raman spectral data, we hypothesize

that these clear differences – not only within the sample groups – but also between the CNs that had interacted with DCs and MΦs highly likely report on the chemical modification the CNs undergo during the phagocytosis/vomocytosis cycles. Interestingly, there is some overlap between double negative CN (late-stage internalization) and single AF488-Ab positive (vomocytosis) groups on the PCA plot for MΦs (**Figure 3.5D**). This result makes sense as late-stage internalization is the step prior to vomocytosis and CN can in this case experience biochemical modification that results in similar expression of these molecular markers. Lastly, a similar pattern can also be seen in the LTRS results of CNs that have interacted with DC (**Figure 3.5B**). Although not clearly overlapping, the double negative and AF488 single positive groups are close to each other therein as well. Taken together, this investigation demonstrates that (1) the reporter system can be used to successfully analyze vomocytosed populations for downstream processes and (2) different reporter-stained CN populations have distinct molecular signatures that can be measured by Raman spectroscopy.

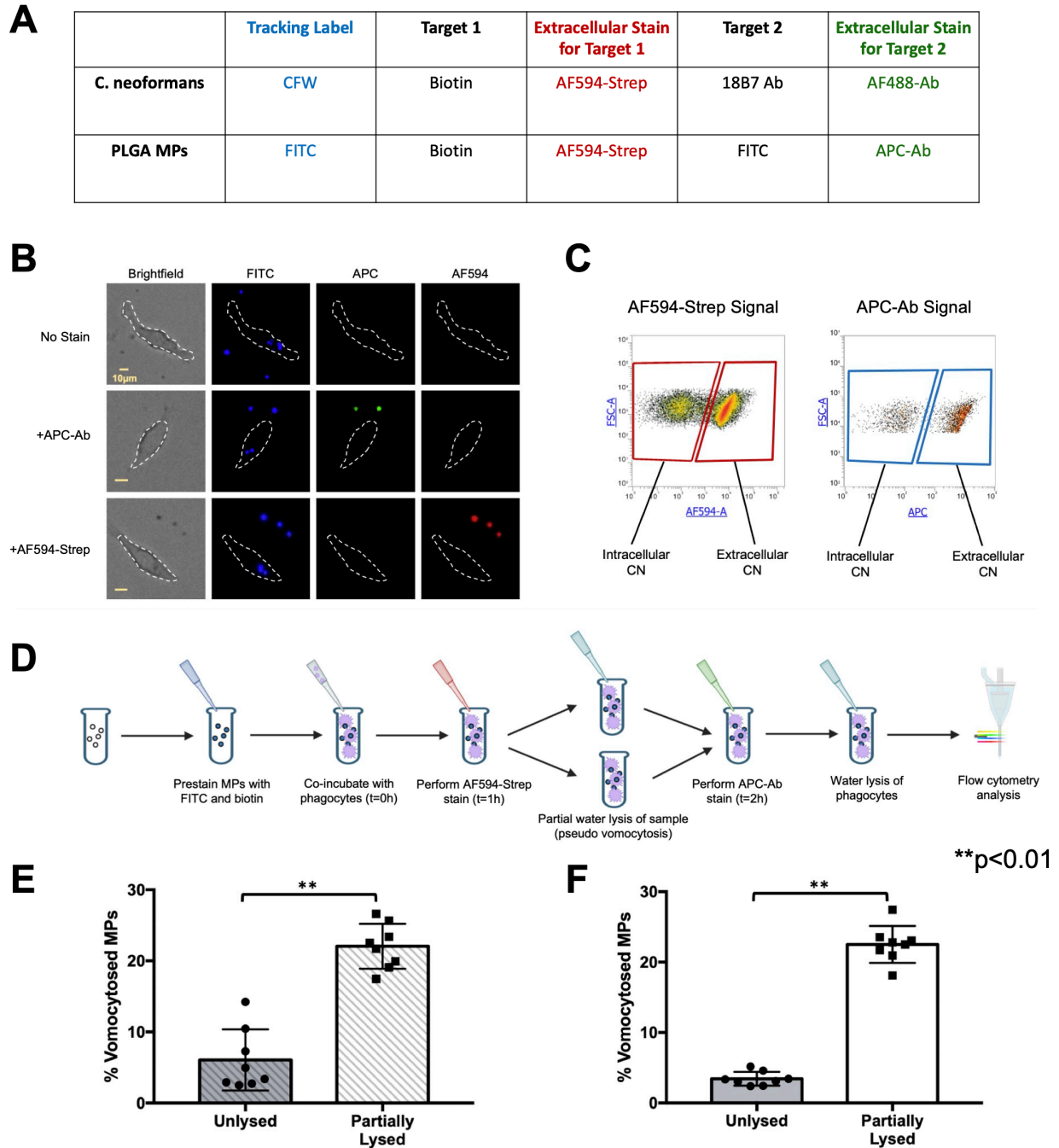| Peak/band	Chemical assignment
788-800	Nucleic acid vibrations[19]
870	Carbohydrate-related vibrations[19]
885	Carbohydrate-related vibrations[19]
895	Carbohydrate-related vibrations[19]
1060-1090	Majorly lipid vibrations[19,20]
1080	Majorly lipid vibrations[19,20]
1110-1120	C-C vibrations in e.g. lipids; C-N amide vibrations in proteins[19]
1295	Protein (amide III)/phospholipid vibrations[38]
1300	Protein (amide III)/ phospholipid vibrations[38]
1305-1360	Protein (amide III)/ phospholipid vibrations[38]
1445	CH_2 and CH_3 deformations in proteins and lipids[18]
1610	Protein vibrations[39]
1650	Amide I vibrations is proteins or C=C stretching in lipids[19]

Table 1. Raman spectra peak/band assignments.

Modified Reporter System Measures Pseudo Vomocytosis Rates of PLGA MPs

Currently, there exist no methods to accurately measure exocytosis of biomaterial particulates. To test the application potential of the reporter system, and to fulfill the need for a method to measure expulsion of particles, we translated the reporter

staining scheme to PLGA MPs. Polymeric PLGA MPs were chose due to their wide usage as a biodegradable biomaterial drug delivery platform with tunable size, chemistry, and release kinetics properties[40]. The key changes to the reporter system for PLGA MPs included replacing the CFW tracker dye with FITC, conjugated via click chemistry. Additionally, the biotin was conjugated to the surface of the PLGA MPs via click chemistry instead of NHS methods used for CN. The fluorescent antibody used for this system was an allophycocyanin (APC) conjugate of an anti-FITC antibody (APC-Ab) targeting the conjugated tracker FITC dye. (**Figure 3.6A**) These alterations were necessary to account for the differences in surface properties of fungal cells and PLGA MPs. To confirm that each reporter component functioned properly, pre-labeled PLGA MPs were incubated with MΦs to allow for phagocytosis and subsequently stained with reporter components. Fluorescence microscopy was used to visualize FITC tracker (blue), AF594-Strep (red), and APC-Ab (green) signal. The pre-labeled FITC tracker displayed clear signal on all PLGA MPs; on the other hand, the AF594-Strep and APC-Ab signals distinctly labeled only extracellular MPs, clearly displaying successful selective staining (**Figure 3.6B**). Additionally, flow cytometry of lysed cultures displayed clear gate-able populations based on AF594-Strep or APC-Ab signal to determine the location of the particle (**Figure 3.6C**). These results indicate that the modified reporter system components act as expected with high resolution and selective staining. Next, this system was tested for its ability to detect expulsion events of PLGA MPs. Biomaterial particles do not inherently perform vomocytosis. Therefore, water was used to lyse open phagocytes to imitate expulsion in order to test the reporter system in PLGA MPs. (**Figure 3.6D**). Compared to an unlysed control, the partially lysed PLGA

126

MP treatment group displayed a significantly higher expulsion rate readout using this reporter system for both MΦ and DC phagocyte types (**Figure 3.6E-F**). Taken together, these data strongly support the potential of this reporter system to measure vomocytosis rates of PLGA MPs from phagocytes and suggest that the system can likely be universally implemented for numerous different pathogens and particles.

A

	Tracking Label	Target 1	Extracellular Stain for Target 1	Target 2	Extracellular Stain for Target 2
C. neoformans	CFW	Biotin	AF594-Strep	18B7 Ab	AF488-Ab
PLGA MPs	FITC	Biotin	AF594-Strep	FITC	APC-Ab

Figure 3.6. Translation of reporter system to biomaterial PLGA MPs and measurement of pseudo-vomocytosis rates. (**A**) Comparison of reporter system staining scheme for PLGA MPs compared to CN. The primary modifications were changing tracking label from CFW to FITC and switching the AF488-Ab to an APC-Ab that targets FITC. Otherwise, the two designs have the same overall fundamental mechanism with a

128

tracker dye and two extracellular stains during infection. (**B**) Fluorescence microscopy confirmation of extracellular staining ability of AF594-Strep and APC-Ab. The particle tracker FITC, shown in blue, is labeled on all PLGA MPs. When AF594-Strep staining (shown in red) is applied, only extracellular particles display signal. If APC-Ab staining (shown in green) is performed, again only extracellular particles display signal. (**C**) Flow cytometry confirmation of extracellular staining. Following either AF594-Strep or APC-Ab staining, both lysed cultures displayed distinct gate-able flow cytometry populations by the respective fluorescence signal. (**D**) Experimental design schematic for measuring pseudo-vomocytosis rates of PLGA MPs. Following PLGA MPs labeling with biotin and FITC, particles were incubated with MΦs or DCs for 1 hour to allow for phagocytosis. Subsequently, a AF594-Strep stain was performed on the culture. To simulate vomocytosis, the tube was then split, and sterile water lysis was performed on half of the culture. Finally, the APC-Ab stain was performed, cultures were fully lysed using water, and PLGA MPs were analyzed via flow cytometry. (**E**) Bar graph showing pseudo-vomocytosis rates of PLGA MPs when co-incubated with MΦ cultures. Rates are shown for both unlysed and partially lysed conditions. (N=3, n=8) (**F**) Bar graph showing pseudo-vomocytosis rates of PLGA MPs when co-incubated with DC cultures. Rates are shown for both unlysed and partially lysed conditions. (N=3, n=8) All statistical analyses were unpaired t-tests performed via GraphPad Prism 9.

3.5 Discussion and Conclusion

This study characterizes a novel reporter staining scheme primarily consisting of two extracellular staining steps during phagocyte infection, followed by flow cytometry

analysis. The AF594-Strep and AF488-Ab stains were verified to selectively stain CN located outside of the phagosome through fluorescence microscopy, flow cytometry, and confocal microscopy. Further, this system was verified to successfully detect real vomocytosis events of CN from both MΦ and DC infections. This approach has the ability to resolve significant differences in expulsion rates of drug treatments affecting phagosomal and actin machinery. Through FACS-sorting and single cell laser trap Raman scattering analysis, different reporter-stained CN populations exhibited unique chemical compositions, indicating differences in biological expression of CN under different phagocyte interaction outcomes. Finally, this reporter methodology was adapted to properly function on biologically inert PLGA MPs to measure pseudo vomocytosis events from partially lysed phagocyte cultures incubated with these particles.

In conclusion, the reporter system we developed is proven to be a simple, high-throughput method to measure vomocytosis with minimal labor and maximal accuracy, whilst only requiring easily accessible resources and equipment. Furthermore, unlike any preexisting methods, this reporter system can be used to detect expulsion events in biomaterial PLGA MPs. A limitation of our technique is that is does require lysis of phagocytes, rendering them unable to be used for downstream analysis or quantification. Additionally, replication of CN may affect reporter gating percentages, especially since the number of expelled CN is counted rather than the number of phagocytes expulsing. However, the impact of fungal replication is minimized by usage a *Cdc24* mutant strain that inhibits replication at 37°C during the infection and CFW gating that prioritizes parent CN during analysis.
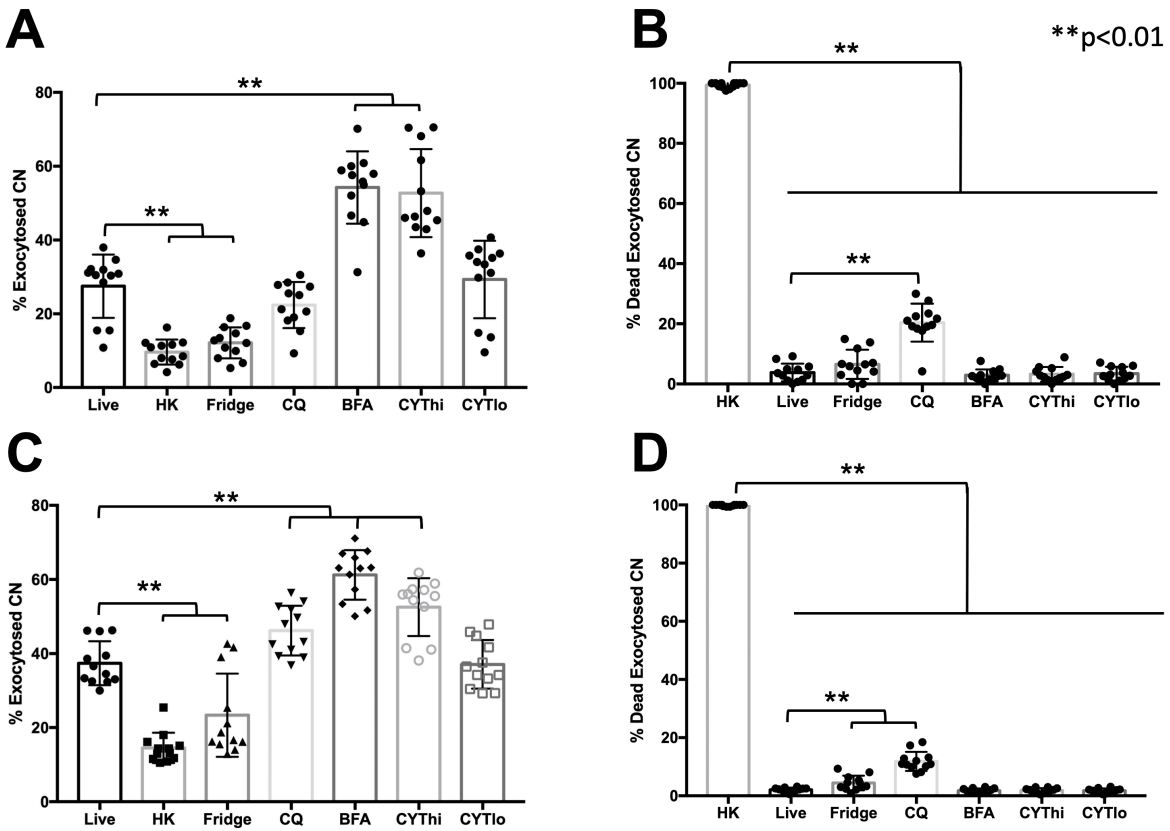
Our improved methodology for studying vomocytosis opens the door for high throughput screening of drug treatments and knockout libraries. Additionally, there is high potential for improved resolution for downstream analyses including proteomics and single-cell RNAseq of CN following reporter staining and sorting. By contributing this powerful tool to the arsenal of vomocytosis research, we hope that it will assist in boosting the amount of new high impact discoveries in this promising field of study, helping to reveal more about the underlying mechanisms of this fascinating phenomenon.

3.6 Acknowledgements

Figure 3.S1. Expulsion rates and viability percentages used to calculate vomocytosis rates. Vomocytosis percentages in the main text represent CN that have been expelled and remain viable, therefore exclude any dead CN that have been exocytosed. Here, bar graphs display (**A**) exocytosed CN from MΦs and (**B**) the percentage of that CN expelled population that are dead. Additionally, for infected DCs, the graphs display (**C**) exposed CN and (**D**) the viability of these CN populations. (Sample size N=4 biological replicates, n=12 technical replicates) All statistical analyses were one-way ANOVAs corrected for multiple comparisons by false discovery rate (FDR) using a two-stage linear step-up procedure of Benjamini, Krieger and Yekutieli via GraphPad Prism 9.
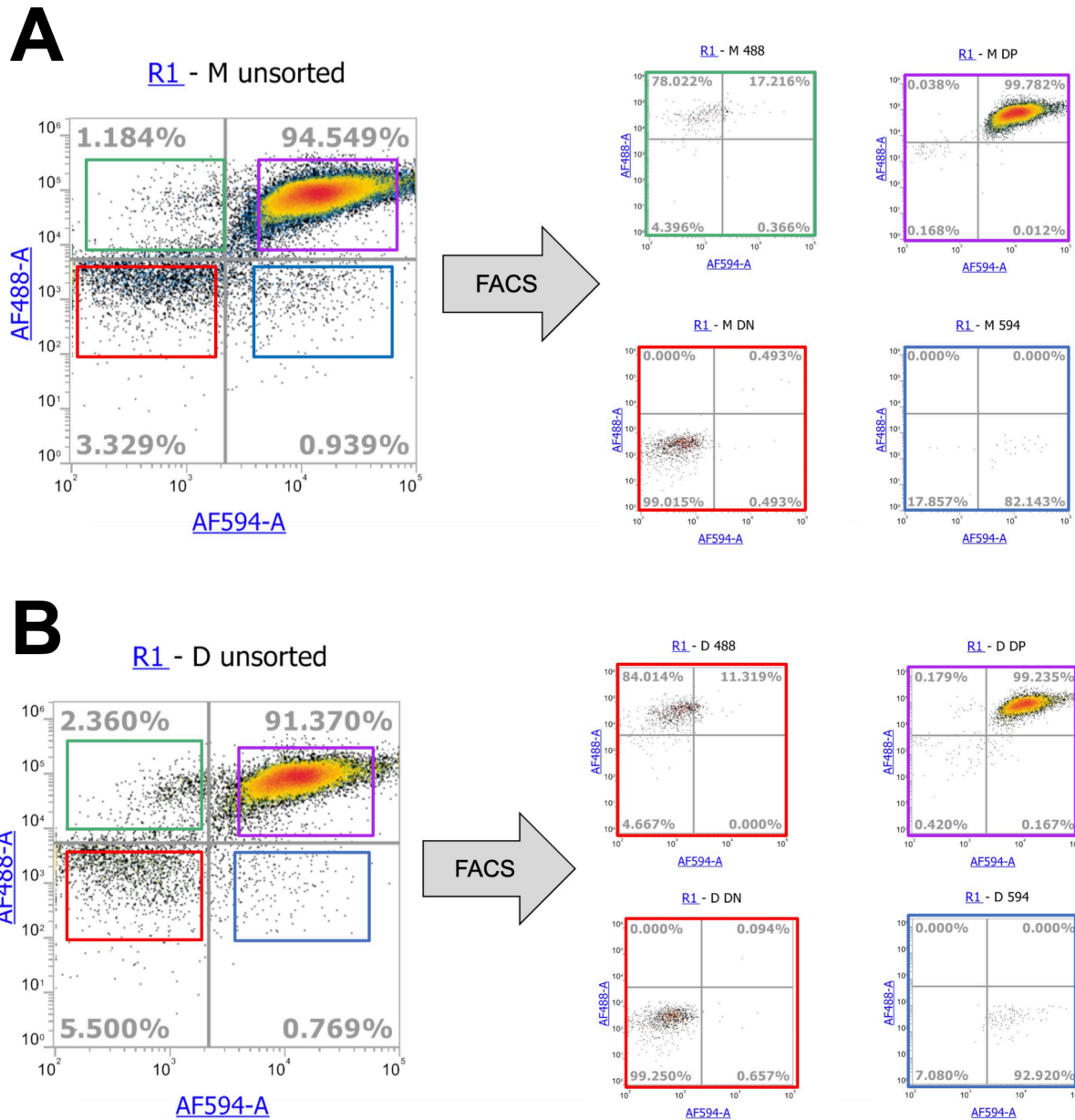
Figure 3.S2. Presort and postsort purity of reporter-stained CN. For (**A**) MΦ infections and (**B**) DC infections, the reporter-stained CN were analyzed via flow cytometry prior to sorting by FACS. Following sorting, the populations were assessed for their purity in the 4 scenarios based on AF594-Strep and AF488-Ab: double positive, double negative, single positive AF594-Strep, and single positive AF488-Ab with a purity of 78% or higher.

3.8 References

(1)   Alvarez, M.; Casadevall, A. Phagosome Extrusion and Host-Cell Survival after Cryptococcus Neoformans Phagocytosis by Macrophages. *Current Biology* **2006**, *16* (21), 2161–2165. https://doi.org/10.1016/j.cub.2006.09.061.

(2)   Ma, H.; Croudace, J. E.; Lammas, D. A.; May, R. C. Expulsion of Live Pathogenic Yeast by Macrophages. *Current Biology* **2006**, *16* (21), 2156–2160. https://doi.org/10.1016/j.cub.2006.09.032.

(3)   Cruz-Acuña, M.; Pacifici, N.; Lewis, J. S. Vomocytosis: Too Much Booze, Base, or Calcium? *mBio* **2019**. https://doi.org/10.1128/mBio.02526-19.

(4)   Seoane, P. I.; May, R. C. Vomocytosis: What We Know so Far. *Cell Microbiol* **2020**, *22* (2), e13145. https://doi.org/10.1111/cmi.13145.

(5)   May, R. C.; Stone, N. R. H.; Wiesner, D. L.; Bicanic, T.; Nielsen, K. Cryptococcus: From Environmental Saprophyte to Global Pathogen. *Nat Rev Microbiol* **2016**, *14* (2), 106–117. https://doi.org/10.1038/nrmicro.2015.6.

(6)   Rajasingham, R.; Smith, R. M.; Park, B. J.; Jarvis, J. N.; Govender, N. P.; Chiller, T. M.; Denning, D. W.; Loyse, A.; Boulware, D. R. Global Burden of Disease of HIV-Associated Cryptococcal Meningitis: An Updated Analysis. *The Lancet Infectious Diseases* **2017**, *17* (8), 873–881. https://doi.org/10.1016/S1473-3099(17)30243-8.

(7)   Yang, X.; Wang, H.; Hu, F.; Chen, X.; Zhang, M. Nonlytic Exocytosis of Cryptococcus Neoformans from Neutrophils in the Brain Vasculature. *Cell Communication and Signaling* **2019**, *17* (1), 117. https://doi.org/10.1186/s12964-019-0429-0.

(8)   Pacifici, N.; Cruz-Acuña, M.; Diener, A.; Senthil, N.; Han, H.; Lewis, J. S.

        Vomocytosis of Cryptococcus Neoformans Cells from Murine, Bone Marrow-

        Derived Dendritic Cells. bioRxiv March 29, 2022, p 2022.03.28.486165.

        https://doi.org/10.1101/2022.03.28.486165.

(9)   Nicola, A. M.; Robertson, E. J.; Albuquerque, P.; Derengowski, L. da S.;

        Casadevall, A. Nonlytic Exocytosis of Cryptococcus Neoformans from

        Macrophages Occurs In Vivo and Is Influenced by Phagosomal PH. *mBio* **2011**.

        https://doi.org/10.1128/mBio.00167-11.

(10)   Frazão, S. de O.; Sousa, H. R. de; Silva, L. G. da; Folha, J. dos S.; Gorgonha, K.

        C. de M.; Oliveira, G. P. de; Felipe, M. S. S.; Silva-Pereira, I.; Casadevall, A.;

        Nicola, A. M.; Albuquerque, P. Laccase Affects the Rate of Cryptococcus

        Neoformans Nonlytic Exocytosis from Macrophages. *mBio* **2020**, *11* (5), e02085-

        20. https://doi.org/10.1128/mBio.02085-20.

(11)   Nicola, A. M.; Albuquerque, P.; Martinez, L. R.; Dal-Rosso, R. A.; Saylor, C.; De

        Jesus, M.; Nosanchuk, J. D.; Casadevall, A. Macrophage Autophagy in Immunity

        to Cryptococcus Neoformans and Candida Albicans. *Infect Immun* **2012**, *80* (9),

        3065–3076. https://doi.org/10.1128/IAI.00358-12.

(12)   Allen, R. P.; Bolandparvaz, A.; Ma, J. A.; Manickam, V. A.; Lewis, J. S. Latent,

        Immunosuppressive Nature of Poly(Lactic-Co-Glycolic Acid) Microparticles. *ACS

        Biomater. Sci. Eng.* **2018**, *4* (3), 900–918.

        https://doi.org/10.1021/acsbiomaterials.7b00831.

(13)   Nichols, C. B.; Perfect, Z. H.; Alspaugh, J. A. A Ras1-Cdc24 Signal Transduction

        Pathway Mediates Thermotolerance in the Fungal Pathogen Cryptococcus

Neoformans. *Molecular Microbiology* **2007**, *63* (4), 1118–1130. https://doi.org/10.1111/j.1365-2958.2006.05566.x.

(14) Perfect, J. R. Cryptococcus Neoformans: A Sugar-Coated Killer with Designer Genes. *FEMS Immunology & Medical Microbiology* **2005**, *45* (3), 395–404. https://doi.org/10.1016/j.femsim.2005.06.005.

(15) Johnston, S. A.; May, R. C. The Human Fungal Pathogen Cryptococcus Neoformans Escapes Macrophages by a Phagosome Emptying Mechanism That Is Inhibited by Arp2/3 Complex-Mediated Actin Polymerisation. *PLOS Pathogens* **2010**, *6* (8), e1001041. https://doi.org/10.1371/journal.ppat.1001041.

(16) Dragotakes, Q.; Fu, M. S.; Casadevall, A. Dragotcytosis: Elucidation of the Mechanism for Cryptococcus Neoformans Macrophage-to-Macrophage Transfer. *The Journal of Immunology* **2019**. https://doi.org/10.4049/jimmunol.1801118.

(17) Ashkin, A.; Dziedzic, J. M.; Bjorkholm, J. E.; Chu, S. Observation of a Single-Beam Gradient Force Optical Trap for Dielectric Particles. *Opt. Lett., OL* **1986**, *11* (5), 288–290. https://doi.org/10.1364/OL.11.000288.

(18) Smith, Z. J.; Lee, C.; Rojalin, T.; Carney, R. P.; Hazari, S.; Knudson, A.; Lam, K.; Saari, H.; Ibañez, E. L.; Viitala, T.; Laaksonen, T.; Yliperttula, M.; Wachsmann-Hogiu, S. Single Exosome Study Reveals Subpopulations Distributed among Cell Lines with Variability Related to Membrane Content. *Journal of Extracellular Vesicles* **2015**, *4* (1), 28533. https://doi.org/10.3402/jev.v4.28533.

(19) Shipp, D. W.; Sinjab, F.; Notingher, I. Raman Spectroscopy: Techniques and Applications in the Life Sciences. *Adv. Opt. Photon., AOP* **2017**, *9* (2), 315–428. https://doi.org/10.1364/AOP.9.000315.

(20) Rojalin, T.; Koster, H. J.; Liu, J.; Mizenko, R. R.; Tran, D.; Wachsmann-Hogiu, S.; Carney, R. P. Hybrid Nanoplasmonic Porous Biomaterial Scaffold for Liquid Biopsy Diagnostics Using Extracellular Vesicles. *ACS Sens.* **2020**, *5* (9), 2820–2833. https://doi.org/10.1021/acssensors.0c00953.

(21) Koster, H. J.; Rojalin, T.; Powell, A.; Pham, D.; Mizenko, R. R.; Birkeland, A. C.; Carney, R. P. Surface Enhanced Raman Scattering of Extracellular Vesicles for Cancer Diagnostics despite Isolation Dependent Lipoprotein Contamination. *Nanoscale* **2021**, *13* (35), 14760–14776. https://doi.org/10.1039/D1NR03334D.

(22) Fu, M. S.; Coelho, C.; Leon-Rodriguez, C. M. D.; Rossi, D. C. P.; Camacho, E.; Jung, E. H.; Kulkarni, M.; Casadevall, A. Cryptococcus Neoformans Urease Affects the Outcome of Intracellular Pathogenesis by Modulating Phagolysosomal PH. *PLOS Pathogens* **2018**, *14* (6), e1007144. https://doi.org/10.1371/journal.ppat.1007144.

(23) Smith, L. M.; Dixon, E. F.; May, R. C. The Fungal Pathogen Cryptococcus Neoformans Manipulates Macrophage Phagosome Maturation. *Cellular Microbiology* **2015**, *17* (5), 702–713. https://doi.org/10.1111/cmi.12394.

(24) Leon-Rodriguez, C. M. D.; Fu, M. S.; Çorbali, M. O.; Cordero, R. J. B.; Casadevall, A. The Capsule of Cryptococcus Neoformans Modulates Phagosomal PH through Its Acid-Base Properties. *mSphere* **2018**. https://doi.org/10.1128/mSphere.00437-18.

(25) Halcrow, P. W.; Geiger, J. D.; Chen, X. Overcoming Chemoresistance: Altering PH of Cellular Compartments by Chloroquine and Hydroxychloroquine. *Frontiers in Cell and Developmental Biology* **2021**, *9*, 170.

(26) Xia, M.-C.; Cai, L.; Zhang, S.; Zhang, X. A Cell-Penetrating Ratiometric Probe for Simultaneous Measurement of Lysosomal and Cytosolic PH Change. *Talanta* **2018**, *178*, 355–361.

(27) Tapper, H.; Sundler, R. Bafilomycin A1 Inhibits Lysosomal, Phagosomal, and Plasma Membrane H+-ATPase and Induces Lysosomal Enzyme Secretion in Macrophages. *Journal of cellular physiology* **1995**, *163* (1), 137–144.

(28) Klionsky, D. J.; Elazar, Z.; Seglen, P. O.; Rubinsztein, D. C. Does Bafilomycin A1 Block the Fusion of Autophagosomes with Lysosomes? *Autophagy* **2008**, *4* (7), 849–850. https://doi.org/10.4161/auto.6845.

(29) Zurier, R. B.; Hoffstein, S.; Weissmann, G. Cytochalasin B: Effect on Lysosomal Enzyme Release from Human Leukocytes. *Proceedings of the National Academy of Sciences* **1973**, *70* (3), 844–848.

(30) Koza, E. P.; Wright, T. E.; Becker, E. L. Lysosomal Enzyme Secretion and Volume Contraction Induced in Neutrophils by Cytochalasin B, Chemotactic Factor and A23187. *Proceedings of the Society for Experimental Biology and Medicine* **1975**, *149* (2), 476–479.

(31) Li, Y.; Wan, Z.; Liu, W.; Li, R. Synergistic Activity of Chloroquine with Fluconazole against Fluconazole-Resistant Isolates of Candida Species. *Antimicrob Agents Chemother* **2015**, *59* (2), 1365–1369. https://doi.org/10.1128/AAC.04417-14.

(32) Levitz, S. M.; Harrison, T. S.; Tabuni, A.; Liu, X. Chloroquine Induces Human Mononuclear Phagocytes to Inhibit and Kill Cryptococcus Neoformans by a Mechanism Independent of Iron Deprivation. *J Clin Invest* **1997**, *100* (6), 1640–1646.

(33) Harrison, T. S.; Griffin, G. E.; Levitz, S. M. Conditional Lethality of the Diprotic

      Weak Bases Chloroquine and Quinacrine against Cryptococcus Neoformans. *The*

      Journal of Infectious Diseases **2000**, *182* (1), 283–289.

      https://doi.org/10.1086/315649.

(34) Jarvis, R. M.; Goodacre, R. Discrimination of Bacteria Using Surface-Enhanced

      Raman Spectroscopy. *Anal Chem* **2004**, *76* (1), 40–47.

      https://doi.org/10.1021/ac034689c.

(35) Maquelin, K.; Kirschner, C.; Choo-Smith, L.-P.; van den Braak, N.; Endtz, H. P.;

      Naumann, D.; Puppels, G. J. Identification of Medically Relevant Microorganisms

      by Vibrational Spectroscopy. *J Microbiol Methods* **2002**, *51* (3), 255–271.

      https://doi.org/10.1016/s0167-7012(02)00127-6.

(36) Butler, H. J.; Ashton, L.; Bird, B.; Cinque, G.; Curtis, K.; Dorney, J.; Esmonde-

      White, K.; Fullwood, N. J.; Gardner, B.; Martin-Hirsch, P. L.; Walsh, M. J.;

      McAinsh, M. R.; Stone, N.; Martin, F. L. Using Raman Spectroscopy to

      Characterize Biological Materials. *Nat Protoc* **2016**, *11* (4), 664–687.

      https://doi.org/10.1038/nprot.2016.036.

(37) Abdi, H.; Williams, L. J. Principal Component Analysis. *WIREs Computational*

      Statistics **2010**, *2* (4), 433–459. https://doi.org/10.1002/wics.101.

(38) Xie, C.; Chen, D.; Li, Y. Raman Sorting and Identification of Single Living Micro-

      Organisms with Optical Tweezers. *Opt. Lett., OL* **2005**, *30* (14), 1800–1802.

      https://doi.org/10.1364/OL.30.001800.

(39) Kengne-Momo, R. P.; Daniel, P.; Lagarde, F.; Jeyachandran, Y. L.; Pilard, J. F.;

      Durand-Thouand, M. J.; Thouand, G. Protein Interactions Investigated by the

Raman Spectroscopy for Biosensor Applications. *International Journal of Spectroscopy* **2012**, *2012*, e462901. https://doi.org/10.1155/2012/462901.

(40) Makadia, H. K.; Siegel, S. J. Poly Lactic-Co-Glycolic Acid (PLGA) as Biodegradable Controlled Drug Delivery Carrier. *Polymers (Basel)* **2011**, *3* (3), 1377–1397. https://doi.org/10.3390/polym3031377.

CHAPTER 4: TRANSCRIPTOMIC ANALYSIS OF MACROPHAGES AND DENDRITIC CELLS DURING VOMOCYTOSIS

4.1 Abstract

Cryptococcus neoformans (CN) is an opportunistic pathogen that utilizes a unique phagosome escape mechanism, called vomocytosis, to disseminate infection throughout hosts. Vomocytosis is a pathogen-induced expulsion in phagocytes that occurs over the course of several hours that leaves both the host and pathogen cells intact. This process is known to regulated by select physicochemical, protein, and immunological cues; additionally, this expulsion behavior has been observed in infected macrophages and, recently, dendritic cells. In this study, to understand more about potential underlying mechanisms of vomocytosis, RNA from CN-infected macrophages (MΦs) and dendritic cells (DCs) was analyzed at multiple expulsion-relevant time points and compared to uninfected and heat-killed CN-infected phagocytes. Differentially expressed genes were filtered through fold change and significance thresholding, as well as comparisons between controls and cell types. KEGG and GO enrichment analysis of the filtered significant gene sets was performed to identify potential pathways involved in infection and vomocytosis. The results of this analysis revealed three candidate regulating pathways of PI3K/Akt, p53, and FoxO signaling, and the 4 top genes with altered expression from each pathway were identified. Together, the results of this study characterize the transcriptome of CN-infected MΦs and DCs, as well as identify key pathways that are actively modulated by live CN over the course of infection in both cell types. The identified genes and signaling pathways potentially modulate vomocytosis or other virulence mechanisms.

4.2 Introduction

As an opportunistic pathogen, *Cryptococcus neoformans* (CN) primarily affects immunocompromised patients and causes 181,000 deaths per year globally[1]. Persistence and dissemination of infection hinges on Cryptococcal evasion and tolerance the host immune system in numerous ways[2]. One chief virulence characteristic is CN's ability to enter and hijack phagocytic immune cells—primarily macrophages (MΦs)—to survive within the normally inhabitable digestive phagosome. Crucially, following several hours of residence within the phagosome vacuole, these Cryptococcal cells are observed to escape intact, without harming the host immune cell, through a mechanism known as vomocytosis, or nonlytic exocytosis[3–6]. This escape mechanism is a key route of dissemination, with an observed significant increase in infection survival outcome when vomocytosis is inhibited[7]. This fascinating expulsion ability has been observed in multiple phagocyte cell types during CN infection including MΦs[4,7], dendritic cells (DCs)[8], and neutrophils[9]. The underlying mechanisms of this process remain to be fully understood. However, since heat-killed (HK) CN cannot perform vomocytosis, this process is likely mediated through active modulation of phagocyte machinery by live CN. Supporting this theory is the observation that vomocytosis is linked to several host cell characteristics[5,6]. For example, vomocytosis has been noted to occur exclusively in non-acidified phagosomes[10], with MΦ expulsion rates are boosted in the presence of weak bases chloroquine and ammonium chloride[11], indicating that this process is likely linked to physicochemical conditions in the phagosome. Additionally, in MΦs the vomocytosis rates have been observed to be enhanced by inflammatory factors (IFN-γ, TNF-α, IL-17,

Poly I•C, IFN-α, and IFN-β) and decreased by tolerogenic cytokines (IL-4 and IL-13), suggesting that immune polarization is a potential regulator of expulsion[12,13]. Lastly, host intracellular proteins have been implicated in this process, with ERK5 pharmacological/genetic inhibition and Annexin A2 knockout causing lower frequency of cryptococcal vomocytosis[7,14]. Still, much remains to be understood about this unique expulsion process. However, like most cellular processes, vomocytosis is likely mediated by protein signaling pathways which are preceded by RNA expression.

In this study, we aimed to use RNA sequencing identify potential pathways and genes involved in regulation of vomocytosis. The gene expression profiles of murine, bone marrow derived MΦs and DCs were evaluated at multiple vomocytosis-relevant time points of 2 hours, 4 hours, and 10 hours during live CN infection. (**Figure 4.1**) For each cell type, a HK-infected control was used to remove overlapped genes to avoid RNA data related to non-pathogen mediated processes such as phagocytosis, inflammation, and antigen processing. Through filtering the gene sets and performing KEGG & GO enrichment analysis, the top three actively regulated signaling pathways in MΦs and DCs were discovered— PI3K/Akt, p53, and FoxO. Further analysis of these pathways and the underlying modulated genes could lead to better understanding of how CN modulates host cells during infection and potentially reveal more of the underlying mechanisms of vomocytic expulsion from phagocytes.
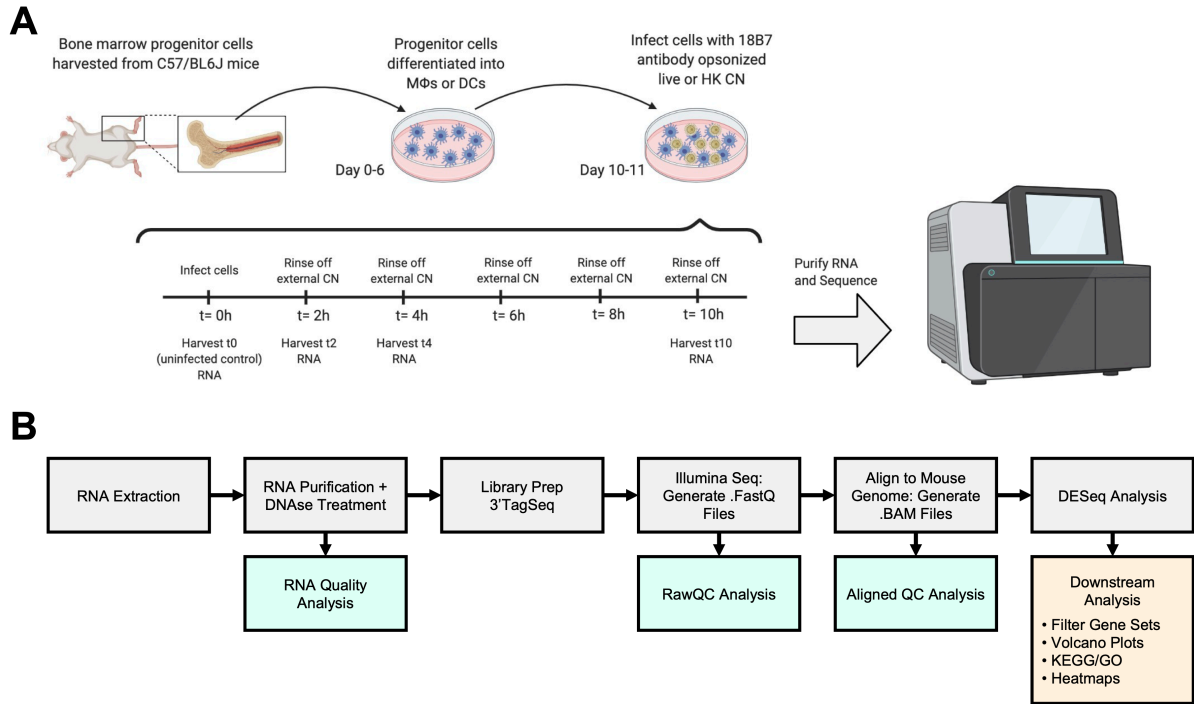
Figure 4.1. Experimental Design. (**A**) Schematic of experimental procedures. Bone

marrow progenitor cells were harvested from C57/BL6J mice and differentiated into

either MΦs or DCs. On day 10 or 11 of culture, the phagocytes were incubated with

either live or heat-killed CN. During infection, RNA was harvested from the phagocytic

cells at 0h, 2h, 4h, and 10h time points while washing away any extracellular CN every

2 hours. Harvested RNA was then purified and sequenced. (**B**) Overview of RNA

procedures and analysis pipeline. Following RNA extraction, the samples were purified

and assessed for quality at the UCD DNA Core. The highest quality samples were sent

to the UCD DNA core for library prep and sequencing to generate FastQ files which

were assessed by RawQC analysis. The reads were then aligned to the mouse

genome, and post alignment QC analysis was performed. Finally, DESeq analysis was

performed for downstream analysis including gene set filtering, volcano plot generation,

KEGG/GO analysis, and heatmap generation.

4.3 Materials & Methods

Bone Marrow-Derived MΦ and DC Culture

Bone marrow progenitor cells were harvested from 8-12 weeks old C57/BL6J mice sourced from The Jackson Laboratory and differentiated to MΦs or DCs as previously described[15]. Progenitor cells were differentiated into MΦs using L929-sourced M-CSF or into DCs using GM-CSF. Aside from differentiating factors, media consisted of DMEM/F-12 1:1 with L- glutamine (Cellgro, Herndon, VA) with 1% sodium pyruvate (Lonza, Walkersville, MD), 1% nonessential amino acids (Lonza, Walkersville, MD), 1% penicillin/streptomycin (Cytiva, Marlborough, MA), and 10% fetal bovine serum. Floating cells were grown and differentiated for 6 days, then adhered to 6 well tissue culture plates (0.5 million MΦs per well or 1 million DCs per well) until usage on day 10 or 11. Cells were grown at 5% CO_2 and 37°C conditions.

Cryptococcus Neoformans *Culture*

A H99 wild-type strain of CN (generously provided by Dr. Angie Gelli, UC Davis, CA) was used for all infections. The fungal cells were grown by first streaking a frozen culture on peptone dextrose (YPD) agar (Thermo Fisher Scientific, Waltham, MA) and incubating at 30°C until colonies were formed. The day prior to experiments, a colony of CN was transferred to YPD broth (Thermo Fisher Scientific) and left shaking at 30°C overnight.

Infection of Phagocytes with Live or HK CN

For infection of phagocytes, CN were first washed 3x with PBS via centrifugation. To prepare HK CN, fungal cells were incubated on a 70°C heat block for 1 hour. Next, live and HK CN cells were opsonized with 10 ug/ml of the anti-capsular IgG1 monoclonal antibody 18B7 (supplied from both Sigma and the Casadevall Lab, Johns Hopkins University, MD) and 50% human AB serum (Sigma, St. Louis, MO) for 30 minutes. Next, opsonized live or HK CN were incubated with MΦs or DCs at a 5:1 CN:phagocyte (0.5 million MΦs with 2.5 million CN; 1 million DCs with 5 million CN) in media containing 10% human serum. Following a 2-hour phagocytosis period, the infected cultures were washed 5x with PBS to remove extracellular CN then replenished with fresh media. Through the 10-hour infection, cultures were washed every 2 hours to remove any new expelled extracellular CN.

RNA Extraction, Purification, Quality Assessment, and Sequencing

From the HK-infected and live-infected MΦ and DC groups, RNA was extracted at 2hr, 4hr, and 10hr time points. Additionally, a 0hr uninfected control group was used for both phagocyte types. Each phagocyte timepoint group consisted of 6 biological replicates from separate mice with 3 technical replicates each. Each well of cells were dissolved using 1 mL of TRIzol Reagent (Thermo Fisher Scientific) to extract RNA. Next, according to manufacturer instructions, 200uL of chloroform was added to each tube for a phase separation procedure. Following centrifugation, the aqueous phase was mixed 1:1 with ethanol to allow for precipitation of RNA. The RNA samples were then transferred to an RNA Clean & Concentrator kit with DNAse treatment (Zymo Research, Irvine, CA)

to further purify the samples according to manufacturer's instructions. In the UC Davis DNA Core, each sample was assessed for RNA concentration & purity using NanoDrop and measured for quality scores using a LabChip GX Nucleic Acid Analyzer. Based on the highest quality scored samples (minimum score of 7), one technical replicate per biological replicate was sent to the DNA Core for 3'-Tag-Seq (QuantSeq) library preparation and sequencing by NextSeq sequencer (Illumina, San Diego, CA) to generate FastQ files containing raw unaligned reads.

Alignment to Mouse Genome and Gene Expression Analysis

Prior to alignment, RawQC analysis was performed for FastQ files of samples using Omicsoft. The generated FastQ files were trimmed and aligned to reference Mouse B39 genome & Ensembl.R105 gene model within Omicsoft to generate aligned BAM files. These files were subsequently assessed for AlignedQC metrics. Next, the gene counts were quantified and compared between groups using the DESeq2OneWayTest module of Omicsoft. The Log2FC and adjusted p-value data for each comparison was exported for further analysis off Omicsoft.

Filtering of Gene Sets

Initial filtering of gene sets was performed by using a threshold of |LogFC|>1 and adjusted p-value<0.05. Next, the gene sets were compared for each time point of each phagocyte type for live-infected vs. control, HK-infected vs. control, and live-infected vs. HK-infected. Comparative analysis was performed using an online Venn diagram tool (https://bioinformatics.psb.ugent.be/webtools/Venn/). From this comparison, the gene

sets for each phagocyte time point were further filtered for only the genes that were not present in the HK-infected vs. control gene set. Each filtered set was named for MΦ time points (M2, M4, and M10) and DC time points (D2, D4, and D10).

KEGG/GO Analysis and Selection of Candidate Genes

For pathway and enrichment analysis, filtered gene sets were analyzed for KEGG, GO biological process, GO cellular component, and GO molecular function terms on the online Enrichr tool (https://maayanlab.cloud/Enrichr/). The gene sets analyzed included M2, M4, M10, D2, D4, and D10 groups, as well as the cumulative M vs. D (M2, M4, & M10 vs. D2, D4, & D10) overlapped gene set, called MD_Overlap. Terms from KEGG/GO analysis were ranked by p-value for each group with a p-value<0.05 threshold of significance. For selected targetable pathways, candidate genes were selected by ranking the pathway-related genes in the M vs. D overlapped gene set by average magnitude LogFC; then, the top 3 genes were selected and plotted for expression at each time point for MΦs and DCs.

*PCA, Volcano, and Heatmap Plot Generation*

Multi-dimensional scaling analysis and generation of PCA plots were performed on Omicsoft. Venn diagrams for comparisons between live-infected, HK-infected, and live vs. HK-infected were created using an online tool (https://bioinformatics.psb.ugent.be/webtools/Venn/). For visualization of gene expression, volcano plots were generated for comparisons using the R EnhancedVolcano package with a threshold of |LogFC|>1 and adjusted p-value<0.05. Heatmaps for each

pathway were generated first by filtering the top 50 genes by average |LogFC| among live-infected comparison groups, then running the resulting gene lists with LogFC values on pheatmap R package.

4.4 Results

RNA samples show sufficient quality pre-sequencing, pre-alignment, and post-alignment

Prior to performing analysis, RNA samples were assessed for LabChip GX RNA quality score. Most samples displayed scores above 7.0 and the highest quality technical replicates were chosen for subsequent analysis (**Figure 4.S1A-B**). Following library preparation and sequencing, unaligned files were assessed for RawQC metrics including GC% (**Figure 4.S1C**). Base distribution, duplication level, Kmer analysis, per sequence quality & GC, sequence length, overrepresented sequences, and overall quality were assessed as well to be sufficient for further analysis (data not shown). After alignment to Mouse genome, alignedQC was performed with uniquely mapped read percentage of ~70% for all samples (**Figure 4.S1D**).
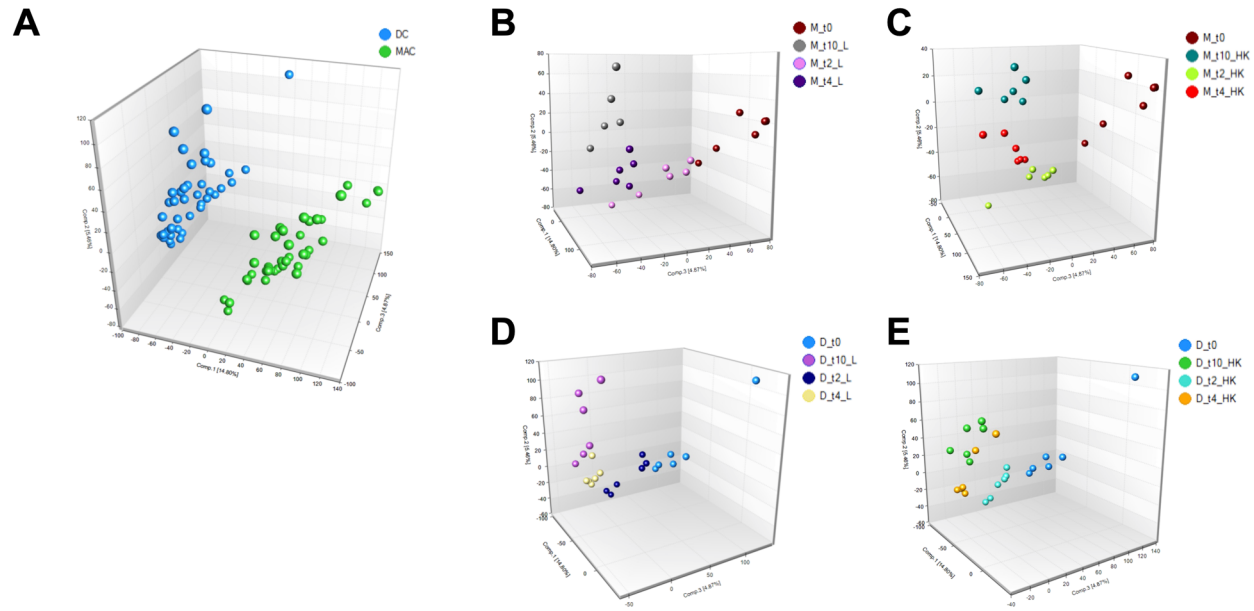
Figure 4.2. Multi-dimensional analysis of sample separation. Principal component analysis charts are shown in 3D plots for separation and clustering between (**A**) cell types, (**B**) MΦ live-infected time points, (**C**) MΦ HK-infected time points, (**D**) DC live-infected time points, and (**E**) DC HK-infected time points. N≥5 for each treatment group. Analysis was performed on Omicsoft.

Multidimensional Scaling Analysis of RNA Sequencing Data Shows High Separation Between Treatment Timepoint Groups

Aligned data files were next assessed for separation and clustering between different groups based on selected factors of analysis. Principal component analysis (PCA) plots display high separation between MΦ and DC cell type samples (**Figure 4.2A**). Additionally, both live and HK infections for both MΦs and DCs showed high separation between time points of infection (**Figure 4.2B-E**). When assessing differences between mouse replicates and gender of mice, no visual differences were seen based on these variables in both MΦs and DCs (**Figure 4.S2A-D**).
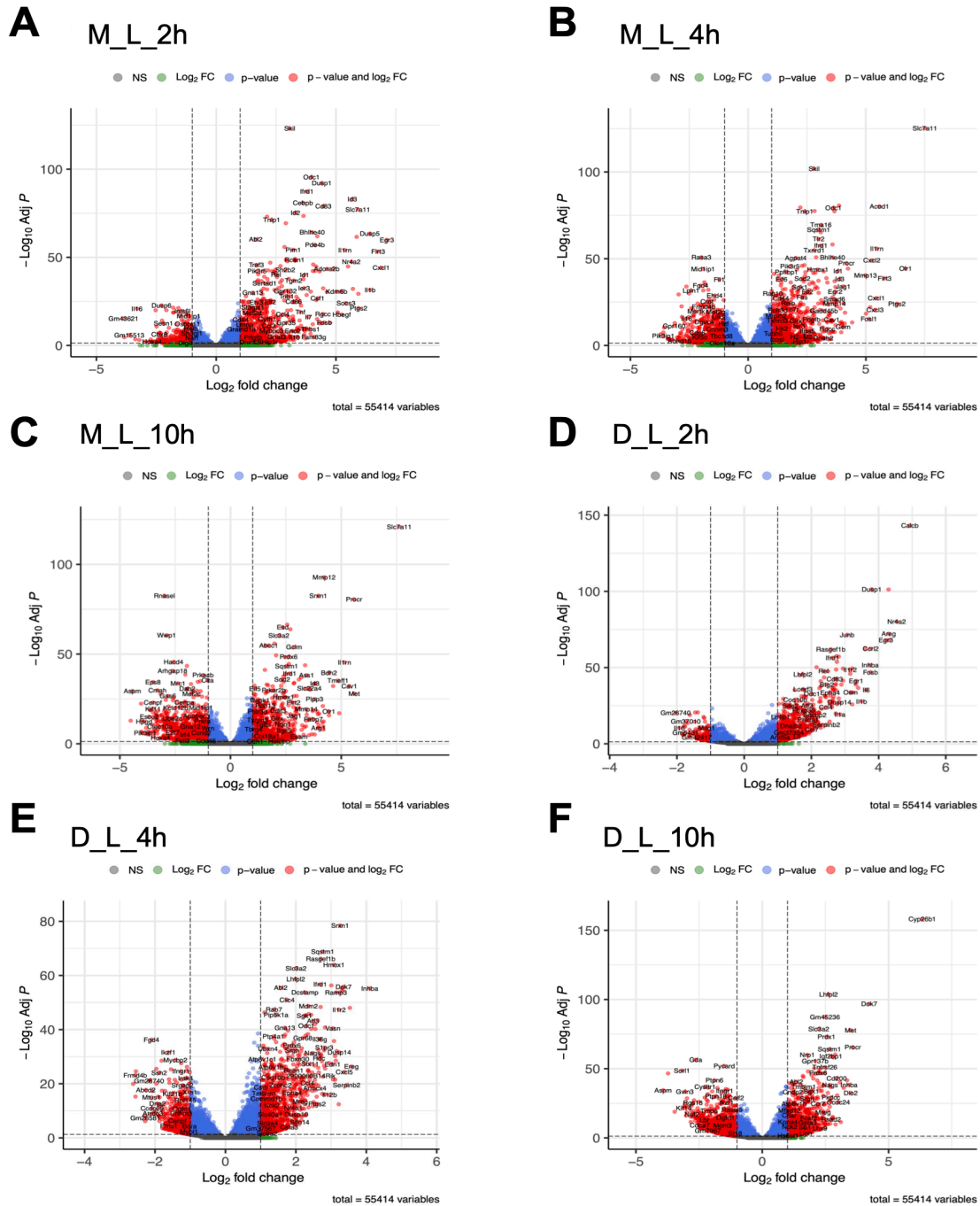
Figure 4.3. Differential gene expression of live-infected MΦ and DC groups. Volcano

plots are shown for live-infected phagocytes for MΦs (**A**) 2hr vs. 0hr, (**B**) 4hr vs. 0hr,

and (**C**) 10hr vs. 0hr; and DCs (**D**) 2hr vs. 0hr, (**E**) 4hr vs. 0hr, and (**F**) 10hr vs. 0hr. The

threshold used for this analysis was |Log2FC|>1 and adjusted p-value < 0.05. Volcano plots were generated using the EnhancedVolcano package on R.

Differential Gene Expression Analysis Reveals Significant Genes for Different Comparison Groups

To find relevant vomocytosis-related genes, a differential gene expression analysis was first performed. Expression analysis quantified comparisons between both live and HK-infections for both MΦ and DC groups across time points. The two key metrics for determining significantly expressed genes were Log2FC levels and adjusted p-values; thresholds used for significance were |LogFC|>1 and adjusted p-value<0.05. Comparisons were performed between 2-hour, 4-hour, and 10-hour time points compared to the 0-hour control point for both live-infected phagocyte groups (**Figure 4.3A-F**) and HK-infected phagocyte groups (**Figure 4.S3A-F**), visualized by volcano plots to display numerous significantly differentially expressed genes. Furthermore, the same analysis was performed for live-infected vs. HK-infected phagocytes at the 2-hour, 4-hour, and 10-hour time points (**Figure 4.S4A-F**), but with much fewer numbers of significantly expressed genes using this analysis method. Based on the thresholds of |LogFC|>1 and adjusted p-value<0.05, each comparison was reduced to a list of genes. At this stage of filtering, live-infected MΦs showed 1167 significant genes for 2hr vs. 0hr ("M_L_2h"), 1825 significant genes for 4hr vs. 0hr ("M_L_4h"), and 1882 significant genes for 10hr vs. 0hr ("M_L_10h"). For HK-infected MΦs there were 1238 significant genes for 2hr vs. 0hr ("M_HK_2h"), 1454 significant genes for 4hr vs. 0hr ("M_HK_4h"), and 1590 significant genes for 10hr vs. 0hr ("M_HK_10h"). For comparisons between live-infected and HK-

infected MΦs, there were 19 significant genes for the 2hr time point ("M_LvHK_2h"), 25 significant genes for the 4hr time point ("M_LvHK_4h"), and 5 significant genes for the 10hr time point ("M_LvHK_10h"). For live-infected DCs, the 2hr vs. 0hr ("D_L_2h"), 4hr vs. 0hr ("D_L_4h"), and 10hr vs. 0hr ("D_L_10h") displayed 842, 1711, and 1858 differentially expressed genes, respectively. Under HK-infected conditions, DCs displayed 712 significant genes for 2hr vs. 0hr ("D_HK_2h"), 1037 significant genes for 4hr vs. 0hr ("D_HK_4h"), and 1258 significant genes for 10hr vs. 0hr ("D_HK_10h"). When comparing between live-infected and HK-infected DC groups, there were 0 significant genes for the 2-hour comparison ("D_LvHK_2h"), 9 significant genes for the 4-hour comparison ("D_LvHK_4h"), and 38 significant genes for the 2-hour comparison ("D_LvHK_10h").
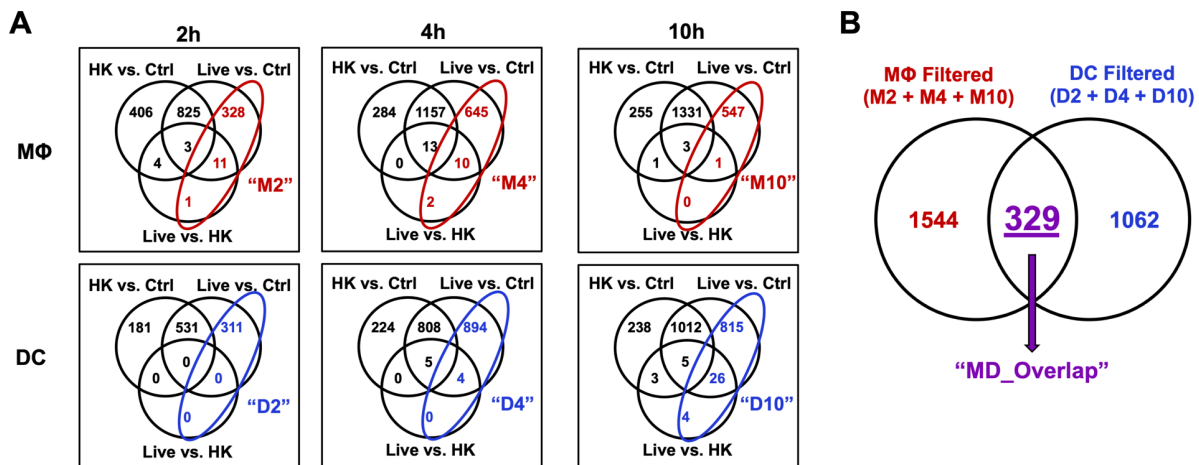
Figure 4.4. Gene filtering via comparisons. Prior to comparison, statistically significant genes (|LogFC|>1, adjusted p-value<0.05) were listed for HK-infected vs. control, live-infected vs. control, and HK-infected vs. live-infected for each cell type and time point of infection. (**A**) Venn diagram comparisons are shown for MΦ 2h, MΦ 4h, MΦ 10hr, DC

2h, DC 4h, and DC 10h groups. Only the genes that were not present in the HK control groups were used for further analysis and for simplicity of naming were labeled as "M2", "M4", "M10", "D2", D4", and "D10". Venn diagrams are shown for comparisons of genes overlapped between filtered MΦ sets and DC sets. (**B**) Lastly, all filtered MΦ (M2 + M4 + M10) and DC (D2 + D4 + D10) sets were pooled and compared, with the overlapped region labeled as "MD_Overlap".

Further Significant Gene Lists Were Generated by Filtering Against HK-Infected Groups and Overlapped MΦ and DC Genes

The generated gene lists from differential gene expression analysis of multiple treatment and control groups were next compared to each other to detect any gene overlaps. For each phagocyte type at each time point, the genes for HK-infected vs. control, live-infected vs. control, and live-infected vs. HK-infected lists were compared and visualized by Venn diagrams (**Figure 4.4A**). For filtering, the genes that were present in the live-infected vs. control and live-infected vs. HK-infected lists, but not present in the HK-infected vs. control lists were created into a new list. For MΦ infection time points, these filtered lists were named M2, M4, and M10. Filtered lists of infected DC time points were named D2, D4, and D10. Additionally, the pooled gene sets from all filtered MΦ lists (M2, M4, M10) and DC lists (D2, D4, D10) were compared (**Figure 4.4B**). The pooled DC and pooled MΦ overlapped gene list ("MD_Overlap") displayed 329 genes that are present in both phagocyte types across the time points, while not being significantly present in the HK-infected control groups.

|	KEGG/GO Terms	D2	D4	D10	M2	M4	M10
KEGG Pathway	TNF signaling pathway	X					X
	Cell cycle		X	X		X	X
	Viral protein interaction with cytokine and cytokine receptor		X				X
	p53 signaling pathway			X			X
	Small cell lung cancer			X			X
	Type II diabetes mellitus	X	X				
	FoxO signaling pathway		X				
	AGE-RAGE signaling pathway in diabetic complications						X
	Chemokine signaling pathway						X
	Homologous recombination						X
	Fanconi anemia pathway						X
	Transcriptional misregulation in cancer			X			X
	Relaxin signaling pathway			X			
GO Molecular Function	protein serine/threonine kinase inhibitor activity (GO:0030291)		X			X	
	cytokine activity (GO:0005125)	X	X	X			X
	1-phosphatidylinositol-3-kinase regulator activity (GO:0046935)	X					
	sphingosine-1-phosphate receptor activity (GO:0038036)	X		X			
	protein kinase inhibitor activity (GO:0004860)		X			X	
	5'-flap endonuclease activity (GO:0017108)						X
	ubiquitin binding (GO:0043130)				X		
	single-stranded DNA helicase activity (GO:0017116)						X
	cytokine receptor binding (GO:0005126)		X				X
	aromatic amino acid transmembrane transporter activity (GO:0015173)				X	X	
	cyclin-dependent protein serine/threonine kinase regulator activity (GO:0016538)		X		X	X	
	C-C chemokine binding (GO:0019957)					X	X
	oxidoreductase activity, acting on a sulfur group of donors, oxygen as acceptor (GO:0016670)					X	
GO Cellular Component	vacuolar proton-transporting V-type ATPase, V1 domain (GO:0000221)		X				
	proton-transporting V-type ATPase, V1 domain (GO:0033180)		X				
	serine/threonine protein kinase complex (GO:1902554)				X	X	
	cyclin-dependent protein kinase holoenzyme complex (GO:0000307)				X	X	
GO Biological Process	cellular response to cytokine stimulus (GO:0071345)	X	X	X			X
	dendritic cell chemotaxis (GO:0002407)		X				X
	dendritic cell migration (GO:0036336)		X				X
	translesion synthesis (GO:0019985)		X			X	X
	positive regulation of lymphocyte proliferation (GO:0050671)						X
	regulation of tyrosine phosphorylation of STAT protein (GO:0042509)	X					
	defense response to protozoan (GO:0042832)	X				X	
	sphingosine-1-phosphate receptor signaling pathway (GO:0003376)	X					X
	regulation of double-strand break repair via homologous recombination (GO:0010569)		X			X	
	positive regulation of T-helper 17 cell differentiation (GO:2000321)						X
	prostaglandin transport (GO:0015732)						X
	regulation of type B pancreatic cell proliferation (GO:0061469)				X		
	cell chemotaxis (GO:0060326)						X
	positive regulation of endothelial cell chemotaxis by VEGF-activated vascular endothelial growth factor receptor signaling pathway						X
	cytokine-mediated signaling pathway (GO:0019221)			X			X
	mitotic DNA damage checkpoint signaling (GO:0044773)			X			X
	positive regulation of cell migration by vascular endothelial growth factor signaling pathway (GO:0038089)						X
	cellular response to mechanical stimulus (GO:0071260)						X
	mitotic G1 DNA damage checkpoint signaling (GO:0031571)			X			
	DNA damage response, signal transduction by p53 class mediator resulting in cell cycle arrest (GO:0006977)			X	X		
	peptidyl-lysine oxidation (GO:0018057)						X
	positive regulation of B cell proliferation (GO:0030890)						X
	regulation of B cell proliferation (GO:0030888)						X
	intrinsic apoptotic signaling pathway in response to endoplasmic reticulum stress (GO:0070059)				X		X
	negative regulation of hormone secretion (GO:0046888)				X		

Table 1. Enrichment analysis of KEGG pathways, GO molecular functions, GO cellular component, and GO biological process. Gene sets used for the analysis were filtered

155

against the negative HK-infected control. Cells in the table are highlighted if the term is statistically significant (p<0.05) for the given gene set.

Enrichment Analysis Reveals Potential Key KEGG and GO Terms Relevant to Vomocytosis

To understand the potential mechanisms of differentially expressed genes, KEGG and GO analyses were performed on the filtered gene sets of M2, M4, M10, D2, D4, and D10. Using a threshold of p-value<0.05, the KEGG, GO Molecular Function, GO Cellular Component, and GO Biological Process terms were ranked by the number of filtered gene sets that displayed threshold significance for each term (**Table 1**). Numerous targetable KEGG Pathway terms were identified including of p53 signaling pathway, FoxO signaling pathway, AGE-RAGE signaling pathway, Relaxin signaling pathway, and others. Significant GO terms were also identified including protein serine/threonine kinase inhibitor activity, 1-phosphatidylinositol-3-kinase regulator activity, ubiquitin binding, sphingosine-1-phosphate receptor activity, and others.

Next, KEGG and GO terms were identified for the MD_Overlap group containing 329 overlapped genes from pooled, filtered MΦ and pooled, filtered DC groups. The significant (p-value<0.05) terms were outlined for this group for KEGG pathways (**Figure 4.5A**), GO cellular components (**Figure 4.5B**), GO molecular functions (**Figure 4.5C**), and GO biological processes (**Figure 4.5D**). This analysis reveals potential key pathways and terms that are significantly affected during both MΦ and DC infections with CN.
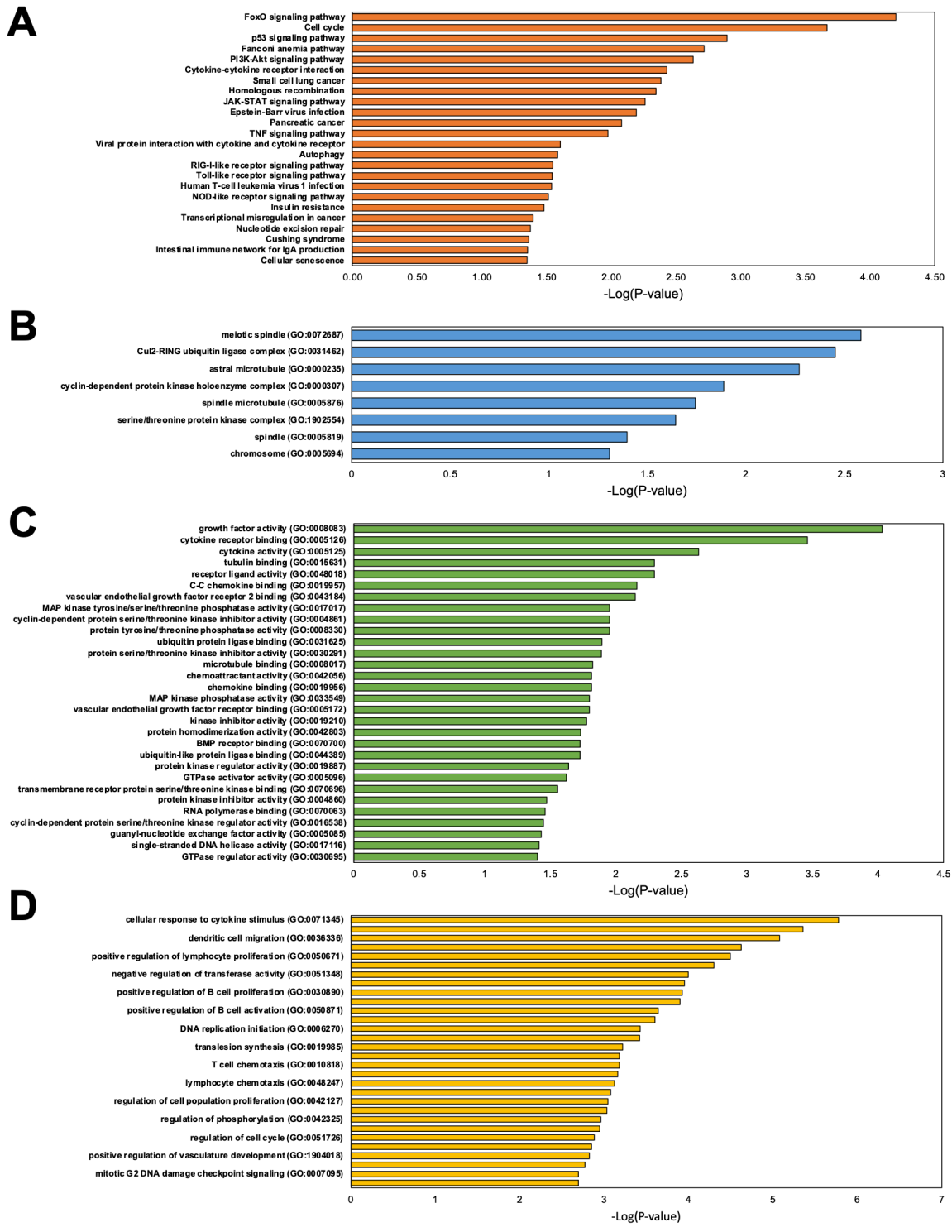
Figure 4.5. Enrichment analysis for gene sets filtered against HK-infected controls and present in both MΦ and DC across all time points. Bar graphs are shown for significant terms (p<0.05) from analysis of (**A**) KEGG pathways, (**B**) GO cellular components, (**C**)

GO molecular functions, and (**D**) GO biological processes. Analysis was performed via Enrichr.

Candidate Pathways and Genes Were Selected by KEGG Pathway Analysis

The KEGG and GO analyses produced numerous potential key pathways and terms that could be involved in vomocytosis regulation. To narrow down the number of candidates, only KEGG pathways from the MD_Overlap gene set analysis were investigated. This group is the most relevant to potential key pathways due to overlapped genes between both phagocyte types and prior filtering against HK-infected control groups. The top 3 targetable KEGG pathways for the MD_Overlap gene set by p-value were FoxO, p53, and PI3K/Akt pathways. The top 50 genes in each pathway (ranked by average |LogFC| across M_L_2h, M_L_4h, M_L_10h, D_L_2h, D_L_4h, and D_L_10h) were displayed in heatmaps, showing high visible correlation across time points and phagocyte types (**Figure 4.6A-C**). Additionally, the top 4 genes found in MD_Overlap set from each pathway, ranked by average |LogFC| across treatment groups were identified. The top 4 genes for PI3K/Akt (*Sgk1*, *Osm*, *N24a1*, and *Areg*), p53 (*Gadd45a*, *Cdkn1a*, *Gtse1*, and *Cdk2*), and FoxO (*Plk2*, *Sgk1*, *Il6*, and *Gadd45a*) expression fold changes are shown plotted for all time points for both phagocyte types (**Figure 4.6D-F**).
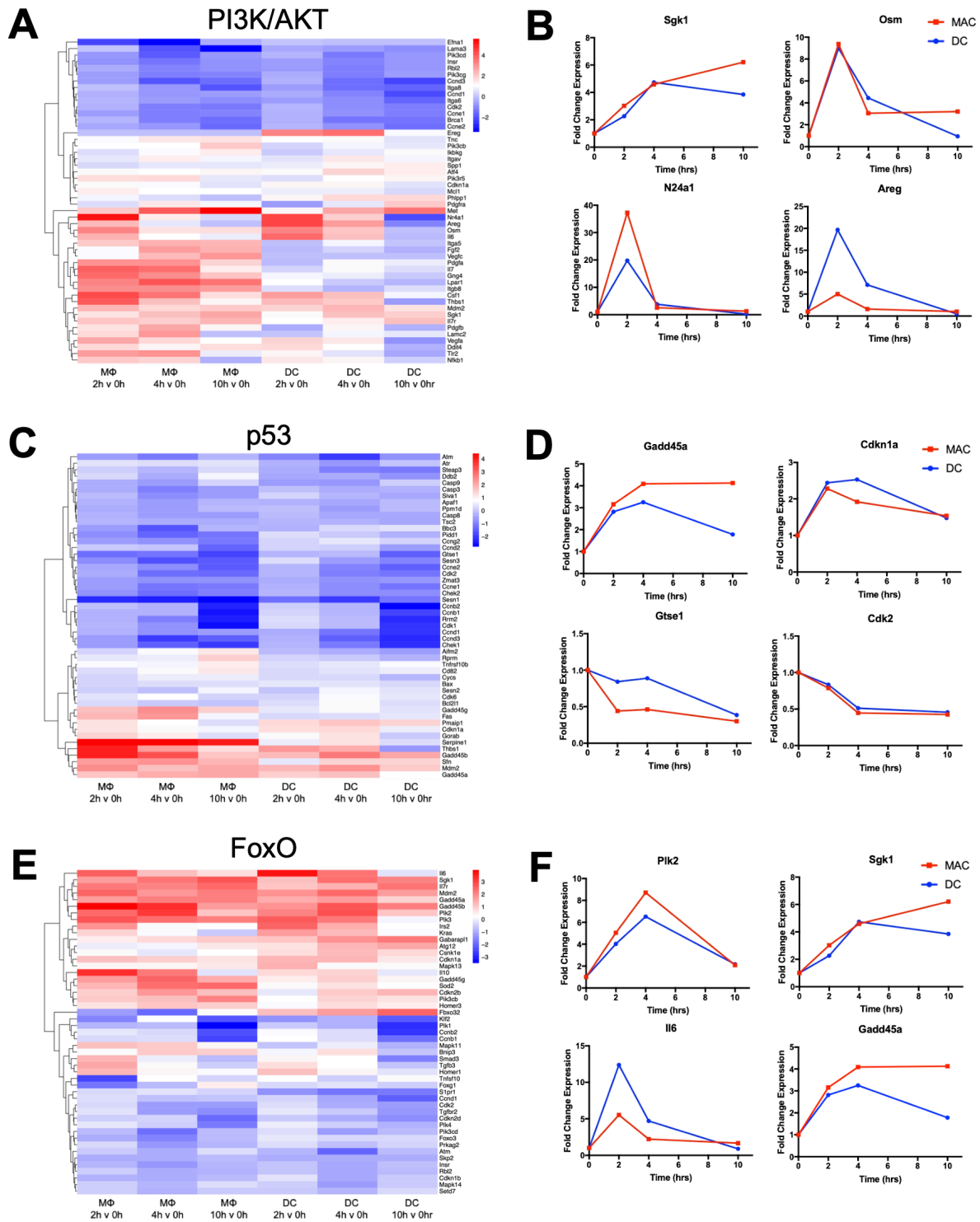
Figure 4.6. Candidate vomocytosis-regulating pathways and potential key genes. From

KEGG analysis, the top three targetable pathways were chosen by p-value to be

159

PI3K/Akt, p53, and FoxO. Heatmaps display the top 50 genes by average magnitude of LogFC for live-infected MΦs and DCs across t2, t4, and t10 timepoints for (**A**) PI3K/Akt, (**B**) p53, and (**C**) FoxO pathways. Line graphs display the expression in live-infected MΦs and DCs over time for the top 4 candidate genes of (**D**) PI3K/Akt, (**E**) p53, and (**F**) FoxO pathways. These genes were selected from the top average magnitude LogFC ranking of overlapped MΦ and DC filtered gene sets from each pathway. Heatmaps were generated using pheatmap package in R.

4.5 Discussion and Conclusion

This study set out to characterize the RNA expression of MΦs and DCs during CN infection with the primary purpose of discovering pathways that could be related to vomocytosis. To achieve this aim, bone marrow derived MΦs and DCs were infected with live or HK CN, and RNA was collected at time points of 0hrs, 2hrs, 4hrs, and 10hrs. Distinct separation and clustering via PCA plots was confirmed for gene expression characteristics between different treatment groups and cell types under incubation with either live or HK CN. Significant gene lists were generated through LogFC and adjusted p-value thresholding, then filtering against the HK-infected control, and finally isolating genes that overlapped between MΦ and DC groups. Interestingly, while there were numerous differentially expressed genes during infection for each comparison, it is worth noting that there were high levels of overlap between the live-infected and HK-infected gene groups. This similarity in gene expression may be due to generic processes for internalizing microbial particulate material, such as phagocytosis machinery and TLR binding pathways. By filtering against the HK-infected control, the analysis pipeline

160

removes most of these genes that are not actively modulated by live CN. Filtering out genes from the HK-infected groups made logical sense for the purpose of discovering genes related to vomocytosis, a process that does not occur in HK CN infections. Additionally, by further filtering for only genes shared between MΦ and DC groups, the expression data is further relevant due to both cell types being able to perform vomocytosis.

By analyzing the filtered gene sets via KEGG/GO analysis, three pathways— PI3K/Akt, p53, and FoxO—were identified to be actively modulated in both phagocyte types during Cryptococcal infection. Due to prior filtering against HK-infected groups and for overlapped genes both MΦ and DC groups, this analysis isolates pathways that are more likely related to vomocytosis. Additionally, all three pathways have been implicated to affect phagocytosis processes in immune cells[16–20]. Since phagocytosis and vomocytosis likely use similar machinery, this correlation strongly supports the validity of these candidate pathways. PI3K/Akt signaling is a highly studied pathway known to be involved in cancer[21] and inflammation[22]. One of the downstream pathways of PI3K/Akt is the mTOR pathway which has been investigated to be actively modulation in MΦ in the presence of CN[23,24], and the PI3K/Akt/mTOR cascade has been characterized to affect MΦ polarization to M1 and M2 phenotypes[25]. The p53 signaling pathway is a cellular stress response network with hundreds of genes and biological processes implicated[26,27]. The primary study of p53 is its role in cancer, with p53 mutation being the most common genetic change associated with human tumor growth[27,28]. This pathway is also involved in immune activation, being potentially connected to the common inflammatory pathways of NF-κB and JAK/STAT. In line with the our findings, other studies have indeed seen p53

activation by RNA sequencing of CN-infected MΦs[23,29]. Lastly, FoxO signaling has been implicated in affecting cell metabolism and tumor suppression[30,31]. This pathway also may be connected to PI3K/Akt signaling[32] and immune regulation[33]. Intriguingly, the FoxO signaling pathway has been observed to be a significantly affected pathway in CN-infected brain tissue via investigation of differentially expressed acetylated protein analysis[34]. Overall, all three candidate pathways (PI3K/Akt, p53, and FoxO) are implicated in various cellular mechanisms with an emphasis on cancer and immune-related processes.

Vomocytosis is a fascinating phenomenon with underlying mechanisms that are mostly unknown. As with most cellular processes, this expulsion event is very likely to be connected to gene expression and signaling pathways of phagocytes during Cryptococcal infection. Through RNA sequencing during various conditions of CN infection, the results of our study reveal potential key pathways and genes that may affect vomocytosis for phagocyte types of MΦs and DCs. The identified genes and pathways establish a foundation for future studies to verify protein expression and screen for their effects in modulating vomocytosis, hopefully unraveling more of the underlying mechanisms of this expulsion process.
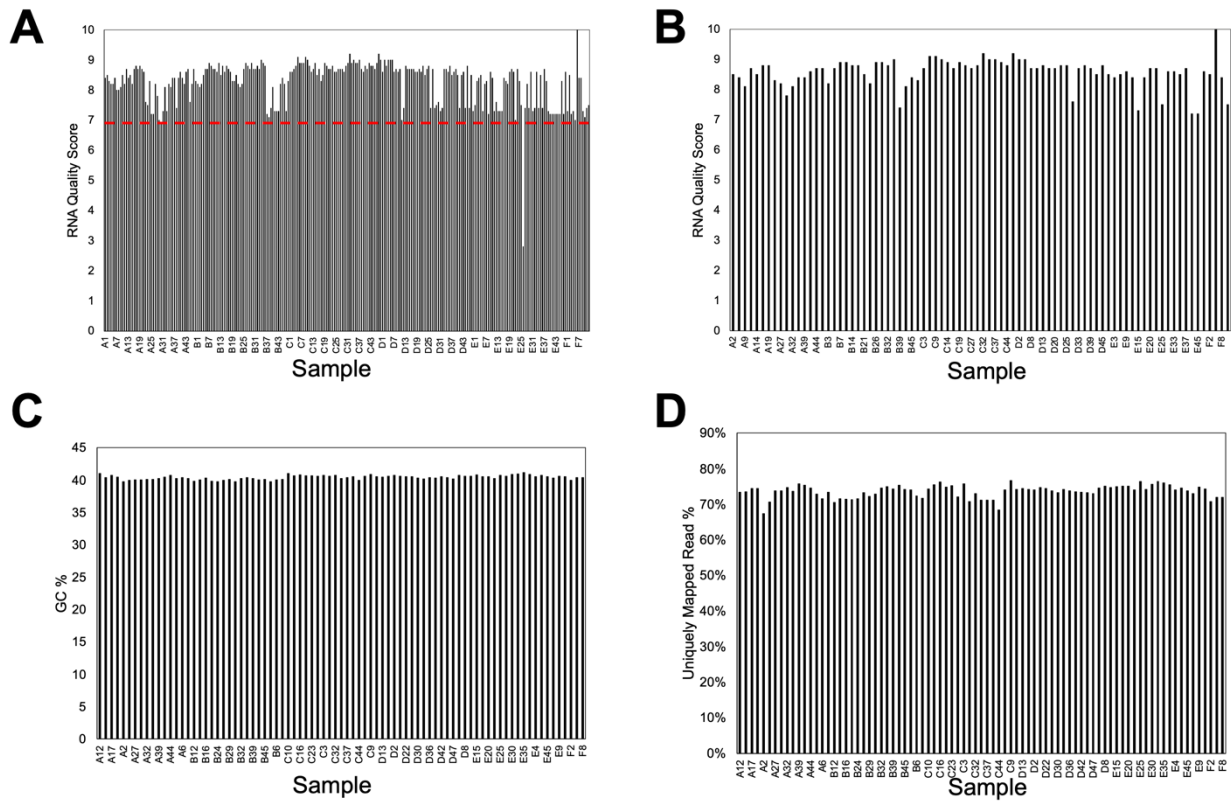
4.6 Acknowledgements

sorting fungal cells for our experiments. Finally, we thank Jian Chen, Jim Rosinski, and

Jeff Aaronson from CHDI Foundation for their guidance on RNA analysis procedures.

## 4.7 Supplemental Figures

Figure 4.S1. Quality analyses. (**A**) Bar graph is shown displaying the LabChip GX-

generated RNA quality scores for all purified samples including technical and biological

replicates. The top scoring technical replicates were chosen for sequencing. (**B**) Bar

graph shows the LabChip GX-generated RNA quality scores for selected samples to be

sequenced. (**C**) Bar graph is shown for GC base pair percentage as a rawQC analysis metric pre-alignment for all sequenced samples. (**D**) Bar graph displays percentage of uniquely mapped reads as a QC metric post-alignment for all sequenced samples. RNA quality scores were generated by LabChip GX and sequenced quality metrics were generated via Omicsoft.
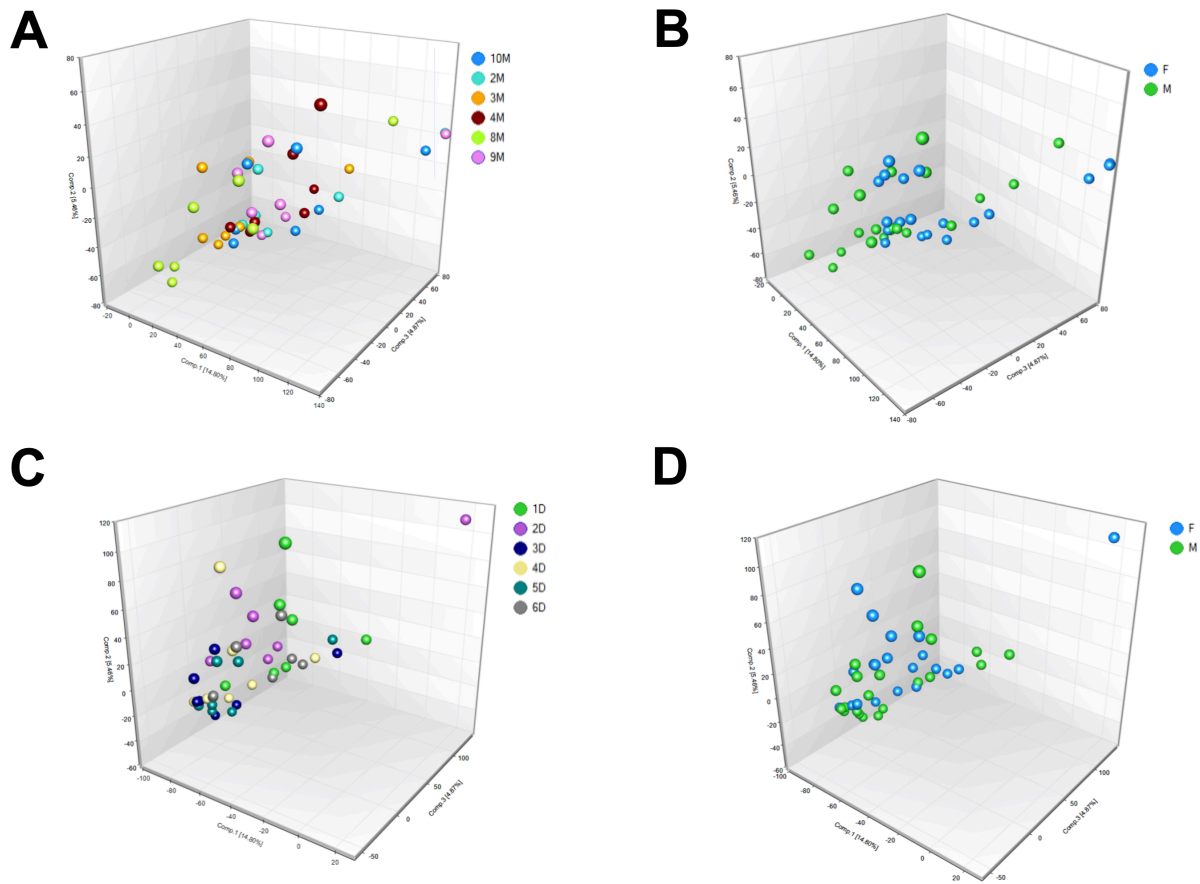

Figure 4.S2. Further multi-dimensional analysis of samples. Principal component analysis charts are shown in 3D plots for (**A**) biological replicate mice used to source MΦs, (**B**) gender of mice used to source MΦs, (**C**) biological replicate mice used to source DCs, (**D**) gender of mice used to source DCs. Analysis was performed on Omicsoft.
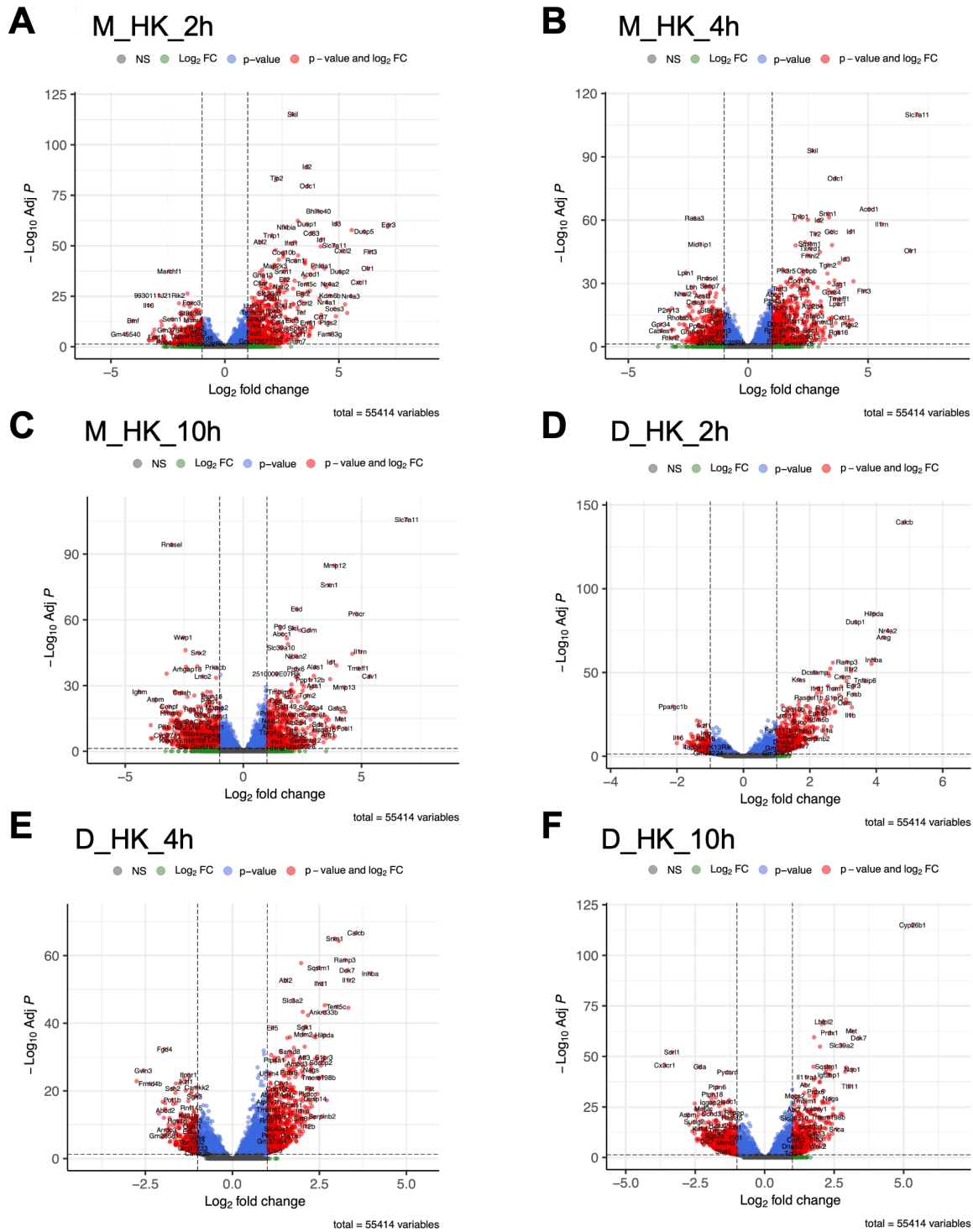
Figure 4.S3. Differential gene expression of HK-infected MΦ and DC groups. Volcano

plots are shown for HK-infected MΦs (**A**) 2hr vs. 0hr, (**B**) 4hr vs. 0hr, and (**C**) 10hr vs.

0hr; and HK-infected DCs (**D**) 2hr vs. 0hr, (**E**) 4hr vs. 0hr, and (**F**) 10hr vs. 0hr. The

threshold used for this analysis was |Log2FC|>1 and adjusted p-value < 0.05. Volcano

plots were generated using the EnhancedVolcano package on R.
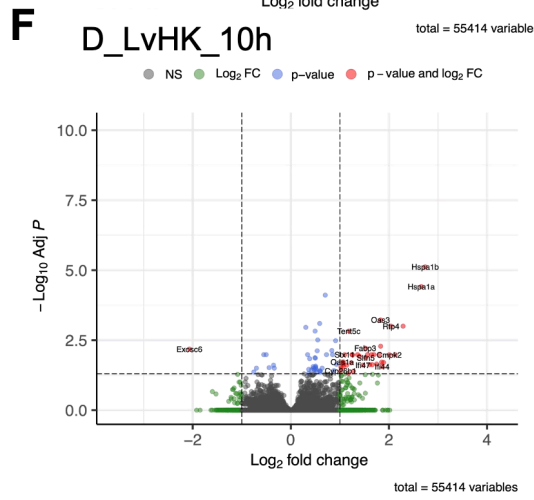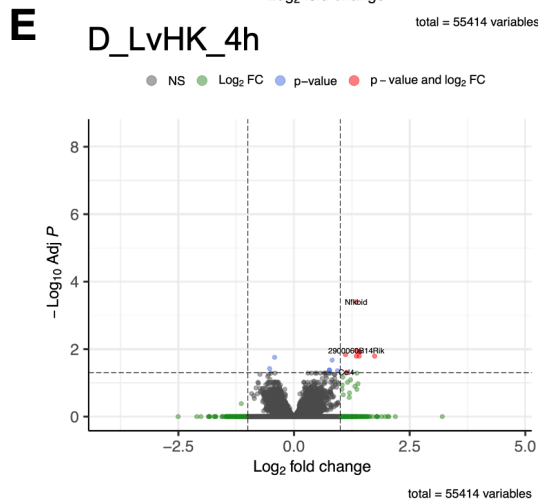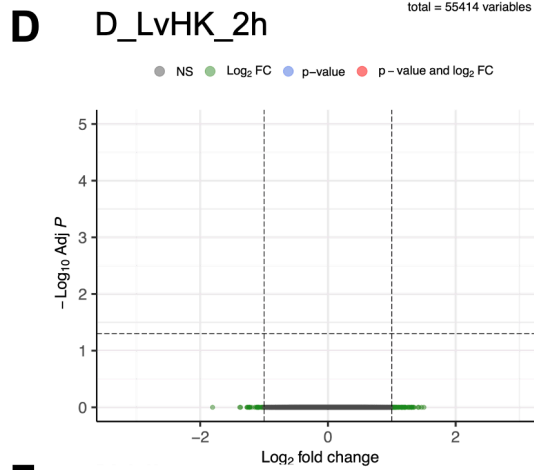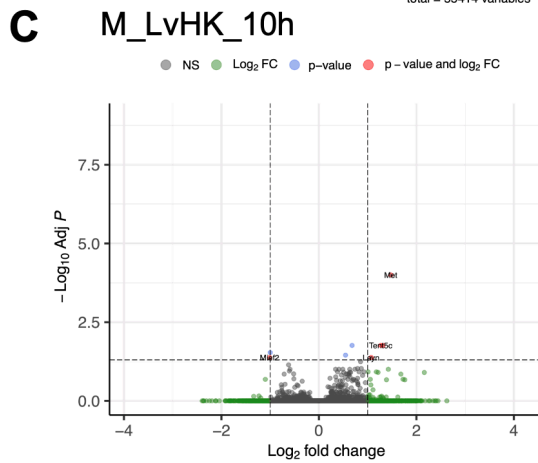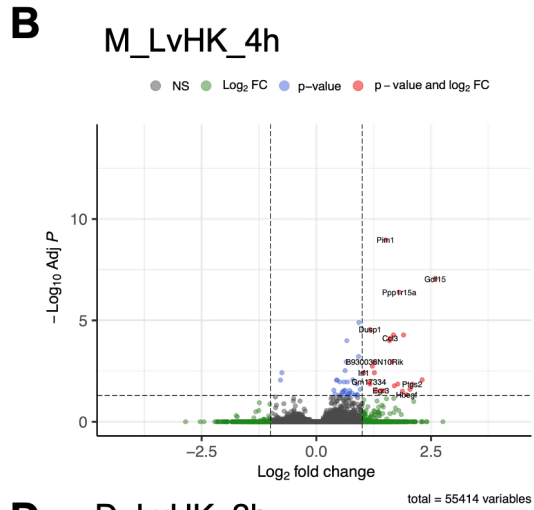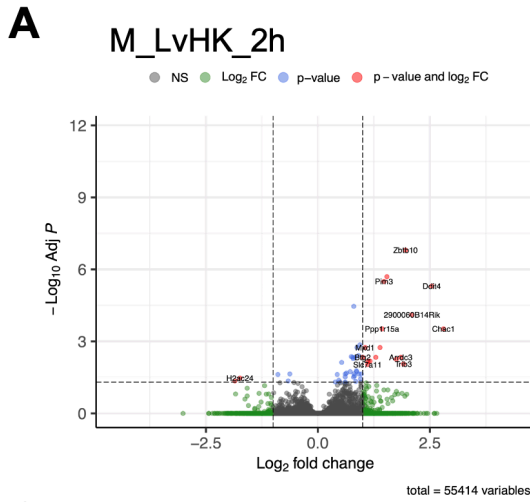
Figure 4.S4. Differential gene expression of live-infected vs. HK-infected MΦ and DC groups. Volcano plots are shown for live-infected vs. HK-infected MΦs at time points of (**A**) 2hr, (**B**) 4hr, and (**C**) 10hr; and live-infected vs. HK-infected DCs at time points of (**D**) 2hr, (**E**) 4hr, and (**F**) 10hr. The threshold used for this analysis was |Log2FC|>1 and adjusted p-value < 0.05. Volcano plots were generated using the EnhancedVolcano package on R.

4.8 References

(1) Rajasingham, R.; Smith, R. M.; Park, B. J.; Jarvis, J. N.; Govender, N. P.; Chiller, T. M.; Denning, D. W.; Loyse, A.; Boulware, D. R. Global Burden of Disease of HIV-Associated Cryptococcal Meningitis: An Updated Analysis. *The Lancet Infectious Diseases* **2017**, *17* (8), 873–881. https://doi.org/10.1016/S1473-3099(17)30243-8.

(2) May, R. C.; Stone, N. R. H.; Wiesner, D. L.; Bicanic, T.; Nielsen, K. Cryptococcus: From Environmental Saprophyte to Global Pathogen. *Nat Rev Microbiol* **2016**, *14* (2), 106–117. https://doi.org/10.1038/nrmicro.2015.6.

(3) Alvarez, M.; Casadevall, A. Phagosome Extrusion and Host-Cell Survival after Cryptococcus Neoformans Phagocytosis by Macrophages. *Current Biology* **2006**, *16* (21), 2161–2165. https://doi.org/10.1016/j.cub.2006.09.061.

(4) Ma, H.; Croudace, J. E.; Lammas, D. A.; May, R. C. Expulsion of Live Pathogenic Yeast by Macrophages. *Current Biology* **2006**, *16* (21), 2156–2160. https://doi.org/10.1016/j.cub.2006.09.032.

(5)   Cruz-Acuña, M.; Pacifici, N.; Lewis, J. S. Vomocytosis: Too Much Booze, Base, or Calcium? *mBio* **2019**. https://doi.org/10.1128/mBio.02526-19.

(6)   Seoane, P. I.; May, R. C. Vomocytosis: What We Know so Far. *Cell Microbiol* **2020**, *22* (2), e13145. https://doi.org/10.1111/cmi.13145.

(7)   Gilbert, A. S.; Seoane, P. I.; Sephton-Clark, P.; Bojarczuk, A.; Hotham, R.; Giurisato, E.; Sarhan, A. R.; Hillen, A.; Velde, G. V.; Gray, N. S.; Alessi, D. R.; Cunningham, D. L.; Tournier, C.; Johnston, S. A.; May, R. C. Vomocytosis of Live Pathogens from Macrophages Is Regulated by the Atypical MAP Kinase ERK5. *Science Advances 3* (8), e1700898. https://doi.org/10.1126/sciadv.1700898.

(8)   Pacifici, N.; Cruz-Acuña, M.; Diener, A.; Senthil, N.; Han, H.; Lewis, J. S. Vomocytosis of Cryptococcus Neoformans Cells from Murine, Bone Marrow-Derived Dendritic Cells. bioRxiv March 29, 2022, p 2022.03.28.486165. https://doi.org/10.1101/2022.03.28.486165.

(9)   Yang, X.; Wang, H.; Hu, F.; Chen, X.; Zhang, M. Nonlytic Exocytosis of Cryptococcus Neoformans from Neutrophils in the Brain Vasculature. *Cell Communication and Signaling* **2019**, *17* (1), 117. https://doi.org/10.1186/s12964-019-0429-0.

(10) Smith, L. M.; Dixon, E. F.; May, R. C. The Fungal Pathogen Cryptococcus Neoformans Manipulates Macrophage Phagosome Maturation. *Cellular Microbiology* **2015**, *17* (5), 702–713. https://doi.org/10.1111/cmi.12394.

(11) Nicola, A. M.; Robertson, E. J.; Albuquerque, P.; Derengowski, L. da S.; Casadevall, A. Nonlytic Exocytosis of Cryptococcus Neoformans from

Macrophages Occurs In Vivo and Is Influenced by Phagosomal PH. *mBio* **2011**. https://doi.org/10.1128/mBio.00167-11.

(12) Voelz, K.; Lammas, D. A.; May, R. C. Cytokine Signaling Regulates the Outcome of Intracellular Macrophage Parasitism by Cryptococcus Neoformans. *Infection and Immunity* **2009**. https://doi.org/10.1128/IAI.00297-09.

(13) Seoane, P. I.; Taylor-Smith, L. M.; Stirling, D.; Bell, L. C. K.; Noursadeghi, M.; Bailey, D.; May, R. C. Viral Infection Triggers Interferon-Induced Expulsion of Live Cryptococcus Neoformans by Macrophages. *PLoS Pathog* **2020**, *16* (2), e1008240. https://doi.org/10.1371/journal.ppat.1008240.

(14) Stukes, S.; Coelho, C.; Rivera, J.; Jedlicka, A. E.; Hajjar, K. A.; Casadevall, A. The Membrane Phospholipid Binding Protein Annexin A2 Promotes Phagocytosis and Nonlytic Exocytosis of Cryptococcus Neoformans and Impacts Survival in Fungal Infection. *The Journal of Immunology* **2016**, *197* (4), 1252–1261. https://doi.org/10.4049/jimmunol.1501855.

(15) Allen, R. P.; Bolandparvaz, A.; Ma, J. A.; Manickam, V. A.; Lewis, J. S. Latent, Immunosuppressive Nature of Poly(Lactic-Co-Glycolic Acid) Microparticles. *ACS Biomater. Sci. Eng.* **2018**, *4* (3), 900–918. https://doi.org/10.1021/acsbiomaterials.7b00831.

(16) Dong, G.; Wang, Y.; Xiao, W.; Pujado, S. P.; Xu, F.; Tian, C.; Xiao, E.; Choi, Y.; Graves, D. T. FOXO1 Regulates Dendritic Cell Activity through ICAM-1 and CCR7. *The Journal of Immunology* **2015**, *194* (8), 3745–3755. https://doi.org/10.4049/jimmunol.1401754.

(17) Dong, G.; Song, L.; Tian, C.; Wang, Y.; Miao, F.; Zheng, J.; Lu, C.; Alsadun, S.; Graves, D. T. FOXO1 Regulates Bacteria-Induced Neutrophil Activity. *Frontiers in Immunology* **2017**, *8*.

(18) Yoon, K. W.; Byun, S.; Kwon, E.; Hwang, S.-Y.; Chu, K.; Hiraki, M.; Jo, S.-H.; Weins, A.; Hakroush, S.; Cebulla, A.; Sykes, D. B.; Greka, A.; Mundel, P.; Fisher, D. E.; Mandinova, A.; Lee, S. W. Control of Signaling-Mediated Clearance of Apoptotic Cells by the Tumor Suppressor P53. *Science* **2015**, *349* (6247), 1261669. https://doi.org/10.1126/science.1261669.

(19) Yamamori, T.; Inanami, O.; Nagahata, H.; Cui, Y.-D.; Kuwabara, M. Roles of P38 MAPK, PKC and PI3-K in the Signaling Pathways of NADPH Oxidase Activation and Phagocytosis in Bovine Polymorphonuclear Leukocytes. *FEBS Letters* **2000**, *467* (2), 253–258. https://doi.org/10.1016/S0014-5793(00)01167-4.

(20) Lv, Y.; Fang, L.; Ding, P.; Liu, R. PI3K/Akt-Beclin1 Signaling Pathway Positively Regulates Phagocytosis and Negatively Mediates NF-KB-Dependent Inflammation in Staphylococcus Aureus-Infected Macrophages. *Biochemical and Biophysical Research Communications* **2019**, *510* (2), 284–289. https://doi.org/10.1016/j.bbrc.2019.01.091.

(21) Vara, J. Á. F.; Casado, E.; de Castro, J.; Cejas, P.; Belda-Iniesta, C.; González-Barón, M. PI3K/Akt Signalling Pathway and Cancer. *Cancer treatment reviews* **2004**, *30* (2), 193–204.

(22) Hawkins, P. T.; Stephens, L. R. PI3K Signalling in Inflammation. *Biochimica et Biophysica Acta (BBA) - Molecular and Cell Biology of Lipids* **2015**, *1851* (6), 882–897. https://doi.org/10.1016/j.bbalip.2014.12.006.

(23) Zhang, L.; Zhang, K.; Li, H.; Coelho, C.; de Souza Gonçalves, D.; Fu, M. S.; Li, X.; Nakayasu, E. S.; Kim, Y.-M.; Liao, W.; Pan, W.; Casadevall, A. Cryptococcus Neoformans-Infected Macrophages Release Proinflammatory Extracellular Vesicles: Insight into Their Components by Multi-Omics. *mBio 12* (2), e00279-21. https://doi.org/10.1128/mBio.00279-21.

(24) Piffer, A. C.; dos Santos, F. M.; Thomé, M. P.; Diehl, C.; Garcia, A. W. A.; Kinskovski, U. P.; Schneider, R. de O.; Gerber, A.; Feltes, B. C.; Schrank, A.; Vasconcelos, A. T. R.; Lenz, G.; Kmetzsch, L.; Vainstein, M. H.; Staats, C. C. Transcriptomic Analysis Reveals That MTOR Pathway Can Be Modulated in Macrophage Cells by the Presence of Cryptococcal Cells. *Genet Mol Biol* **2021**, *44* (3), e20200390. https://doi.org/10.1590/1678-4685-GMB-2020-0390.

(25) Vergadi, E.; Ieronymaki, E.; Lyroni, K.; Vaporidi, K.; Tsatsanis, C. Akt Signaling Pathway in Macrophage Activation and M1/M2 Polarization. *J Immunol* **2017**, *198* (3), 1006–1014. https://doi.org/10.4049/jimmunol.1601515.

(26) Prives, C.; Hall, P. A. The P53 Pathway. *The Journal of Pathology* **1999**, *187* (1), 112–126. https://doi.org/10.1002/(SICI)1096-9896(199901)187:1<112::AID-PATH250>3.0.CO;2-3.

(27) Levine, A. J. P53: 800 Million Years of Evolution and 40 Years of Discovery. *Nat Rev Cancer* **2020**, *20* (8), 471–480. https://doi.org/10.1038/s41568-020-0262-1.

(28) Bosari, S.; Viale, G. The Clinical Significance of P53 Aberrations in Human Tumours. *Vichows Archiv A Pathol Anat* **1995**, *427* (3), 229–241. https://doi.org/10.1007/BF00203389.

(29) Subramani, A.; Griggs, P.; Frantzen, N.; Mendez, J.; Tucker, J.; Murriel, J.; Sircy, L. M.; Millican, G. E.; McClelland, E. E.; Seipelt-Thiemann, R. L.; Nelson, D. E. Intracellular Cryptococcus Neoformans Disrupts the Transcriptome Profile of M1- and M2-Polarized Host Macrophages. *PLOS ONE* **2020**, *15* (8), e0233818. https://doi.org/10.1371/journal.pone.0233818.

(30) Farhan, M.; Wang, H.; Gaur, U.; Little, P. J.; Xu, J.; Zheng, W. FOXO Signaling Pathways as Therapeutic Targets in Cancer. *Int J Biol Sci* **2017**, *13* (7), 815–827. https://doi.org/10.7150/ijbs.20052.

(31) Gross, D. N.; van den Heuvel, A. P. J.; Birnbaum, M. J. The Role of FoxO in the Regulation of Metabolism. *Oncogene* **2008**, *27* (16), 2320–2336. https://doi.org/10.1038/onc.2008.25.

(32) Tzivion, G.; Dobson, M.; Ramakrishnan, G. FoxO Transcription Factors; Regulation by AKT and 14-3-3 Proteins. *Biochimica et Biophysica Acta (BBA) - Molecular Cell Research* **2011**, *1813* (11), 1938–1945. https://doi.org/10.1016/j.bbamcr.2011.06.002.

(33) Peng, S. L. Foxo in the Immune System. *Oncogene* **2008**, *27* (16), 2337–2344. https://doi.org/10.1038/onc.2008.26.

(34) Li, H.; Li, Y.; Sun, T.; Du, W.; Zhang, Z.; Li, D.; Ding, C. Integrative Proteome and Acetylome Analyses of Murine Responses to Cryptococcus Neoformans Infection. *Frontiers in Microbiology* **2020**, *11*.

CHAPTER 5: CONCLUSIONS AND FUTURE DIRECTIONS

The overarching goal of this dissertation was to further the understanding of vomocytosis. Together, the work outlined provides evidence for successful completion of this goal on multiple fronts.

First, the discovery of vomocytosis in dendritic cells (DCs) was documented and characterized. Prior to this study, only macrophages (MΦs) and neutrophils were known to display this expulsion ability during *Cryptococcus neoformans* (CN) infection. Dendritic cells are an important innate immune cell type with antigen presentation abilities and unique lymph node trafficking abilities. The outlined work in this dissertation characterized the vomocytosis rates, timing, and CN per phagosome of DCs under different infection ratios, immune phenotypes, and drug treatments. Overall, this finding of vomocytosis occurrence in DCs could be a crucial puzzle piece for understanding how CN infection progression occurs, as this cell type may traffic fungal cells to guarded organs in a similar "Trojan Horse" manner to MΦs. Furthermore, this work, combined with prior discovery of vomocytic ability MΦs and neutrophils, confirms this shared expulsion behavior of three total phagocyte types derived from the myeloid progenitor cell lineage. The conserved process between these cells suggests that there is likely shared machinery used in vomocytic expulsion that is found in multiple phagocyte cell types.

Next, this dissertation aimed to develop a new, improved fluorescent tool for measuring vomocytosis events. Prior to developing this new tool, the field of vomocytosis study was lacking in facile methods to measure expulsions. The standard in literature is manual counting of events via analysis of time lapse videos. Unfortunately, this approach has several limitations including expensive equipment requirements, low accuracy levels,

and high labor needs. To address this deficiency, we developed a new fluorescent staining scheme that assists in quantifying vomocytosis events in a simple, high throughput manner. This reporter system consists mainly of a fungal pre-labeling step followed by two fluorescent extracellular stains—streptavidin and antibody—during CN infection of phagocytes. This approach was proven to be effective in measuring vomocytosis rates for MΦs and DCs via flow cytometry; significant rate changes in drug treated conditions were able to be distinguished. Furthermore, molecular compositional differences were observed between reporter-sorted CN using single cell laser trap Raman scattering. This confirms reporter staining-based phenotypic identities of CN and suggests that these biochemical changes likely are involved in inducing vomocytic expulsion. Finally, the reporter stain was adapted for use in measuring vomocytosis rates of inert poly(lactic-co-glycolic acid) (PLGA) microparticles (MPs). This modified protocol was successful in measuring lysis-induced expulsion events of particles from phagocytes, showing that the reporter scheme has potential to be used as a universal system for measuring expulsions.

The final section of this dissertation was a transcriptomic analysis of phagocytes during CN infection, with the goal of identifying potential key pathways and genes involved in vomocytosis. RNA was collected and sequenced from MΦs and DCs infected with live CN and heat-killed (HK) CN. This sequencing data was used for differential gene expression analysis at multiple time points during infection up to 10 hours, compared to an uninfected or HK-infected control. The analysis yielded gene lists that were filtered for fold change expression and adjusted p-value, then further filtered by omitting any significant genes from HK-infected comparisons to isolate only genes that were actively

induced by live CN. Next, KEGG & GO analysis was conducted on genes overlapped between MΦ and DC sets to identify PI3K/Akt, p53, and FoxO as targetable candidate signaling pathways involved in vomocytosis. The top 4 genes of each pathway were identified for PI3K/Akt (*Sgk1, Osm, N24a1, and Areg*), p53 (*Gadd45a, Cdkn1a, Gtse1, and Cdk2*), and FoxO (*Plk2, Sgk1, Il6, and Gadd45a*).

The significant findings of the work outlined in this dissertation provide a foundation for further studies. The developed reporter system can be used to screen libraries of drugs and knock out strains for assessment of vomocytosis ability. Furthermore, the RNA pathway analysis results will be confirmed for protein expression confirmation via western blot and flow cytometry staining. Then, pathway modulation via pharmacological or RNA silencing treatments could be screened using the reporter system to measure the downstream effect on vomocytosis rates. We hope the outlined discoveries of new methods, cell types, pathways, and genes will guide future vomocytosis studies for improved mechanistic understanding of this phenomenon, stemming new innovative discoveries in Cryptococcal therapies and biomaterial drug delivery designs.